An Experimental Study of Positron Moderation and Accumulation and the Laser Ionisation of Positronium

Serena Jayne Kerrigan MPhys

Submitted to Swansea University in fulfilment of the requirements for the degree of Doctor of Philosophy

Swansea University
Prifysgol Abertawe

2011

Abstract

The laser excitation of positronium has long been an objective of researchers in Swansea and recent progress towards attaining this goal is presented here. A description of the equipment used and a review of measurements previously conducted are given. A new laser arrangement, currently being constructed, will be outlined in this thesis.

Positron plasmas, produced in a Penning trap, have been manipulated using a rotating wall electrode, in order to optimise their properties for antihydrogen production. This investigation looks at plasma manipulation using both dipole and quadrupole rotating electric fields, and the effect that an additional cooling gas, namely CO_2, has on the resulting plasma. The results presented herein show that the optimal conditions for plasma compression occur when a dipole electric field is employed in the presence of CO_2. This configuration allows for greater compression of the plasma with higher positron yield. The radial profiles of the plasmas produced as part of this investigation were imaged using a phosphor screen and CCD camera and the resulting shapes have been studied.

Research into methods of positron moderation, for the production of low energy positron beams, has been conducted for a number of years. One such study, motivated by research conducted elsewhere, is presented here. A series of argon moderators have been grown and subsequently plated with an additional gas in an attempt to improve moderator efficiency, through the production of a charged layer. Three gases were used for plating, namely N_2, O_2 and air. The effect of moderator growth with respect to pressure and temperature has also been investigated. While no increase in positron yield was observed, this study indicates that a negatively charged layer has been produced on the moderator surface, resulting in a lower average kinetic energy of the emitted beam.

DECLARATIONS AND STATEMENTS

DECLARATION

This work has not previously been accepted in substance for any degree and is not concurrently being submitted in candidature for any degree.

Signed _____ (candidate)

Date _____

STATEMENT 1

This thesis is the result of my own investigations, except where otherwise stated. Other sources are acknowledged in footnotes or by giving explicit references. A bibliography is appended.

Signed _____ (candidate)

Date _____

STATEMENT 2

I hereby give consent for my thesis, if accepted, to be available for photocopying and for inter-library loan, and the title and summary to be made available to outside organisations.

Signed _____ (candidate)

Date _____

Contents

Acknowledgements

There are a number of people that I wish to thank for their contributions, both academic and personal, towards my PhD. The first of which are Dirk and Mike who have been my supervisors for the past four years. Their knowledge in the field and assistance in the laboratory with the equipment has been invaluable to me.

The support staff are the backbone of the physics department, and the author would like to make a special mention of two in particular, Julian and Hugh. Over the years I have asked them to assist me with a number of tasks from building equipment to providing advice on components purchased. They play a crucial role in the day to day running of the lab and their support has been very much appreciated.

Additional to the above, I have worked very closely with a number of other students, Aled, Chris and Peter, all of which have made significant contributions to the experiment. Without them the experiment would not be where it is today. You have been a pleasure to work with, diolch.

Helmut and Richard have generously devoted their time and efforts to the development of the laser system and have always been available to answer any queries that I may have, I am very grateful to them both. I would also like to thank the ALPHA collaboration for allowing me the time on their system to conduct the research that makes up a large part of this thesis.

On a more personal note, I wish to thank my fellow students and friends who have provided endless entertainment and sometimes much needed distractions, In particular Kelly, Parisa and Azaria.

To my family, especially my mum and dad, you have been a constant source of support and guidance, and I don't think words can express how much that has meant to me. Thank you all.

And finally Aaron, you have been with me every step of the way with never ending patience and the constant ability to make me laugh. I couldn't have done it without you.

List of Figures

List of Tables

Chapter 1

Introduction

The study of the fundamental components of matter and their interactions has been of great interest to scientists for many years. Increasingly, from the early 20th century to the present day, antimatter has played a significant role. Every fundamental charged particle has an antimatter equivalent i.e. a particle of equal mass but opposite charge. It is thought that when the universe was created, matter and antimatter were produced in equal quantities and that we reside in a matter dominated region of the cosmos, or indeed a universe devoid of bulk antimatter. It is hoped that the study of matter-antimatter interactions will lead to an insight into the behaviour of the early universe.

The most abundant antiparticle is the positron, produced via pair production or through the beta-plus decay of a radioactive source. The discovery of positrons [1] meant that for the first time scientists could entertain the possibility of producing anti-atoms. The next big step towards achieving this goal came in 1954 with the invention of the Bevatron at Lawrence Berkeley National Laboratory (LBL). The Bevatron was designed to accelerate protons to energies of around 6.2 GeV and collide them with stationary protons to produce antiprotons. The antiproton was subsequently discovered in 1955 by Chamberlain and Segrè [2] who received the Nobel Prize for their efforts in 1959. The antineutron was discovered a year later, also at the Bevatron, by Cork *et al.* [3]. In 1995, the PS210 experiment based at the Low Energy Antiproton Ring (LEAR), CERN, produced the first ever antihydrogen ($\overline{\mathrm{H}}$) atoms, observing 11 of the anti-atoms at high en-

ergy [4]. In this experiment an antiproton beam was steered around the LEAR ring and clusters of xenon atoms were passed through the antiproton beam causing electron-positron pairs to be produced. In some cases the antiproton 'caught' the positron and became bound, thus creating antihydrogen. The antihydrogen was not confined in the ring and so left LEAR into a detection region. Here the antihydrogen was ionised and its consituent particles analysed. In 1997, the E862 experiment based at Fermilab, produced 57 $\overline{\mathrm{H}}$ atoms using a similar method [5].

In 2002, a nested Penning trap capable of trapping both antiprotons and positrons simultaneously, and then combining them, was implemented by the ATHENA collaboration to produce 50,000 low energy antihydrogen atoms [6], at the Antiproton Decelerator (AD) in CERN. Less than a month later, the ATRAP (The Antihydrogen TRAP) collaboration, also at the AD, confirmed these findings through a similar experiment. The ATHENA collaboration has since been replaced by ALPHA (Antihydrogen Laser PHysics Apparatus), described in more detail in chapter 5.

This thesis is divided into five main sections; chapters 1, 2 and 3 examine the theory that is relevant to all aspects of the research presented here, such as; positrons and positronium, positron moderation and positron accumulation. Chapter 4 outlines the goals, apparatus and results of the research conducted into the laser ionisation of positronium. The production of small dense positron plasmas through the use of a rotating wall system alongside a cooling gas is described in chapter 5. Chapter 6 details the system and data produced through research into positron moderation. Finally, conclusions and suggestions for future work will be reviewed in chapter 7.

1.1 Positrons

The positron is the most accessible antimatter particle for research. Its existence was first predicted in 1931, when Dirac, whilst developing his theory of the electron [7], discovered that there were four solutions to the relativistically invariant wave equation. For the free electron case, and neglecting spin, the solutions for the total energy, E, of a particle are given by:

$$E^2 = m^2c^4 + p^2c^2, \tag{1.1}$$

where the particle has rest mass m and momentum p, with c being the speed of light in a vacuum. The negative solutions of this equation were found to be of physical significance and led Dirac to the conclusion that there had to be electron states between $-mc^2$ and $-\infty$. These states would be unobservable but occupied according to the Pauli Exclusion Principle. A positively charged particle, with a positive rest mass would be evident if a void in these electron states occurred. Initially this was thought to be the proton, being the only positively charged particle known to be present at the time. This assumption was quickly altered and it was realised that a new particle must exist of equal rest mass to the electron, but with opposite charge; the positron.

In 1933, Anderson discovered the first positron during his work studying cosmic rays in a cloud chamber [1]. His findings were confirmed, later that year, by Blackett and Occhialini [8] who also observed pair production. A flurry of research into the possible annihilation routes for a positron in the presence of an electron ensued. It was shown that when a positron annihilates with an electron two gamma rays are emitted almost colinearly, with energy 0.511 MeV. Further work into this [9] determined that the two gamma rays were not emitted exactly colinearly, but that the angle between them was dependent upon the motion of the bound electrons in the bulk of the material with which the positron annihilated. Positrons can therefore be used as a tool to investigate the internal structure of materials [10].

1.2 Positronium

In 1951, the quasi-stable bound state of a positron and an electron was discovered by Deutsch [11]. It was named positronium and given the chemical symbol Ps. Theory dictates that the internal energy level structure of positronium is similar to that of hydrogen. The binding energy of positronium is around 6.8 eV, approximately half that of hydrogen ($\sim$13.6 eV), due to the reduced mass term in the Schrödinger equation and therefore the energy levels in positronium are scaled

Table 1.1: The states of positronium for principal quantum numbers $n = 1$ and $n = 2$ [12]. Here J is the total angular momentum and P is parity.

		J	P
$n = 1$	$^1S_0$	0	-1
	$^3S_1$	1	-1
$n = 2$	$^1S_0$	0	-1
	$^3S_1$	1	-1
	$^1P_1$	1	1
	$^3P_2$	2	1
	$^3P_1$	1	1
	$^3P_0$	0	1

by a factor of two. The orbital angular momentum, L, in each level is restricted so that $L \leq n - 1$, where n is the principal quantum number. The total spin, S, is the sum of the spins of the positron (S_+) and electron (S_-),

$$S = S_+ + S_-. \tag{1.2}$$

The states of positronium corresponding to $n = 1$ and $n = 2$ can be seen in table 1.1. The parity of the states, P, is also given, and can be calculated via:

$$P = P_{e^+} P_{e^-} (-1)^L = (-1)^{L+1}, \tag{1.3}$$

where the parity of an electron, $P_{e^-} = 1$ and a positron, $P_{e^+} = -1$, L is as previously defined. As parity is said to be invariant in electromagnetism, positronium can be used as a test of conservation laws in quantum mechanics namely, quantum electrodynamics (QED).

Looking specifically at the case where $n = 1$, two well defined spin states are given; $S = 0$ and $S = 1$. The singlet state $^1S_0$, is known as para-positronium (p-Ps). It occurs when the spins of the positron and the electron are anti-parallel and the Ps atom has a lifetime of 125 ps in vacuum. When the spins are parallel the triplet state, $^3S_1$ is produced and is known as ortho-positronium (o-Ps). The lifetime of the triplet state in vacuum is 142 ns. When either of these states decay,

photons are emitted. The number of photons, n_p, produced is dependent upon the spin and the orbital angular momentum of the state and can be calculated using equation 1.4, as

$$(-1)^{n_p} = (-1)^{L+S}. \tag{1.4}$$

From equation 1.4 it can be determined that, in their respective ground state, p-Ps must decay with the emission of an even number of photons, whereas in the case of o-Ps an odd number of photons are produced. The dominant process in both cases is the lowest order process available i.e. 2 gamma rays in the p-Ps case, emitted back to back with energies of 0.511 MeV, and 3 gamma rays for o-Ps[1]. While higher order photon emission is possible [13] annihilation via zero or one gamma ray emission is forbidden in vacuum.

[1]This is due to the conservation of angular momentum and to ensure CP invariance.

Chapter 2

Moderation of Positrons

Positrons, e^+, are produced via the beta-plus decay of a radioactive source, for instance ^{22}Na, (equation 2.1) as,

$$^{22}\mathrm{Na} \rightarrow \ ^{22}\mathrm{Ne}^* + e^+ + \upsilon_e. \tag{2.1}$$

Positrons given off in this reaction have an energy spread ranging from 0 to 0.545 MeV (see figure 2.1). With such a broad energy range, the positrons are unsuitable for most research applications and must be moderated. Positron moderation allows positrons produced from a radioactive source to be emitted into vacuum with energies of the order of a few eV. These positrons can then be conveniently manipulated into a tunable low energy beam. Although β^+ decay is not the only way of obtaining positrons [14], it is the preferred method for beamline systems, with most groups favouring ^{22}Na due to its relatively long half life of 2.6 years.

The following sections detail the historical progression of positron moderation, provide a theoretical description of the process and will introduce the concept of field assisted moderation. The latter has been investigated as part of the scope of this thesis: our experimental findings will be described in chapter 6.

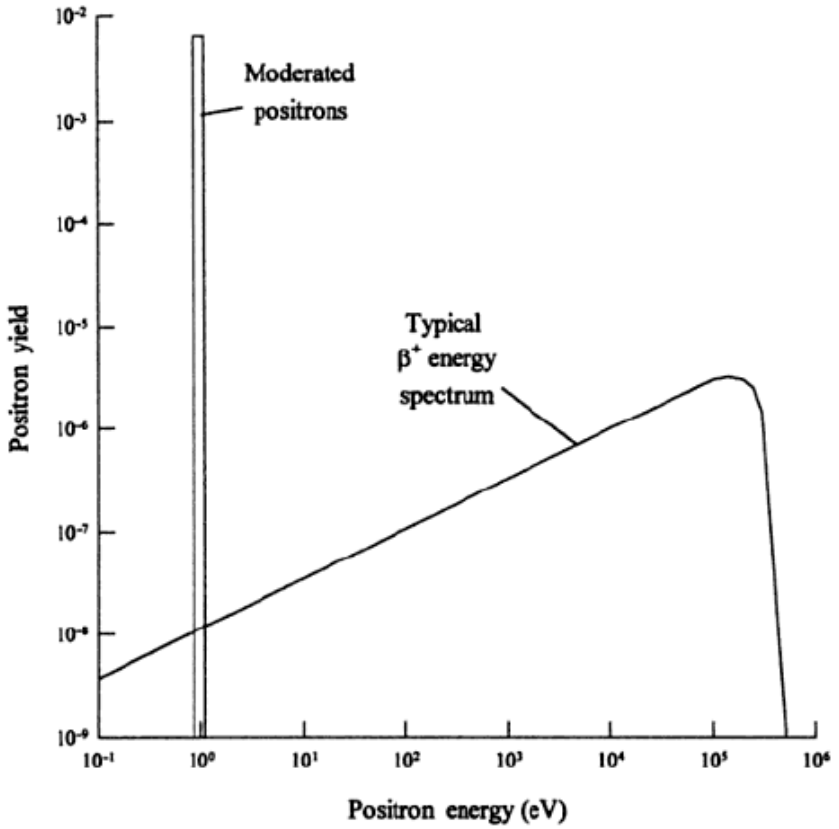

Figure 2.1: A graph to show the typical β^+ emission energy spectrum in contrast to the narrow distribution of the moderated positrons [15]. Note the massive increase in yield at very low energies achieved using moderation.

2.1 Historical Remarks

In 1950, Madansky and Rasetti began the search for a positron moderator [16]. They used ^{64}Cu, of varying strengths (from 10 - 30 mCi), as a positron source and a range of moderating materials, both metallic and dielectric. All their experiments proved to be fruitless with no slow positrons being detected from any of the materials they used. They hypothesised that the reasons for this were: (1) that positrons cannot diffuse through a crystal lattice, but instead become trapped inside potential minima and annihilate before travelling a significant distance; (2) they can diffuse through the lattice but become trapped at the

surface, or (3) that positronium is formed. It turns out that, depending on circumstance, all are true, but it is likely that all their samples contained defects which acted as positron trapping centres, reducing the positron diffusion length (see section 2.2).

In 1958 the first breakthough was made in positron moderation. Whilst working towards his PhD thesis, W. H. Cherry accidentally produced the first ever positron moderator [17], observing an excess of emission of very low energy positrons following β^+ bombardment of a surface held in vacuum. The material was chromium-on-mica and an efficiency of slow e^+ production (defined as the total number of mono–energtic positrons incident upon a target per unit time divided by the total source activity) of 10^{-8} was recorded, though these results were never published in a journal.

Eleven years later, in 1969, Madey released the first official publication of an observation of the effects of positron moderation [18]. The positrons (which originated from a ^{58}Co source) travelled through a layer of polyethylene with an aluminium film on top and later passed through a graphite filter before being annihilated on a target. The energy range of these re-emitted positrons was measured and shown to have a peak around 20 eV.

Prior to this publication, Groce *et al.* 1968 [19] reported, at a meeting of the American Physical Society, the successful observation of low energy positrons. In this case positrons were produced via pair production, using a 55 MeV electron LINAC and some thin tantalum targets. The high energy positrons produced were passed through a gold-plated mica sheet. A time-of-flight technique, with the start pulse being the LINAC signal and the stop pulse being the gamma rays emitted from the annihilation at the target, was used as the method of detection. The energies of the emitted positrons were measured to be between 1 and 2 eV. These measurements were repeated, over a period of four years, with other materials used in place of mica. No shift in the energy spectrum was observed, hence it was concluded that the moderation process had occured in the gold layer, which had been present in all of their moderators, rather than the mica [20]. A theoretical discussion by Tong in 1972 provided some justification for this observation [21], stating that the moderation process was due to the "negative work function" of the metal (see below).

Also in 1972, Canter *et al.* published a paper on their research aimed specifically at measuring the cross sections for low energy positron-helium interactions [22]. Here positrons were produced from a ^{22}Na radioactive source and moderated by backscattering off a series of gold blades, 1.4 mm wide, coated in smoked magnesium oxide (MgO) powder. The vanes were mounted in a venetian blind geometry at an angle of 45° to the tube axis. After moderation these positrons were shown to have energies around 1.5 eV, measured using a time-of-flight technique. Although the moderator only had an efficiency of 3×10^{-5}, its existence made the possibility of low energy, laboratory based, positron beams a reality.

This research was followed up in 1974 by Canter, Mills and Berko [23] who used a series of MgO coated gold surfaces in a similar configuration to produce a moderator with an efficiency an order of magnitude higher. In 1979, Mills [24] discovered a moderator having an efficiency up to 10^{-3}, consisting of single crystal copper (100), the first true ultra-high vacuum moderator. This moderator was quickly replaced by the tungsten moderator in 1983 [25]. Tungsten moderators are highly efficient, very robust and can be used in both non-UHV and UHV systems.

Since then, much research has been carried out into positron moderators, with research groups striving to produce ever higher efficiencies. Currently, the most efficient moderating materials are either metals (with a negative work function) such as tungsten, or rare gas solid (RGS) moderators boasting an efficiency of up to 1 % [26]. In general the type of moderator used is chosen according to the application of the positrons. For instance, metal moderators have a lower yield but a narrower energy spread in comparison to RGS moderators.

2.2 The Process of Moderation

When an energetic positron enters a solid it loses energy in three ways. Firstly via inelastic collisions with core and conduction electrons, followed by plasmon excitation and finally through phonon scattering (this occurs when the energy of the positron is in the eV range)[1]. The energy loss mechanism is very dependent

[1]Each process occurs on a different timescale.

upon the moderating material. In the case of metals, electron-hole pair excitation can allow the energy of the positrons to decrease to very low energies. Hence, thermalisation is rapid (on the ps timescale). For rare gas solids, once the energy has fallen below the lowest inelastic threshold, i.e. the threshold for positronium formation, further energy loss can only occur via production of acoustic phonons. In this case thermalisation is substantially retarded and many of the positrons will annihilate at epithermal energies. The diffusion length of a thermalised positron

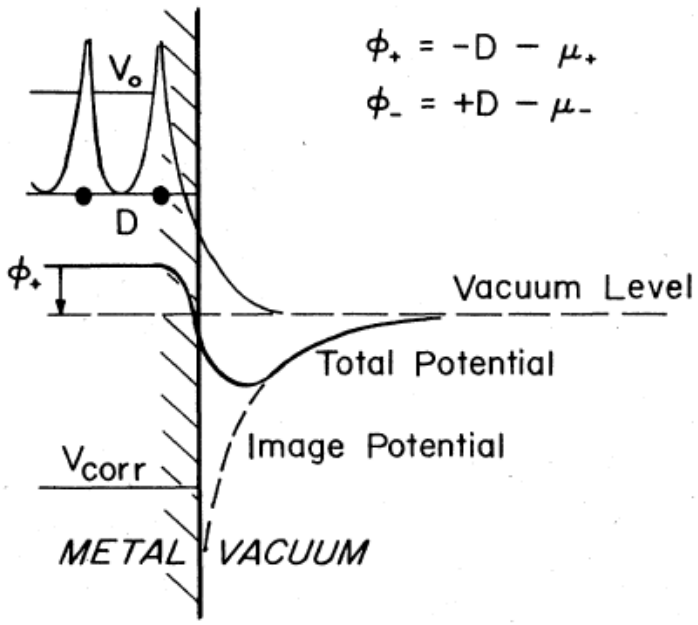

Figure 2.2: An illustration of the single particle surface potential experienced by a thermalised positron near the surface of a metallic material. The work function ϕ_+ is a combination of the the surface dipole layer D and the bulk chemical potential μ_+. The positron chemical potential includes a correlation term from the interaction with conduction electrons, V_{corr}, and the repulsive interaction with the ion cores, V_0. The sign of D, as shown, is opposite for positrons relative to electrons which is important and can result, in many cases, in a negative ϕ_+, as in the example shown here [15].

in a material can be defined as the average distance travelled in its lifetime, i.e. the distance travelled by the positron through the solid before annihilation. Positrons which are thermalised within a few diffusion lengths of the surface

may diffuse back to the surface itself. Thermalised positrons which reach the surface can either: (a) fall into a surface well where they eventually annihilate, (b) capture an electron from the material and leave as positronium, or (c) leave as free positrons into the vacuum. The latter is the one of interest here and is dependent upon the positron work function of the material, ϕ_+, where

$$-\phi_+ = \mu_+ + D. \tag{2.2}$$

Here μ_+ is the positron chemical potential in the bulk of the material and D represents the surface dipole potential; see figure 2.2. A work function can be defined as the minimum energy required to remove an object from the bulk of a solid to a point an infinite distance outside the solid. For the case of a negative ϕ_+, which can lead to spontaneous emission, the energy with which the positron leaves the surface is determined by ϕ_+. For a negative ϕ_+, from figure 2.2, it can be seen that $\mu_+ + D > 0$.

In the case of rare gas solid (RGS) moderators, such as neon and argon, the positron work function is positive. Energetic positrons lose energy via inelastic collisions which cause electronic transitions from the valence band to the conduction band. Further energy loss occurs through the creation of electron-hole pairs, and exciton or positronium formation. Once the positron energy drops below the thresholds of these it can only lose energy through the creation of acoustic phonons. This final process usually takes longer than the annihilation lifetime of the positron in the material meaning that in general positrons moderated in an RGS remain at epithermal energies. Positrons that reach the surface of the moderator with kinetic energy (perpendicular to the moderating surface) greater than the work function of the material can escape into the vacuum. The emitted positrons, in this case, have energies ranging from zero to around the band gap of the moderating material.

The fraction of moderated positrons is dependent upon a number of factors and can be estimated using a one-dimensional analysis as follows. An important quantity is the absorption coefficient, μ_{imp} (m^{-1}), of the β^+, which determines the stopping profile of the particle in a solid, and which has been determined

empirically [27] to be:

$$\mu_{imp} = \frac{17\rho}{E_m^{1.14}}. \tag{2.3}$$

Here ρ is the density of the material measured in gcm^{-3} and E_m is the endpoint energy of the β^+ emission spectrum (in MeV) as shown in figure 2.1. Using this quantity the implantation profile $P_{imp}(x)$, can be found from

$$P_{imp}(x) = \mu_{imp} e^{-\mu_{imp} x}, \tag{2.4}$$

for β^+ particles stopping a distance x from a surface.

As previously stated the diffusion length of a positron in a material can be defined as the average distance travelled by the positron during its lifetime. This model is generally accepted for metals (with a negative work function) where the diffusion is a thermal process, however it is assumed that it can also apply to the RGS case where this process would be epithermal. For the positron to be emitted from the surface it must diffuse to it. The diffusion length is given by

$$L_+ = (D_+ \tau)^{\frac{1}{2}}, \tag{2.5}$$

where D_+ is the diffusion coefficient and τ is the lifetime of the positron in the material. The probability of a positron diffusing over a distance x to the surface is thus,

$$P_{diff}(x) = e^{-x/L_+}. \tag{2.6}$$

Upon reaching the surface, the surface branching ratio (y_0) becomes important. To be emitted as a free particle in vacuum, the positron must either possess energy higher than that of the positron work function, ϕ_+,[2] or reach a negative work function surface. The emission probability, ξ, of a positron from a surface is therefore determined via,

$$\xi = y_0 \int_0^\infty P_{diff}(x) P_{imp}(x) dx. \tag{2.7}$$

[2]In the case of an RGS moderator.

Substituting in from equations 2.4 and 2.6 this can be written as,

$$\xi = y_0 \mu_{imp} \int_0^\infty e^{-(\mu_{imp} + \frac{1}{L_+})x} dx. \tag{2.8}$$

Integrating this gives,

$$\xi = y_0 \mu_{imp} \frac{L_+}{(1 + \mu_{imp} L_+)}. \tag{2.9}$$

In general the implantation depth is significantly larger than the diffusion length i.e. $\mu_{imp} L_+ << 1$, therefore the following approximation can be made:

$$\xi = y_0 \mu_{imp} L_+. \tag{2.10}$$

From this it can be seen that the moderator efficiency is dependent upon only a few factors, namely the surface branching ratio of the material, the implantation depth and the diffusion length. While the branching ratio is out of our control the implantation depth can be changed through the choice of radioactive source used, however this choice is limited by what is commercially available. The diffusion length is dependent upon the material used and moderator quality.

In the case of a RGS moderator, defects at the moderator surface can cause a broadening of the energy spread, through scattering and energy loss, of the emitted positrons. This effect can be reduced through annealing. Annealing is the process of heating the moderator to its sublimation point and then re–condensing it onto the cone of the coldhead assembly, see sections 4.3.1.1, 5.2.1.1 and 6.2.1.

2.3 Field Assisted Moderation

In field assisted moderation (FAM), the fraction of positrons implanted in a material that reach the surface is enhanced by the application of an electric field. The applied field provides a small drift velocity to the positrons, which increases the fraction of positrons reaching the surface. The drift length, L_d, replaces the diffusion length, L_+ (see section 2.2), and can be significantly higher (of the order of 10-100 times larger [28]). The drift length can be written as,

$$L_d = \nu\tau, \tag{2.11}$$

where ν is the drift velocity imparted to the positron by the electric field and τ is the lifetime of the positrons in the material. Electrical contacts are required on either side of the moderator in order to apply an electric field, which could be achieved either through a thin metallisation or ion implantation doping, however in both cases the near-surface structure would be drastically modified.

This concept was first proposed and attempted in 1979 by Lynn and McKee [29]. Positrons were drifted through a Si layer with a 200 Å thick gold layer at the emitting surface. A small increase in positron yield was observed with the increase of the electric field however the overall efficiency was very low. It was thought that defects in the gold layer and the presence of a thin layer of SiO_2, between the Si and the gold contact, had contributed to the lack of success.

In 1986, Beling *et al.* [30], proposed that efficiencies of up to 10 % could be achieved using epitaxially grown silicide contacts alongside a silicon crystal (Si(111)) moderator. They predicted that transmission through the silicide layer would be nearly 100 % efficient, however, in order to be sucessful the silicide layer had to have a negative work function that was lower than that of the Si(111). Subsequently it was found that the Si(111) work function was positive.

It was later proposed that metal on semiconductor systems could be a candidate FAM, with Si-GaAs being considered the most promising [28]. In 1994, Shan *et al.* [31] produced a semi-insulating GaAs layer which allowed, when an electric field was applied to it, around 10 % of the positrons entering the layer to drift through it to the metal overlayer. The emission of these positrons into the vacuum was more difficult with two main problems being highlighted. The first was that the metal-semiconductor interface contained many vacancies within which the positrons could become trapped and subsequently annihilate. This could be overcome through epitaxal growth on the GaAs layer. The second of the difficulties was related to the type of metal used as an overlayer, with the conclusion that a thin film metal, which allows tunnelling emission into the vacuum, such as gold, must be used.

It has been shown that the efficiency of RGS moderators can be improved

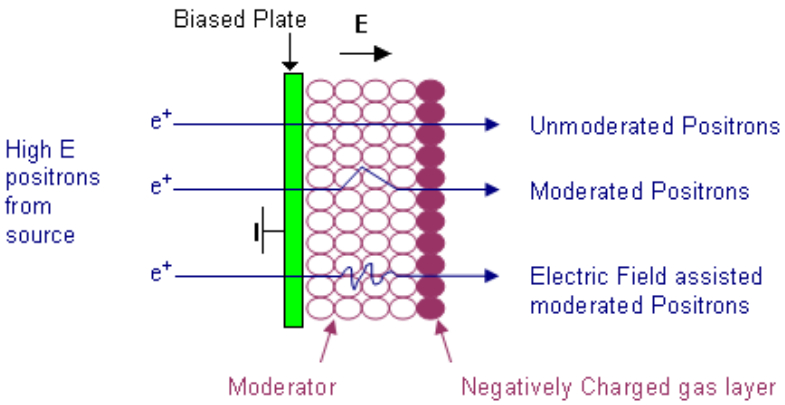

Figure 2.3: Positron moderation showing the concept of electric field assisted moderation.

through the use of a charging layer [32]. A small amount of a second gas can be deposited directly upon the moderator surface. Positrons (in the form of energetic β^+particles) bombard the moderating material and cause secondary electrons to be produced and possibly trapped in the surface gas layer. This results in the layer becoming negatively charged, as shown in figure 2.3. An electric field is set up between the surface charge and a biased plate, behind the RGS surface. The electric field imparts a small amount of drift velocity to the positrons, which enhances the fraction reaching the surface.

This technique was demonstrated in 1992 by J. Merrison and co-workers who grew both argon and krypton moderators with an overlayer of oxygen which they then bombarded with electrons from a heated tungsten filament [32]. With the bombardment of the e^-s they reported a three-fold enhancement in yield.

In 1995, Jørgensen *et al.*, followed up this research by examining the re-emission of positrons from a surface charged argon moderator [33], with respect to the implantation energy of the positrons and the electric-field produced. Positrons from a ^{22}Na radioactive source were moderated by a tungsten mesh moderator to produce a beam of 2×10^4 e^+s^{-1}, with an energy spread of $\sim$ 4 eV. The beam was passed through a filter at 100 eV before the particles were accelerated, providing implantation energies of 1-10 keV. An argon layer was grown on top of a copper target with an overlayer of oxygen. The oxygen was charged via

bombarding the surface with low energy electrons from a tungsten filament. The charge produced in the overlayer could be increased by repeated bomabardment of electrons. Jørgensen found that, for a range of implantation energies, the yield of positrons re-emitted from the RGS layer was maximised at an electric field of 7 $kVmm^{-1}$, however at higher fields the yield was reduced. It was observed that no change in positron number occurred with respect to implantation energy with the electric field set at 7 $kVmm^{-1}$.

Preliminary research performed at UCL [34], has shown that when a layer of gas, namely nitrogen, oxygen or air is deposited upon a rare gas solid moderator the yield of low energy positrons can increase by a factor of three. This increase in positron moderator efficiency has provided the motivation for the Swansea group to begin the investigation of plated solid rare gas moderators, the results of which are presented in chapter 6.

Chapter 3

Positron Accumulation and Rotating Wall Techniques

Antimatter has a large focus in the scientific community with many groups currently working in various areas of research such as anti-atom production [35, 36] and positronium studies [37, 38]. To be successful both these fields require high intensity positron beamlines to be successful. As positrons are emitted via radioactive decay, in order to produce the required intensity, strong sources with highly efficient moderators, e.g. RGS moderators, (previously described in section 2.2) are required. In addition to this, while there are some high intensity positron beams in existence, in order to allow experimentation involving large numbers of positrons to be conducted in a laboratory environment, charged particle traps need to be used.

In 1989, Surko and co-workers devised a charged particle trap, based on the Penning trap, capable of trapping moderated positrons [39]. This new trap allowed large numbers (3.3×10^5) of positrons to be collected to form a plasma, and is known today as a positron accumulator. Two such traps have been used for the research conducted for this thesis, and will be described in sections 4.3.1.2 and 5.2.1.2. With the introduction of the rotating wall technique described in section 3.4, positron plasmas could finally be tailored to suit a variety of applications. This chapter will introduce the concept of positron trapping, beginning with the Penning trap and moving on to the now widely used positron accumulator. The

rotating wall technique, used for the manipulation of positron plasmas, will be explained in section 3.4.

3.1 The Penning Trap

The Penning trap, originally invented in 1959 by Hans Dehmelt [40], is a charged particle trap designed to hold species through the use of electric and magnetic fields. In its original form it consists of a ring electrode with two end cap electrodes in the shape of hyperboloids of revolution, and a magnetic field, $\mathbf{B}$, in the z direction, as shown in figure 3.1.

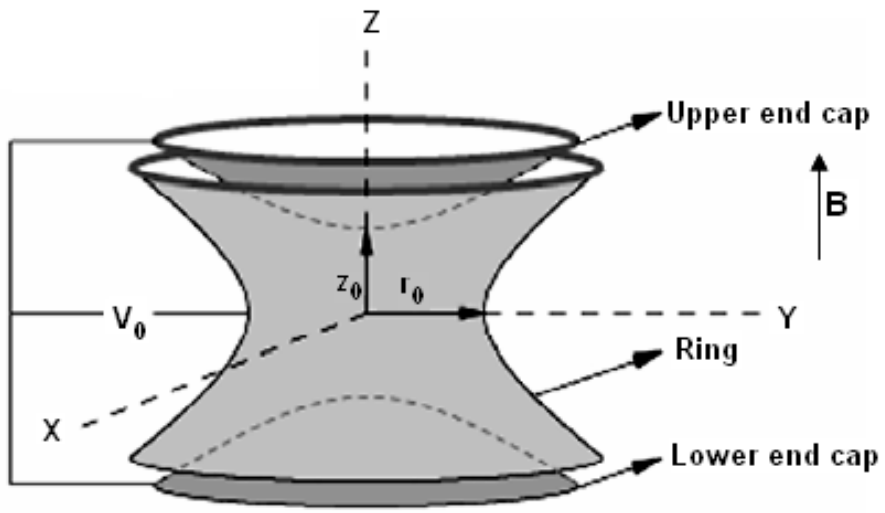

Figure 3.1: Schematic illustration of a Penning trap. Here V_0 is the applied potential, r_0 is the radial distance from the centre of the trap to the ring elecrode and z_0 is the axial distance to an end cap [41].

The force, $\mathbf{F}$, acting on a particle of mass m, and charge q, moving with a non-relativistic velocity $\mathbf{v}$ travelling in a uniform magnetic field, can be determined via,

$$\mathbf{F} = q(\mathbf{v} \times \mathbf{B}). \tag{3.1}$$

This gives rise to a rotation in the xy plane known as cyclotron motion, with the

characteristic cyclotron frequency, ω_c, given by

$$\omega_c = \frac{q|\mathbf{B}|}{m}. \tag{3.2}$$

As can be seen from equation 3.2, ω_c is dependent purely upon the magnetic field applied, that radially confines the trapped ions which rotate around the magnetic field lines present, as illustrated in figure 3.2.

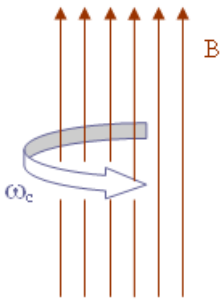

Figure 3.2: An illustration showing the precession of the ions around the magnetic field lines with frequency ω_c.

By applying an electrostatic quadrupole potential,

$$V = \frac{V_0}{2d^2}(z^2 - \frac{r^2}{2}), \tag{3.3}$$

across the electrodes (i.e. for trapping positive ions a positive potential is applied to the end caps relative to the ring) a saddle point is produced at the centre of the trap which provides axial confinement. Here d is the characteristic trap dimension given by,

$$d^2 = \frac{r_0^2}{2} + z_0^2. \tag{3.4}$$

The applied electric field causes an oscillation in the axial direction of the trap which is independent of the magnetic field applied and behaves according to simple harmonic motion. The axial bounce frequency is given by,

$$\omega_z = \left(\frac{qV_0}{md^2}\right)^{\frac{1}{2}}. \tag{3.5}$$

The forces produced in the $\mathbf{E} \times \mathbf{B}$ interaction of the trap induce an additional oscillation, namely magnetron motion and causes the cyclotron motion to be modified. The angular frequencies of these two radial motions are given by the following equation:

$$\omega_{\pm} = \frac{1}{2}(\omega_c \pm (\omega_c^2 - 2\omega_z^2)^{\frac{1}{2}}), \tag{3.6}$$

where the magnetron motion, $\omega_m = \omega_-$, and ω_+ is the reduced cyclotron motion. The magnetron motion can also be written as,

$$\omega_m = \frac{\omega_z^2}{2\omega_c}. \tag{3.7}$$

It should be noted here that this is a leading order approximation for $\omega_z \ll \omega_c$. The three types of motion experienced by a light, low q, particle in a Penning trap, are illustrated in figure 3.3, where in general $\omega_c \gg \omega_z \gg \omega_m$.

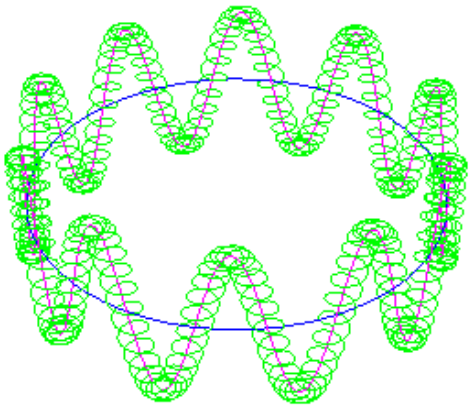

Figure 3.3: The three types of motion, axial (seen here in pink), cyclotron (green) and magnetron (blue), experienced by a charged particle in an ideal Penning trap.

The cylindrical Penning trap is an array of cylindrical electrodes electrically isolated from oneanother. In a trap of this type charged particles can both enter and exit the trap if allowed by the potentials on the initial and final electrodes. This makes a trap of this type considerably more convenient for loading "rare" particles, such as e^+ and $\overline{p}$.

Hans Dehmelt recieved the Nobel Prize in physics in 1989 for his efforts in ion trapping. Although it was a joint prize, with W. Paul (the inventor of the Paul radio-frequency trap), the construction of the Penning trap opened up a whole new field in physics.

3.2 Positron Accumulation

In order for efficient trapping to occur the particles must quickly lose energy upon entering the trap. This is done through the use of a buffer gas, namely nitrogen. The routes of energy loss available to a positron interacting with a nitrogen molecule are as follows: ionisation, electronic excitation, vibrational excitation, rotational excitation and momentum transfer. All these mechanisms (with the exception of momentum transfer) have an energy threshold, with the dominant process being that of electronic excitation.

In 1992, Murphy and Surko [42], investigated inelastic collisions of positrons with nitrogen molecules. Positrons from a ^{22}Na radioactive source were moderated with a 1 μm single crystal tungsten foil moderator and subsequently trapped and stored in an accumulator. They found that three processes were in competition. Positrons with energy less than 8 eV were unable to lose sufficient energy and hence could not be captured. In this case the energy loss mechanisms were that of rotational and vibrational excitation, as follows:

$$e^+_{(<8eV)} + N_2 \rightarrow e^+ + N_2^{rot/vib}. \tag{3.8}$$

The threshold for positronium formation occurs around 8.8 eV the mechanism is shown in equation 3.9. Murphy and Surko found that for e^+ with kinetic energy above 11 eV, the number of particles lost to positronium formation was equivalent to those trapped through electronic excitation,

$$e^+_{(>8.8eV)} + N_2 \rightarrow Ps + N_2^+. \tag{3.9}$$

This meant that an energy window of ~ 3 eV existed within which efficient energy loss could occur, equation 3.10, to promote trapping of the antiparticle,

$$e^{+}_{(8-11eV)} + N_2 \rightarrow e^{+} + N_2^{*}. \tag{3.10}$$

The positron accumulator (see figure 3.4), consists of cylindrical electrodes which increase in diameter over the length of the trap. Three different diameters are used across an array of eight electrodes making this trap a 3-stage accumulator. Nitrogen gas is introduced into the first stage of the positron accumulator as a buffer gas. The three 'tubes' behave as pumping restrictions and when pumped from both sides, three distinct nitrogen pressure regions are produced.

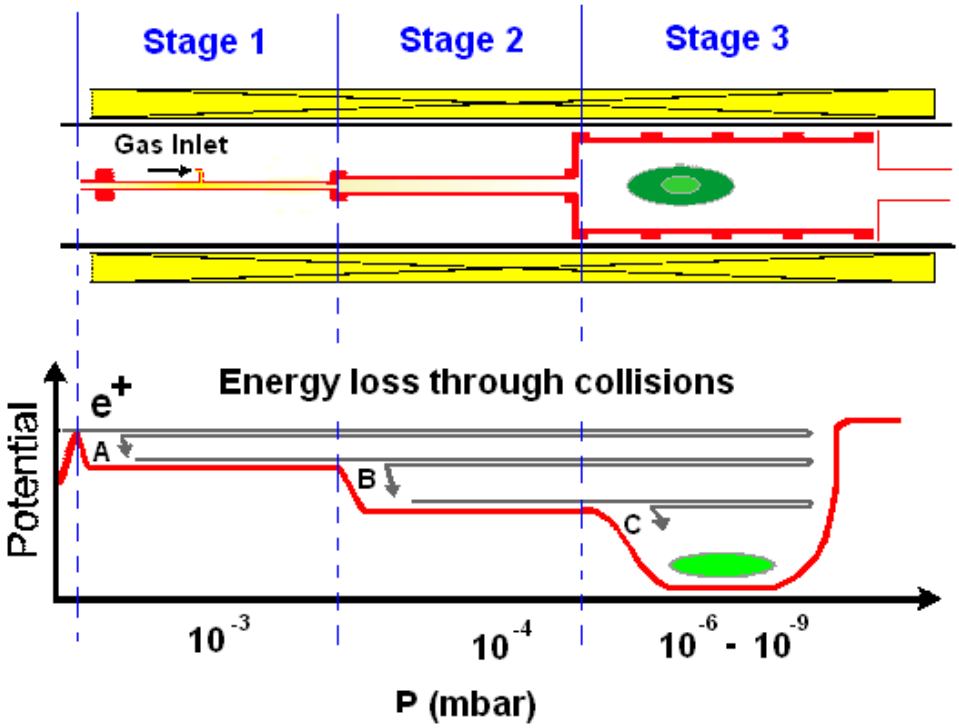

Figure 3.4: An illustration of the positron accumulator used in the ALPHA experiment, showing the electrode configuration of the trap and a representation of the trapping scheme. The nitrogen buffer gas is inserted in the centre of electrode 2. A, B and C represent interactions with nitrogen molecules which involve electronic excitation of the molecule.

As shown in figure 3.4, moderated positrons with kinetic energies in the tens of eV range enter the trap and subsequently lose energy. The dominant loss process is that of excitation of the nitrogen molecules, however positronium formation

and direct annihilation[1] of the positrons can occur. Almost all of the positrons will collide with a nitrogen molecule as they pass through stage 1 of the trap with a large ($\sim$ 40 %) fraction losing around 9 eV in the interaction (point A on figure 3.4). The energy loss causes the positron to become trapped within the accumulator where it experiences a second collision (B) causing it to become trapped in stages 2 and 3. An additional collision (C) causes it to become trapped in the third stage where it cools to room temperature. Electrode 7 of the trap acts as a gate and is set at a higher potential than the initial kinetic energy of the positron, which is now trapped. The process of loading the trap continues until sufficient particles have been captured and a plasma/cloud can be formed. At this point the gate electrode potential is dropped ejecting the positron cloud/plasma from the trap.

In 2006, Swansea University pioneered a novel, two-stage, version of the positron accumulator [43]. It consists of two stages instead of the regular three and is capable of operating at 10 Hz, producing a cloud of the order of 10^5 positrons. The operation of the two-stage accumulator is more-or-less identical to that of the three-stage system however, there are only two pressure regions, as shown schematically in figure 3.5. The two stages of the Swansea accumulator are constructed of more electrodes with 15 in the first stage and 5 in the second. Essentially a three stage potential configuration can be established over the two regions, which can be seen in figure 3.5. The Swansea accumulator also uses nitrogen as a buffer gas, which is injected into the system through a hole in electrode 8, which is at the centre of the first stage. More detail on the Swansea accumulator can be found in section 4.3.1.2 and references [43, 44].

The accumulation rate, R, can be determined via,

$$R = I_0 \epsilon, \tag{3.11}$$

where I_0 is the intensity of the incoming beam and ϵ is the trapping efficiency in the first stage of the accumulator given by:

$$\epsilon = f(1 - e^{-DP}). \tag{3.12}$$

[1]This is negligible in comparison to positronium formation and electronic excitation.

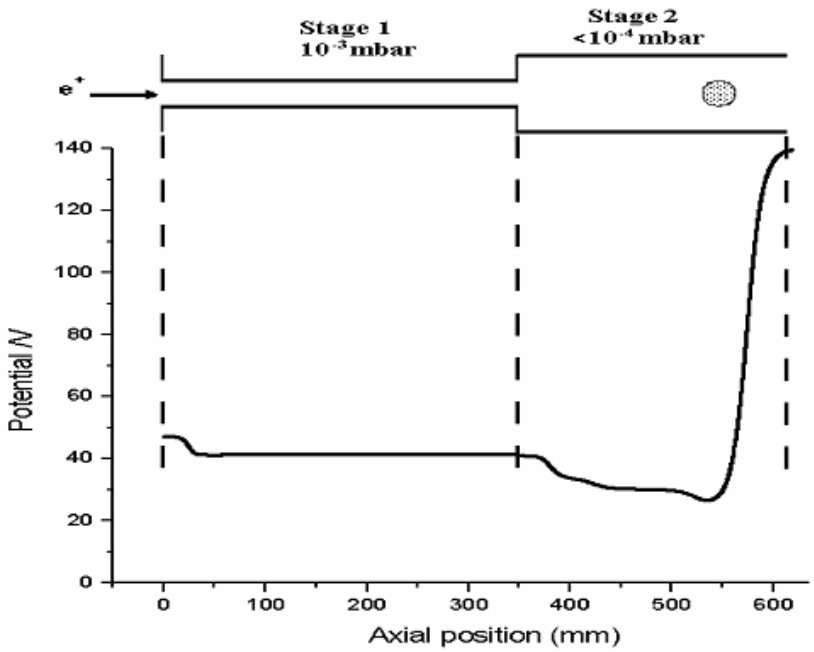

Figure 3.5: An example of of trapping potentials that can be applied to the electrodes to produce the well used to trap the positrons [43]. The two stages of the accumulator are shown along with an indication of the pressure in each stage.

Here P is the average nitrogen gas pressure in the first stage, D is a constant proportional to the total scattering cross section for positron-nitrogen interactions and f is a branching ratio determined by the ratio of the cross sections for electronic excitation and positronium formation.

The lifetime, τ, of the particles accumulated in the trap is governed by the pressure of the nitrogen gas present, as this is maintained at a certain value, the lifetime can be assumed to be a constant. The annihilation rate, λ_{ann}, with respect to the gas pressure is inversely proportional to the lifetime with $\lambda_{ann} = 1/\tau$. It can therefore be seen that the number of e^+ lost is proportional to the number of particles in the trap at any given time, leading to

$$\frac{dN(t)}{dt} = R - \lambda_{ann} N, \tag{3.13}$$

where $N(t)$ is the number of particles in the trap at time t. Integrating both sides

and rearranging for $N(t)$, equation 3.13 can be solved to give:

$$N(t) = \frac{R}{\lambda_{ann}}(1 - e^{-\lambda_{ann}t}). \tag{3.14}$$

As $t \to \infty$, a saturation value, $N(\infty)$, is achieved. At this point $dN/dt = 0$ and $N(\infty) = R/\lambda_{ann}$. From this equation, 3.14 can be written as:

$$N(t) = N(\infty)(1 - e^{\frac{-t}{\tau}}). \tag{3.15}$$

3.3 Non-Neutral Plasmas

As mentioned in section 3.2, large numbers of positrons can be trapped through the use of a positron accumulator. When the number of trapped particles, per unit volume, becomes sufficiently large a so-called non-neutral plasma is formed. A plasma is characterised according to the Debye screening length, λ_D, which must be much smaller than any of the dimensions of the positron cloud. The Debye length given by,

$$\lambda_D = \left(\frac{k_B T_e \epsilon_0}{n_e e^2}\right)^{\frac{1}{2}}. \tag{3.16}$$

Here e is the charge of an electron, k_B is Boltzmann' s constant, n_e is the positron density, ϵ_0 is the permitivity of free space and T_e is the temperature of the particles.

The Debye screening length is the distance over which the particles at the plasma edge shield the external electric fields. The particles in the plasma are close enough together that they influence each other and can behave as a single body, which reacts collectively to electric and magnetic fields. A self-generated radial electric field is produced inside the plasma, which in the presence of a **B** field causes a natural drift in the plasma whose frequency is given by,

$$f = \frac{n_e e}{2\pi\epsilon_0 \mathrm{B}}. \tag{3.17}$$

In 1959, Trivelpiece and Gould investigated the modes which exist in plasmas

[45]. They discovered that space-charge waves exist in stationary plasmas in the prescence of a magnetic field. While their work focussed on the modes of the electron component of a neutral plasma, similar modes exist in a non-neutral plasmas with the main difference being the existence of a Doppler-shift in the mode frequencies. A more detailled discussion of these modes can be found in [45]. Exploitation of modes such as these allow for plasma manipulation, e.g. the use of a rotating wall technique for plasma compression, described in more detail in section 3.4, and plasma diagnostics [46].

3.4 The Rotating Wall Technique

Accumulated positrons, to produce either a cloud or a plasma, have a finite lifetime, which limits the overall number that can be held. In an ideal accumulator the lifetime should be determined by the annihilation rate on the gas, λ_{ann}, only. However, this is often not the case, due to electric and magnetic field asymmetries in the trap and the presence of background gases (which cause a collision-induced drift) in the system. These asymmetries cause a radial drift which, if it becomes sufficiently large, can cause the positrons to annihilate on the trapping electrodes, resulting in loss of particles and a decreased lifetime [47].

Research into methods of counteracting the radial drift began with efforts initially focused on producing a steady state plasma. One such investigation was reported by Heinzen *et al.* [48] in 1991. Here energy was imparted to a $^{9}Be^{+}$ non-neutral plasma, contained in a cylindrical Penning trap, through the use of a laser beam. The additional energy introduced a torque to the plasma causing the angular momentum of the plasma to change. Cooling lasers were employed to maintain thermal equilibrium, by counteracting the energy introduced by the torque-inducing laser. Using this method the rotation rate of the plasma could be controlled. This technique has also since been used to compress plasmas resulting in an increase in particle density and lifetime.

Sideband cooling has also been shown to be successful at counteracting the drag on particles held in a harmonic Penning trap [49]. In this case an oscillating electric field is applied to a cloud of particles causing the magnetron and axial bounce motions of the particles to become coupled. Resistive cooling of the

bounce motion in turn cools the magnetron motion resulting in radial compression. This method has been employed to compress electron clouds, of the order of $10^3 - 10^4$ particles, but is ineffective on large plasmas as both the magnetron and bounce motions are dominated by space-charge effects.

In 1997, Huang *et al.* [50], developed a technique using a rotating electric field to balance the radial drift in a Mg^+ plasma. An eight segmented cylindrical electrode was used to drive a rotation in the electric field (in the direction of the natural plasma rotation). The drive frequency was tailored to balance the radial drift creating a steady state or, in certain conditions, to compress the plasma. They reported that using this method the plasma could be confined in a steady state for very long time periods (of the order of weeks) or that up to 20 % compression of the plasma could be achieved. Using the rotating wall for compression did however introduce a heating element to the plasma, which can result in loss of plasma equilibrium (between the plasma and the field). The compression of the plasma was therefore limited by the heating component.

Experiments conducted with electron plasmas [51], showed that the heating caused by the drive could be suppressed by the use of a superconducting magnet. In 1998, Anderegg *et al.*, confined 3×10^9 electrons in a 4 T field with the application of a rotating electric field. In this case the strength of the magnetic field permitted the particles to cool through emission of cyclotron radiation allowing for increased compression. This method of cooling is not however always possible as in some cases the high B-fields can be detrimental to the experiment being conducted.

In 2000, Hollmann *et al.* [52], confined a plasma of 3×10^9 electrons over a period of weeks through the use of a rotating wall electrode. They determined that the rotating wall transferred a torque to the plasma which excited the aforementioned Trivelpiece-Gould modes (see section 3.3). They reported that if the modes rotated faster than the natural rotation of the plasma then the background drag could be counteracted and radial compression could occur, however if the modes rotated slower, then opposite was true and expansion of the plasma occurred. Later that year Greaves and Surko [53] reported the same effects in a positron plasma, declaring that a coupling of the rotating wall frequency to the Trivelpiece-Gould modes of the plasma was responsible.

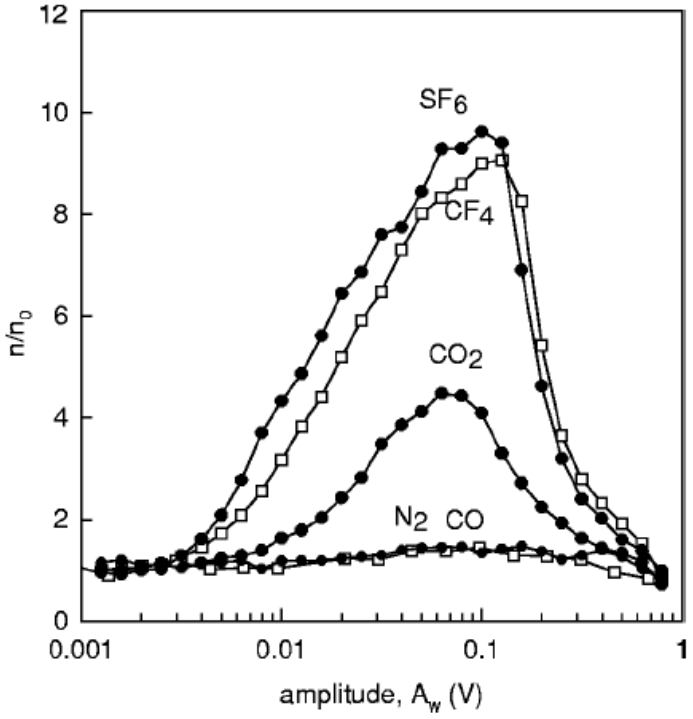

Figure 3.6: Results of compression of a positron plasma in the presence of a cooling gas from [54]. Here the rotating wall frequency has been kept constant (2.5 MHz) whereas the amplitude has been adjusted. n/n_0, is a measure of the density enhancement achieved using the rotating wall. It is clear from these data that SF_6 is the most effective cooling gas with N_2 being the least effective.

In 2001 Greaves and Surko [54] published results of an investigation using a gas additional to the buffer gas of the accumulator to act as a cooling element. In order for the gas used to be sucessful in cooling positrons, it needed to have a low annihilation cross section, a large cross section for inelastic processes i.e. vibrational and rotational excitation, and a low elastic collision cross section. The gases tested were SF_6, CF_4, CO_2, CO and N_2. The results obtained can be seen in figure 3.6, from this it is clear that SF_6 is the most effective at cooling the plasma.

Recent research, aimed at the development of a multicell trap [55], employed the rotating wall technique to compress and excite diocotron modes within an electron plasma. Electron plasmas were used for developing techniques and test-

ing purposes before attempting to trap positrons. Positrons will be accumulated and transferred into a manipulation region where a rotating wall will be applied for plasma compression. By exciting the diocotron modes the plasma can be moved off axis into one of 95 cells. Each of the cells consist of a Penning-type trap capable of holding up to 10^{10} particles. The multicell trap will allow large numbers ($\sim 10^{12}$) of positrons to be trapped inside the same vacuum and magnetic field.

Subsequent measurements by the Surko group have used a Penning-type trap to extract small (50 μm) electron beams from a plasma [56, 57]. Electrons were trapped in an accumulator where a rotating electric field is applied compressing the particles into a plasma. Radial profiles of the plasmas and extracted beams were imaged using a phosphor screen. The images showed flat topped and Gaussian profiles, similar to those presented in chapter 5. By slightly lowering the gate potential for a short amount of time (15 μs) the particles at the plasma centre can escape forming a narrow, bright beam.

While this thesis will focus on the use of the rotating wall with plasmas, it should be noted that the particle densities obtained using the Swansea accumulator are not high enough to be termed a plasma, and so the cloud produced falls under the catagory of the so-called single particle regime. More recently, Greaves and Moxom [58] have conducted research into the use of a rotating wall technique in this regime. Using this technique positron clouds were compressed with the aid of cooling gas. It is not however clear as to the mechanism causing this as no coupling to Trivelpiece-Gould modes was observed. In order to improve the understanding of this, research is currently being conducted in Swansea, into cooling gases used with a rotating wall in the single particle regime. Whilst this will not be discussed here the interested reader is directed to the thesis of Isaac [59].

Chapter 4

The Laser Ionisation of Positronium

4.1 Introduction

Resonance Ionisation Spectroscopy (RIS) is a process for ionising matter through the use of laser radiation; a process based on quantum mechanical principles. The most simple form is two photon RIS, where a laser is tuned to deliver one photon of a specific wavelength which is absorbed by the atom causing an electron to be excited from its ground state to a bound excited state. A second photon of exactly the same wavelength then ionises the atom. When the second photon is of a different wavelength to the first, the process is known as two colour RIS. By adjusting the wavelength of the second photon different energy levels can be attained by the electron. If the levels reached lie lower than vacuum, the second photon can be used to probe the high n-states of the atom, and a third photon is employed for ionisation. Due to its high efficiency and selectivity RIS is a prime candidate to investigate the energy levels of positronium.

To date, a number of measurements on the excitation of positronium have been performed. In 1982, Steven Chu and Allen Mills performed a measurement of the transition from the 1^3S_1 state to the 2^3S_1 state of Ps [60]. This was

done using Doppler-free two photon spectroscopy[1] of positronium produced from a hot copper target. In these measurements a frequency tripled, Q-switched, laser pulse from a Nd:Yttrium Al Garnet (Nd:YAG) laser produced a 100 mJ, 12 ns FWHM laser pulse at a wavelength, $\lambda = 355$ nm to pump a dye laser with an intercavity etalon amplified to give a pulse of 18 mJ with a 10 ns FWHM at $\lambda = 486$ nm. The photon flux then ionises the atom from the 2^3S_1 state in ~ 1 ns. The positrons from the ionisation are then separated from positive ions produced from the target and accelerated towards a multi-channel plate detector (MCP) for detection. This research was continued by Chu and Mills using a different experimental set-up which they published in 1984 [61]. In this case the pump laser was a XeCl excimer laser pumping a C.W. ring dye laser amplified by a 4 stage single pass amplifier to produce a 20-25 mJ, 10 ns laser pulse. The use of a C.W. laser instead of a pulsed system allowed the measurement to be made with greater accuracy, as longer interaction times could be used. Again the positrons from the ionisation were accelerated onto an MCP. Subsequent measurements [62, 63], have allowed the accuracy of the 1^3S_1 - 2^3S_1 transition to be determined to be a factor of 3.3 smaller than the 1984 measurement, in these instances the experimental arrangement was as in the 1984 case but the ionised positrons were detected using a channel electron multiplier (CEM).

In 1990 Ziock *et al.* sucessfully observed the optical saturation of the 1^3S to the 2^3P transition in positronium [64]. By bombarding a clean copper target heated to 1000 K with positrons, positronium was produced which drifted back out of the sample to the laser interaction region. Laser pulses of $\lambda = 485.9$ nm and bandwidth 0.4 nm were produced from an excimer pumped dye laser. By doubling the frequency of the laser pulses, UV radiation of wavelength of 242.953 nm (in air) was produced and passed directly in front of the copper target. The UV pulse interacted with the Ps cloud, optically saturating the transition. Later that year this research was expanded to explore the resonant excitation of the high-n states ($n = 13$-19) of Ps [65]. In this case the $n = 1$ to $n = 2$ transition, described above, was used as an intermediate level where a second photon, produced by a dye laser

[1]This is a process where two photons are used to promote a transition in an atom. One of the photons is moving towards the atom whereas the other moves away. The Doppler shift of both these photons is equal in magnitude but of opposite sign, cancelling each other out, meaning, that to first order, no Doppler broadening is observed.

pumped from the same excimer laser, performed the transition from $n = 2$ to $n = 13-19$. The second dye laser could be tuned to match a specific transition and had a bandwidth of 0.4 nm. A broadband pulse was chosen specifically to maximise the overlap with the Doppler profile of the Ps. Two transitions in particular were focused on, $n = 2$ to $n = 14$ and $n = 2$ to $n = 15$, where wavelengths of 744.094 nm and 741.993 nm respectively were required. By monitoring the annihilations of the Ps they were able to confirm the resonant ionisation of the high-n states.

More recently, Cassidy *et al.* [66] performed a similar measurement. Positrons were produced from a radioactive source and accumulated using a two-stage accumulator similar to that used in this research see section 4.3.1.2. These positrons were dumped into a third, high vacuum, accumulation region capable of producing positron plasmas containing 1×10^8 positrons, however the plasmas used in this research only contained 2×10^7 particles. The plasmas produced were implanted into a porous silica target at various implantation energies and formed Ps. The positronium drifted back out of the silica where it interacted with a laser pulse. A Nd:YAG laser was used that could emit fundamental radiation as well as the second and third harmonics. The green laser pulse ($\lambda = 532$ nm) pumped a dye laser to produce radiation of $\lambda = 772$ nm, which was later combined with the 355 nm pulse to produce a UV laser pulse of $\lambda = 243$ nm. The interaction of the Ps cloud with the UV radiation caused the Ps to be excited from the ground state into the $n = 2$ state. The transition was detected through the use of a Single Shot Positron Annihilation Lifetime Spectroscopy (SSPALS) technique. The eventual goal in this case was not the ionisation of Ps but to use it as an initial step towards performing spectroscopy of molecular positronium or Ps_2, a four-particle matter-antimatter system first discovered by Cassidy and mills in 2007 [67].

It has long been a goal of researchers in Swansea to exploit laser spectroscopy to investigate the energy levels of positronium. A laser system was purpose-built to be tunable allowing pulses with wavelengths from 243 nm to 1055 nm to be obtained. The available excitation schemes of positronium can be seen in figure 4.1.

As shown in figure 4.1, there are two possible methods for ionising the positro-

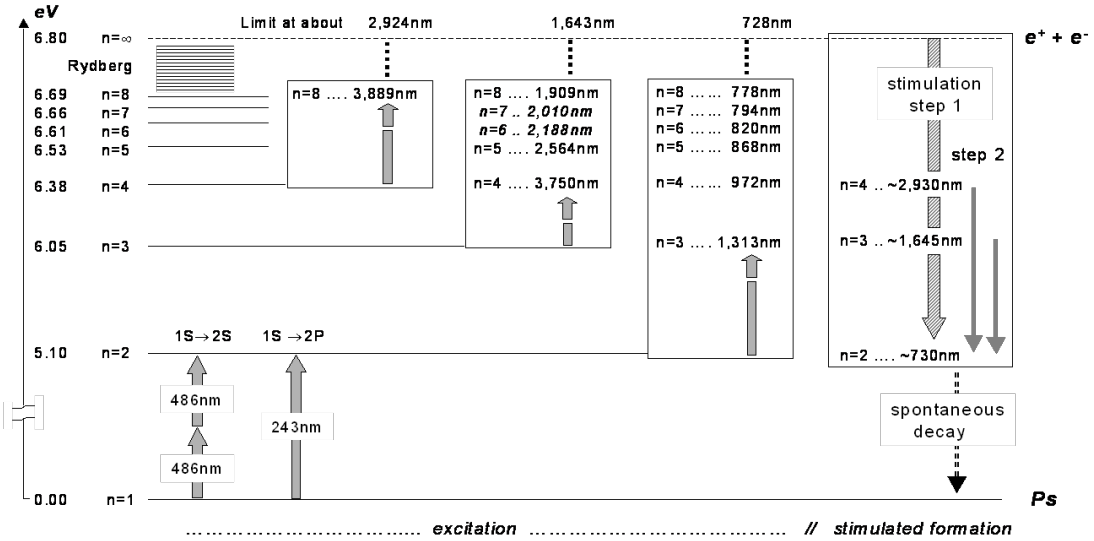

Figure 4.1: Avaliable laser excitation schemes for positronium, produced for the original research proposal [68].

nium. The first is two-step, one colour, RIS where two photons of 243 nm are used. The first photon causes the transition of the positronium from the 1S to the 2P state, where the second photon can then further photoionise the positronium. This scenario was attempted as part of the research of Griffiths [69], however the measurements proved unsuccessful. It was thought at the time that the reason for this was one of two things; (i) the overall laser excitation/ionisation probability was insufficient, or (ii) the overlap between the laser pulse and the positronium cloud was not correct. Subsequently the experiment was changed to a scheme of two colour ionisation. In this scenario the positronium would be excited from the 1S to the 2P state using one photon of wavelength 243 nm and from there a second photon of 728 nm could excite it further. More information regarding these preliminary measurements can be found in the thesis of Griffiths [69].

The positronium used in this research is produced via bombarding a porous silica target with a cloud of positrons from a positron accumulator (see chapter 3). More information regarding the positron apparatus can be found in the following sections. A mini-trap assembly system outlined in section 4.3.2 is used to trap the ionised positrons before they are re-dumped on the target plate where they annihilate. Gamma rays given off in the annihilation are then detected by two

CsI detectors.

The motivation of this research was to master techniques to produce Rydberg positronium as a method of producing antihydrogen. In 1990, Charlton published an article that discussed antihydrogen production by combining excited state positronium with a $\overline{\mathrm{p}}$ beam [70]. Here charge exchange would occur in the collision of the Ps^* with the anitproton as can be seen in reaction 4.1,

$$\mathrm{Ps}^* + \overline{\mathrm{p}} \rightarrow \overline{\mathrm{H}}^* + \mathrm{e}^-, \tag{4.1}$$

where * denotes an excited state. The above paper proposed that the probability of this reaction occurring would be greatest if the velocities of the $\overline{\mathrm{p}}$ and e^+ in the Ps atom were matched, and that the $\overline{\mathrm{H}}^*$ formation cross section has a classical scaling of n_{Ps}^4, where n_{Ps} is the principal quantum number of the positronium. Another advantage of using Ps^* is that the annihilation lifetime of the excited states is longer than its ground state. The experimental considerations regarding antihydrogen formation, as described by reaction 4.1, have been presented in [71]. This method for $\overline{\mathrm{H}}$ production has been favoured by the AeGis (Antimatter experiment:Gravity, Interferometry, Spectroscopy) experiment, currently being established in CERN, which aims to measure the earths gravitational acceleration on a cold, collimated $\overline{\mathrm{H}}$ beam [72, 73]. This chapter will outline the apparatus used for this research, initial measurements made and the current status of the experiment.

4.2 Positronium Formation

Positronium can be formed in many ways the most common being through the interaction of a positron with an atom or molecule in the gaseous state, i.e.

$$e^+ + X \rightarrow Ps + X^+. \tag{4.2}$$

In this case the positronium formation threshold is

$$E_{Ps} = E_i - \frac{6.8}{n_{Ps}^2}\mathrm{eV}. \tag{4.3}$$

Here E_i is the ionisation threshold of the atom or molecule and $6.8/n_{Ps}^2$ is the binding energy of the positronium. The dominant process, in most cases, is formation into the ground state ($n_{Ps} = 1$) [13].

In the case of metals positronium cannot form in the bulk but is instead created as the positron passes through the surface of the metal. This is due to the density of the electrons at the surface being considerably lower than in the bulk. Positronium formed at the surface is then emitted into vacuum with kinetic energy $\leq -\epsilon_{Ps}$, the positronium formation potential, which can be determined via;

$$\epsilon_{Ps} = \phi_+ + \phi_- - \frac{6.8}{n_{Ps}^2}. \tag{4.4}$$

In general ϵ_{Ps} is negative, for the ground state, allowing positronium emission.

What is of more interest, for the research presented here, is the formation of positronium in an insulator. In this case, positronium can be formed not only at the surface of the insulator, but also in the bulk. Positronium formed in the bulk can diffuse to the surface and be emitted into the vacuum with kinetic energy $\leq -\phi_{Ps}$, the positronium work function determined via,

$$\phi_{Ps} = -\mu_{Ps} + E_B - \frac{6.8}{n_{Ps}^2}. \tag{4.5}$$

Here μ_{Ps} is the chemical potential of the positronium and E_B is the binding energy of the positronium in the solid. For a more detailled description of positronium formation see e.g. Schultz and Lynn [15], Charlton and Humberston [13], or Brusa and Dupasquier [74].

As previously stated the target used for positronium formation in this experiment was a porous silica target, manufactured and provided by L. Liskay and co-workers [75]. The implantation energy of positrons in such a sample is important. Liskay *et al.* reported that 40 - 50 % of the incident positrons were re-emitted as positronium, from the silica target, when implantation energies between 1 and 3 keV were used. Positronium created at the surface of a pore has a kinetic energy around 1 eV, however positronium can also be created in the bulk of the silica. The positronium formed in the bulk is also produced with an energy

of around 1 eV but loses energy in the pores. Using a time-of-flight technique, Liskay and co-workers observed that the Ps produced was emitted from the silica with energies < 100 meV, when implantatation energies greater than 1 keV were used.

4.3 Experimental Set-up

4.3.1 The Positron Beamline

The main positron beamline in Swansea is used for experiments ranging from rotating wall studies, magnetised positronium and positronium excitation. For this reason the beamline can be divided into two stages, with stage one being the positron accumulator and stage two being the high B-field and laser interation region. A schematic of the beamline (excluding the high field region which has not been used in the present work) is shown in figure 4.2. A 1.85 GBq ^{22}Na positron source is mounted on the front of a cryogenic coldhead and is cooled to a temperature of around 7 K, (see section 4.3.1.1). The positrons are moderated (see chapter 2) by a thin film of neon gas condensed onto the coldhead. The moderated positrons are steered around a 'kink', used for energy selection, in the source chamber by a series of three water cooled magnetic coils. These coils produce a field of around 30 mT (at the centre) when a current of 40 A is passed through them.

A transport solenoid, providing a magnetic field of approximately 50 mT, guides the positrons into the first cross of internal diameter 160 mm, where an electron gun is located. The positron accumulator (explained in more detail in section 4.3.1.2), is situated inside a second solenoid (also providing a field of 50 mT) connecting crosses 1 and 2. The two transport solenoids are also water cooled. A series of 9 additional coils provide the magnetic field in the crosses. These coils are supplied with currents of around 6 A, have 400 turns and produce an axial field of approximately 6 mT.

Cross 2 contains two metal plates attached to a vertical linear drive. The lower plate is solid and can be used to intercept the beam for alignment purposes. The second plate has a 1 mm hole in the centre which can be used complementary to

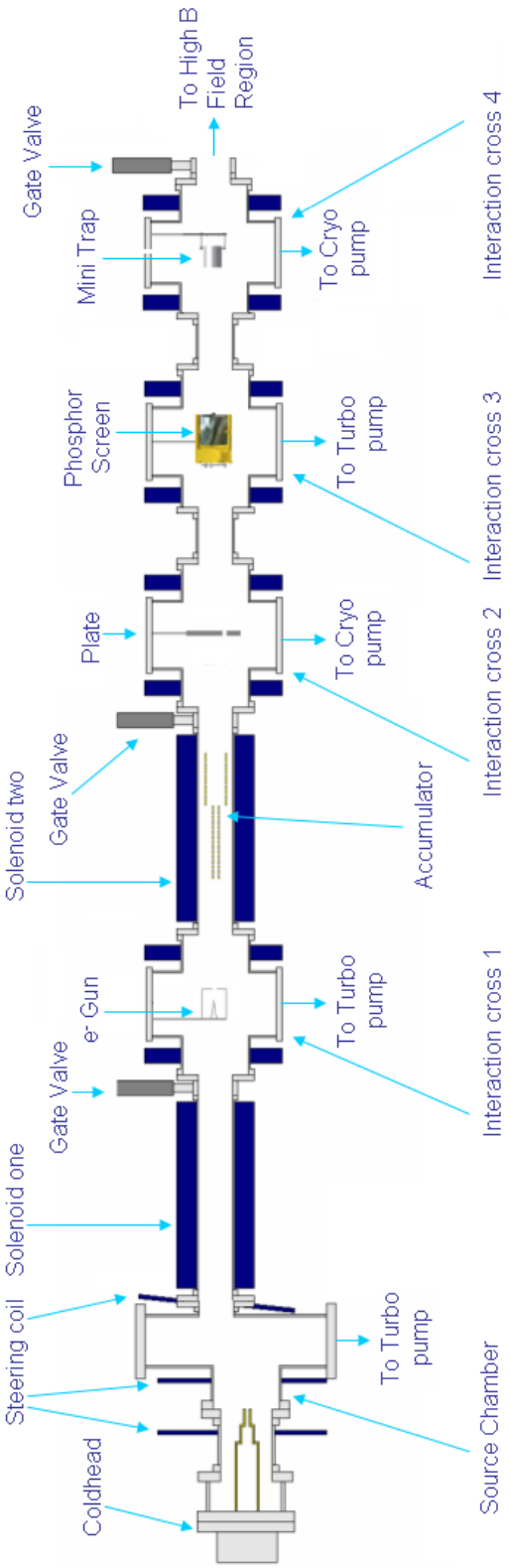

Figure 4.2: Schematic of the positron beamline used for the laser ionisation of positronium.

a phosphor screen, positioned in cross 3 (section 4.3.1.3), to measure the central density of the positron cloud produced by the accumulator.

The laser interaction cross, cross 4, was designed by Beddows for the purpose of allowing pulsed laser beams to pass through the vacuum system. The positrons are incident upon a silica target, mounted on the back plate of the mini-trap (described in section 4.3.2), and form positronium. The lasers interact with the positronium directly in front of the silica target. The mini-trap is mounted on a vertical linear drive that can be removed from the beam path to allow the second stage of the system to be used.

The second stage of the positron beamline contains an array of 35 cylindrical electrodes of 1 cm inner diameter. A cryogenically cooled 5 T superconducting magnet provides an axial magnetic field used to study positronium in high **B** fields [76]. The electrode array can also be used to investigate electron/positron plasma mixing. The electron source for this is the previously mentioned electron gun, which can also be used for testing apparatus, such as the phosphor screen. The second stage of the system was not used for any of the results presented in this thesis and therefore will not be discussed further.

The vacuum in the system is maintained by a series of magentically levitated, water-cooled turbomolecular pumps, two APD cryogenic pumps, and an ion pump. The backing line for these pumps is supplied by a series of oil-free scroll pumps and a piston pump. A schematic of the pumping system can be seen in figure 4.3. A residual gas analyser (RGA) is located inside the source chamber to test for impurities in the vacuum. The low pressures (10^{-8} mbar) of the vacuum system are monitored with Pirani gauges and full range cold-cathode gauges. A neon gas inlet line connects directly into the source chamber from a gas regulator, with the option of using a purification stage. The purification stage allows neon to pass through zeolite, an adsorbant material, cooled to liquid nitrogen temperatures. Some of the impurities in the neon are frozen onto the zeolite. A piezo-electric valve (PEV) controlled by a labview program with an integrated proportional-integral-derivative (PID) controller and pressure monitor regulates the amount of neon allowed into the chamber. The gate valve in front of cross 2 can divide the system into its two halves. A CsI detector is located at this point: positrons can annihilate on the valve (when closed) to give a count

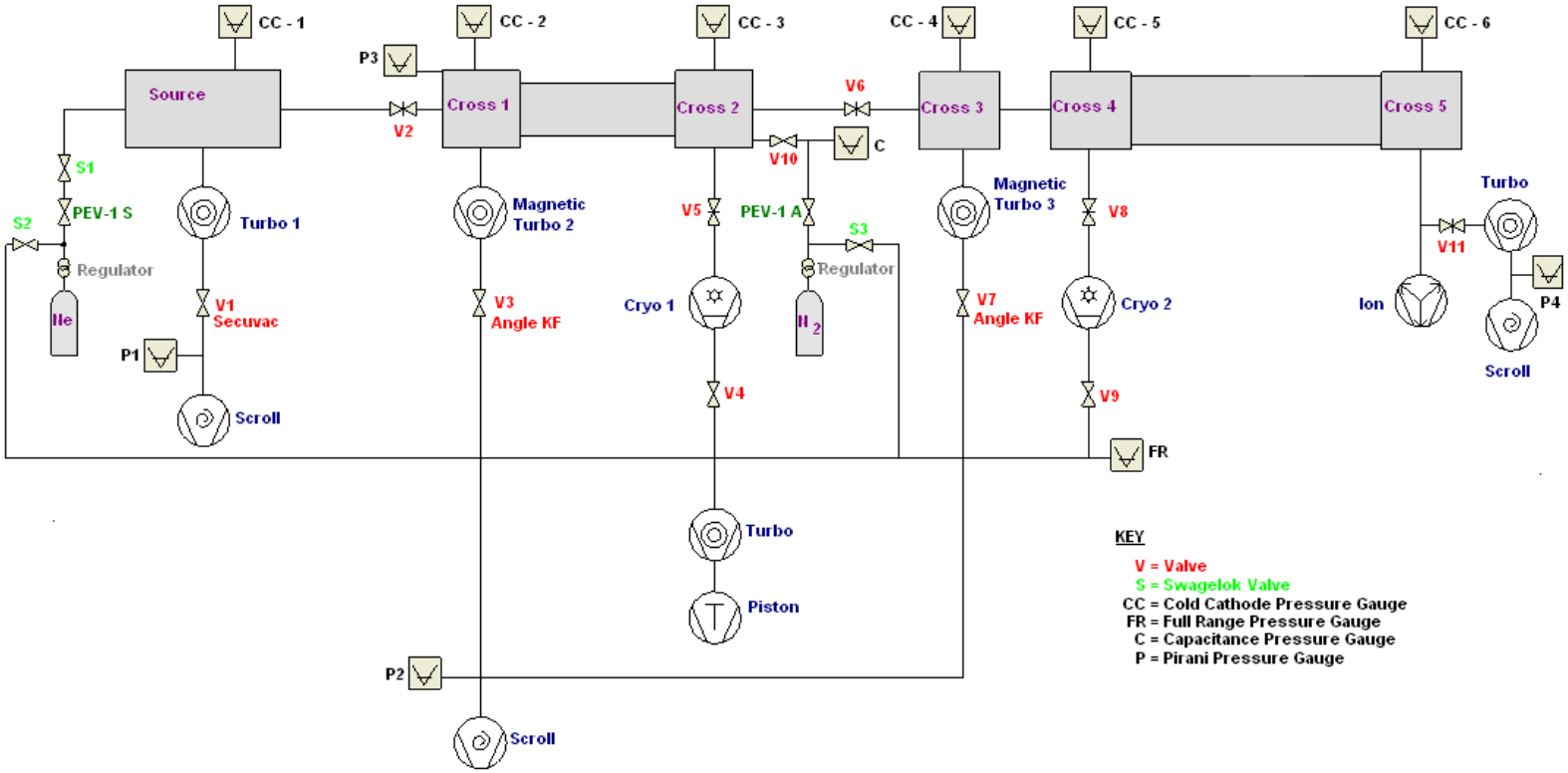

Figure 4.3: A diagram of the pumping system in use as part of the Swansea positron beamline.

rate that is monitored by a second labview program to assess moderator growth and for measurement of the beam strength.

4.3.1.1 The Coldhead and Coldhead Assembly

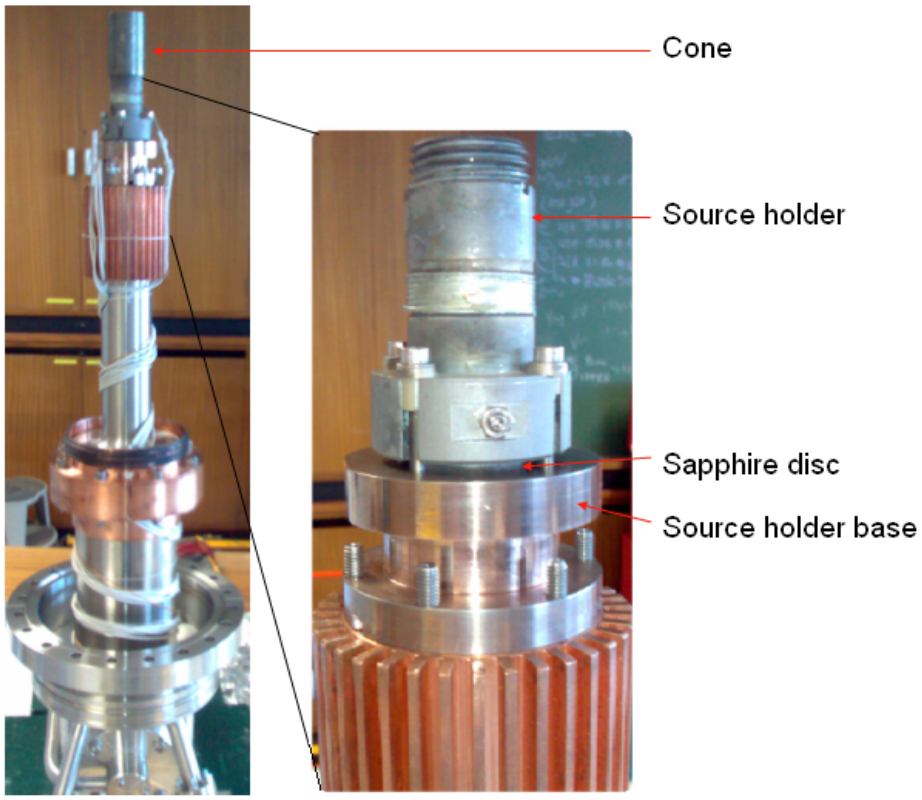

Figure 4.4: A photograph of the coldhead used in the Swansea beamline with a close up view of the coldhead assembly. The thermocouples, wires supplying power to the heater and the bias wire are clearly visible. The source is positioned on the source holder, inside the cone.

The radioactive source employed in the system is a sealed ^{22}Na source. It is mounted in a holder connected to the cold finger of a Sumitomo SRDK-408E coldhead (see figure 4.4). A cone is placed directly on top of the source to enhance the yield of moderated positrons. The cone is a piece of metal, generally copper or Elkonite, a copper tungsten alloy, that is cylindrical in shape with a central conical recess. During operation the cone is biased to +50 V. The cone is isolated,

electrically, from the coldhead itself through the use of a 2 mm thick sapphire disk of diameter 20 mm. The source holder and cone assembly are surrounded by a gold-plated copper heatshield, connected to the first stage of the coldhead. Two chromel-gold (0.07 % Iron) thermocouples are attached to the coldfinger and the base of the source holder to monitor the temperatures at the first and second stages of the coldhead. These temperature readouts are monitored by a Lakeshore 331 temperature controller. In order to allow neon to condense on the cone a temperature of around 7 K, or lower, needs to be maintained.

4.3.1.2 The 2-Stage Positron Accumulator

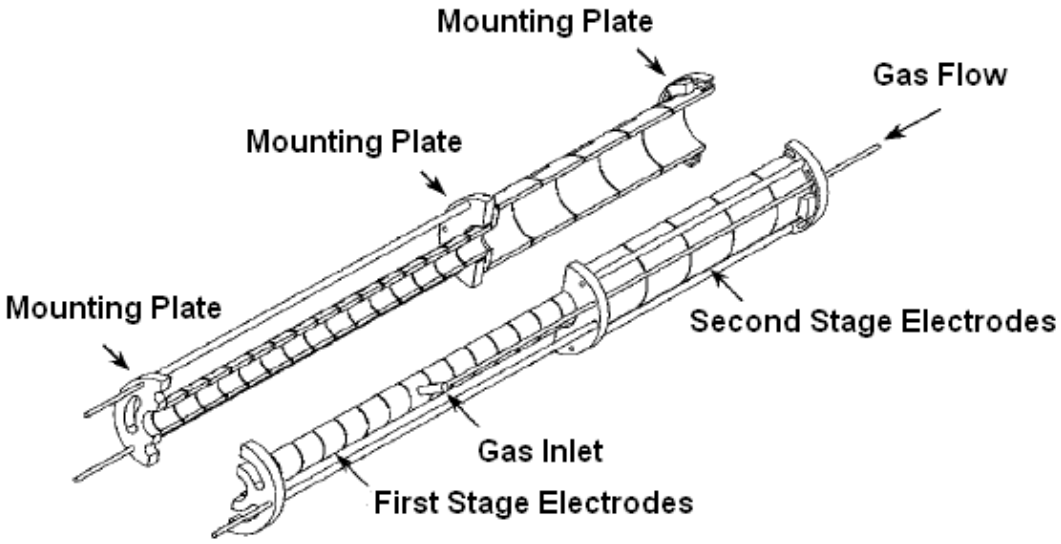

Figure 4.5: Schematic of the 2-stage positron accumulator employed for use in the Swansea beamline system (re-labelled from [43]).

The positron accumulator is a Penning-Malmberg type trap similar to that developed by Surko and co-workers [39]. It is constructed of 20 electrically isolated electrodes of varying size. The device is made up of two stages; the first stage has 15 electrodes of internal diameter 16 mm and length 24 mm. The second stage is comprised of 5 electrodes, 49 mm long and having an internal diameter of 41 mm. All the electrodes are separated by 2 mm diameter sapphire balls. A gas inlet allows nitrogen as a buffer gas to enter the trap at the centre of the first stage

(see figure 4.5). The buffer gas pressure is regulated using a PEV controlled by a PID algorithm written into a labview program. With a pump at either end of the accumulator the smaller diameter electrodes behave as a pumping restriction, meaning that there is a pressure difference between the first and second stages. Electrode four of the second stage of the trap is split into two electrodes of lengths 25 mm and 24.5 mm respectively. The first of these is divided into four equal, electrically isolated segments, which make up the rotating wall electrode. The potentials on the electrodes are controlled via a series of labview programs, allowing different routines to be run which can be tailored to the experiment being conducted. The most common of these is the trap and dump cycle which will be discussed later. Positrons in the trap can then be held and manipulated using the rotating wall technique (see section 3.4) before being dumped out of the trap. This system operates at 10 Hz (to coincide with the laser capabilities) and typically produces clouds[2] of 10^5 positrons.

4.3.1.3 The Phosphor Screen

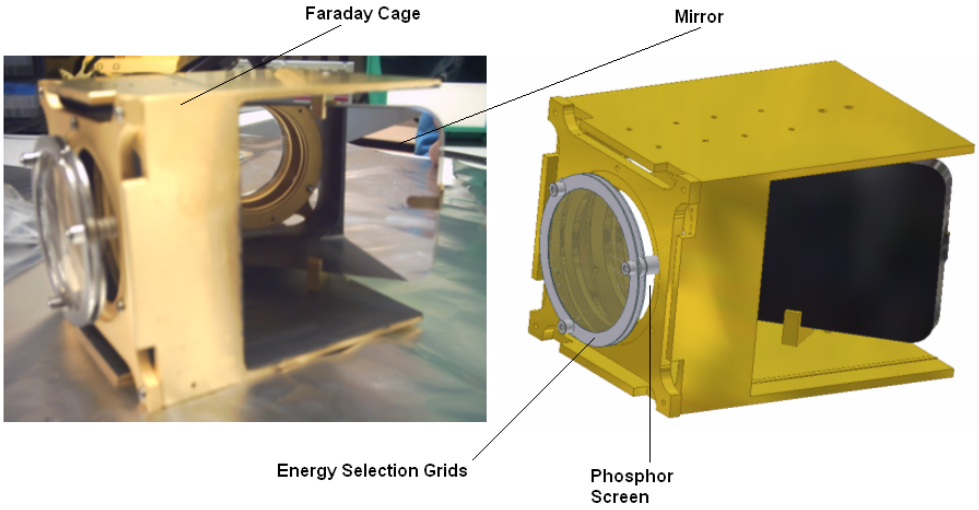

Figure 4.6: The phosphor screen assembly.

An image of the accumulated positron cloud can be taken using a phosphor

[2]The term cloud is used when there is an insufficient number of particles contained in a given volume to form a plasma, as in the case of the Swansea positron accumulator.

screen assembly system, (see figure 4.6). The phosphor screen assembly consists of two electrically isolated grids, a phosphor screen and a mirror, all mounted onto a gold plated Faraday cage. A layer of P43 phosphor deposited on a glass substrate makes up the phosphor screen, as shown in figure 4.7.

Type P43 phosphor is a gadolinium, oxygen and sulphur composite doped with terbium (GdO_2S:Tb). It emits light in the range of 360-680 nm with the maximum being typically at 545 nm, which corresponds to visible green light. The light intensity decays from 100 - 1 % in around 3 ms. It is mounted just inside the Faraday cage, where a potential of -7 kV (or $+7$ kV for imaging electrons) can be applied. The chromium ring and indium tin oxide layer seen in figure 4.7 provide a conducting base.

The first grid acts as a shield to mask the high potential on the screen whereas the second grid can be used for energy selection. Both grids were grounded for all measurements outlined in this thesis. The applied potential accelerates the cloud or plasma towards the screen where the impact of the particles causes the screen to fluoresce. A CCD camera, positioned outside the vacuum system, takes a photograph from the reflection of the mirror mounted approximately 4.5 cm from the front of the Faraday cage and 45 degrees to the screen itself. The images obtained from the screen can be imported into a Labview program to establish the central density of the particles and the cloud size. The annihilations of the positrons on the screen can be used in both Swansea and ALPHA to establish the number of particles in the cloud/plasma. At present this measurement is not automated for the positronium beamline but can be measured using an oscilloscope from a signal filter box attached to the feedthrough.

4.3.2 The Mini-Trap

Positrons are ejected from the accumulator with energy around 50 eV and enter an E $\times$ B trap, the mini-trap. Potentials are applied to the trap which serve to increase the implantation energy of the positrons before bombarding a porous silica target, described in section 4.2. Here the positrons interact with surface and bulk electrons and are subsequently re-emitted into the vacuum as positronium. The mini-trap, as seen in figure 4.8, consists of a tube, a grid and an electrode

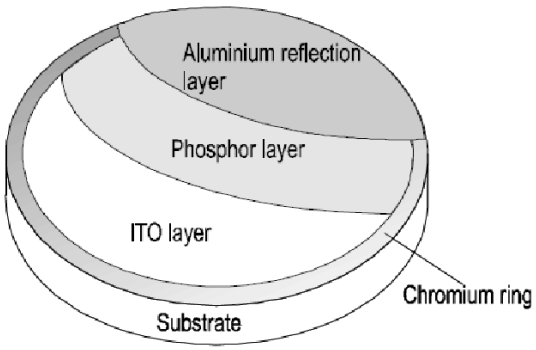

Figure 4.7: The layered structure of the phosphor screen from [77]. A layer of indium tin oxide (ITO) provides a conductive base.

all electrically isolated from each other. The porous silica target is located on a plate at the back of the mini-trap.

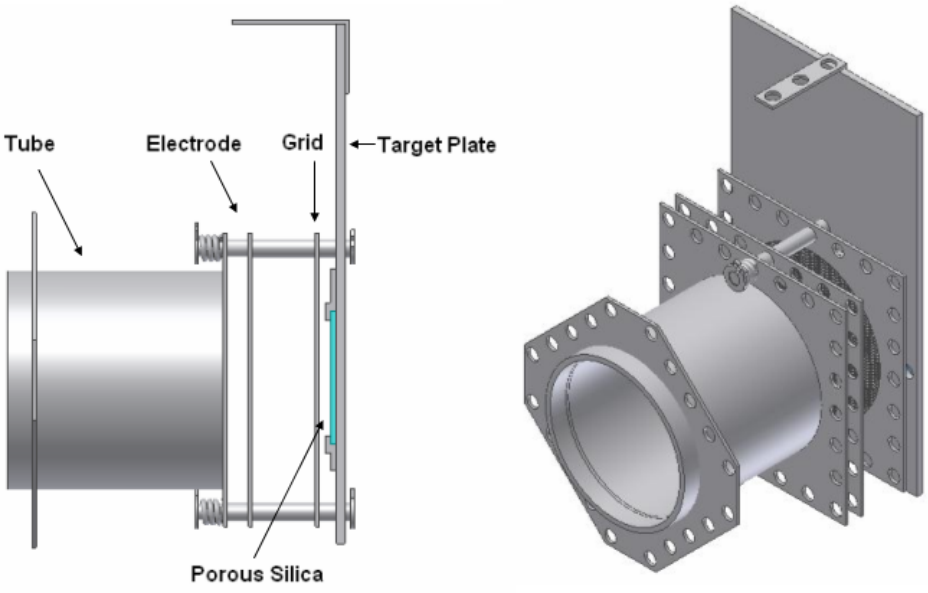

Figure 4.8: Schematic of the mini-trap showing the tube, grid, electrode, silica and target plate. Each of these were isolated from oneanother using ceramic spacers.

Directly in front of the silica target the positronium interacts with two laser pulses. The first excites the positronium from the $n = 1$ to $n = 2$ state, the second then ionises the positronium. The laser system employed for this research

is described in section 4.3.3. Potentials are applied to the mini-trap such that a small potential well of depth ~ 1 V is created between the grid and the electrode. The positronium, being of neutral charge, is not constrained by the potentials and drifts into the laser interaction region. Upon ionisation, the electrons are attracted to the electrode and lost whereas the ionised positrons become trapped within the potential well. They are then held for a short period of time (~ 1 μs) before being dumped back into the target plate, where they annihilate. The annihilation signal is detected by two CsI detectors mounted onto the back of the target plate. In order to reduce the diameter of the positron cloud two Nd permanent magnets were mounted on the back of the target plate directly behind the silica target.

4.3.3 The Laser Apparatus

The laser system was built for purpose with six lasers in total divided into two tables, as shown schematically in figure 4.9. The first is the UV table which houses two titanium sapphire (Ti:Sapp) lasers pumped by an LQ-129 Nd:YAG laser. The radiation produced from the LQ-129 is split 50:50 to the two Ti:Sapp lasers. One of these lasers is currently not employed in this scheme and so the radiation to this laser is blocked. The other laser uses the YAG radiation to pump a Ti:Sapp crystal. The radiation produced goes into a holographic selector which is controlled by a stepper motor for wavelength tuning. The pulse from the Ti:Sapp crystal is totally internally reflected by the holographic selector so that light of the correct wavelength is emitted. This radiation passes through a compensator and a doubler crystal, also controlled by stepper motors, to enter the LG-312 third harmonic generation (THG) unit. The radiation going into the LG-312 is tripled to produce light in the UV spectrum at 242.95 nm. This light is then directed using a series of optics through the laser enclosure and into the vacuum system where it can interact with the positronium to stimulate the 1S-2P transition. The 243 nm pulse has a diameter of around 2 mm, and a duration of around 13 ns, the power of the resultant pulse is 380 μJ. A second laser beam delivered by another LQ-129 Nd:YAG pulse provides a pulse of wavelength 532 nm to the positronium cloud for ionisation. The laser system can be triggered by an external TTL pulse

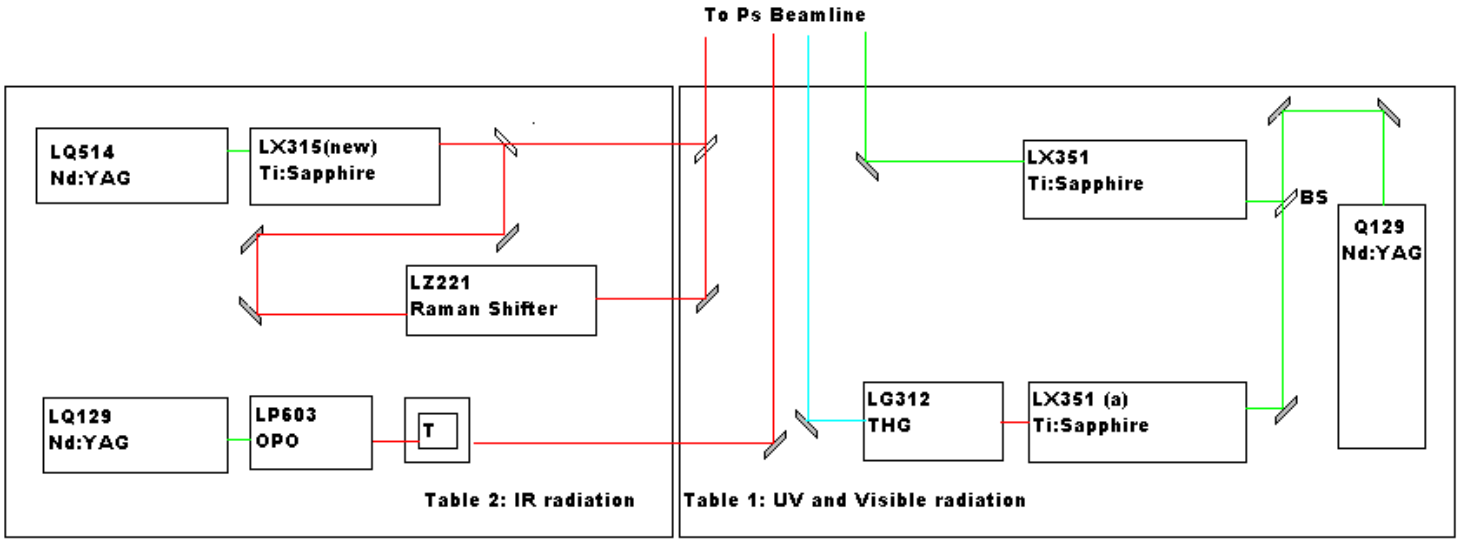

Figure 4.9: Schematic of the original laser system employed as part of the positronium measurements based in Swansea.

of 12 V delivered by a sequencer. A series of LABVIEW programs were written to control the internal motor positions and the laser triggering.

4.4 Discussion

A series of measurements were conducted in order to investigate if the equipment previously described was capable of saturating the $n = 1$ to $n = 2$ transition in positronium. Positrons were accumulated as described in section 4.3.1.2, providing a cloud of around 10^5 positrons. A series of triggers were delivered to the laser system and the accumulator. The accumulator then dumped the positron cloud into the silica target where positronium was formed. Upon recieving the trigger signals the 532 nm Nd:YAG pulse was emitted creating the 243 nm pulse via the Ti:Sapp laser and THG unit. The 532 nm and 243 nm pulses were directed through the laser enclosure and into the vacuum system in order to coincide with the positronium cloud. The resonance of the 243 nm pulse was stepped through in linewidth increments and an annihilation signal was expected to be observed from the CsI detectors.

It was thought that approximately 90 % of the positrons emitted from the accumulator would be incident upon the silica target. As the conversion efficiency of positronium formation from the incident positron cloud was measured to be around 50 % [75], the resulting positronium cloud would consist of around 4.5×10^4 ortho-positronium atoms. Calculations conducted at the time determined that approximately 30 positronium atoms would be excited from the 1S to the 2P state and that 100 % of the positronium atoms would be ionised by the 532 nm pulse. Unfortunately no annihilation signals were observed. A detailed discussion of these measurements can be found in the thesis of Watkeys [78].

It has been determined that the main cause of the null result is related to the Doppler profile of the positronium. The Doppler width, $\Delta\nu_D$, of positronium can be determined via;

$$\Delta\nu_D = \left(\frac{2.35}{\lambda}\right)\left(\frac{k_B T}{m}\right)^{1/2}, \tag{4.6}$$

where λ is the wavelength, k is Boltzmanns constant, T is the Ps temperature and m is the Ps mass. In the aforementioned measurements the Ps would have been

emitted from the silica with a kinetic energy of around 1 eV, corresponding to a temperature of ∼10000 K. Due to the high temperature and low mass of the Ps, the Doppler width is very broad. The output pulse of the Ti:Sapp laser described in section 4.3.3 has a linewidth of ∼10 GHz, thus only a very small fraction of the Ps produced would have been probed. Additionally the power of the 243 nm pulse was insufficient to saturate the 1S-2P transition. In order to overcome these issues, the laser linewidth needs to be broadened, and the temperature of the Ps decreased.

The Ps loses energy via collisions within the silica therefore, higher implantation energies are required to reduce the temperature of the emitted Ps. The current mini-trap is not suitable for the application of high voltages and so needs to be altered, additional to this the laser system had to be reconfigured. The designs for both are outlined in the following sections however, both are still in progress at the time of submission of this thesis and so no physical data can be presented.

4.4.1 The New Scheme

In order to broaden the UV pulse a new scheme of producing the UV radiation has had to be developed. The new proposal exploits frequency mixing of the three harmonics of the Nd:YAG laser, and a schematic of the proposed setup can be seen in figure 4.11. Fundamental and second harmonic radiation from an LQ-129 Nd:YAG is emitted from the laser. A beam splitting prism divides the 532 nm radiation into two pulses of equal power. One of these pulses enters an Optical Parametric Oscillator (OPO) unit where radiation of 770 nm is produced, whilst the other is recombined with the fundamental in a tripling crystal to produce pulses of the three harmonics of the laser, 1064, 532 and 355 nm. These three pulses enter a harmonic separator unit where the 1064 nm and 532 nm pulses are separated from the 3ω and dumped. The third harmonic, or 355 nm, pulse then moves into the LG-312 unit where it meets the 770 nm pulse and is combined to produce a single pulse of 243 nm. A prism is then used to separate any additional wavelengths hidden in the outgoing pulse, which are then dumped. As in the previous scheme the UV radiation is directed through the laser enclosure

and into the laser interaction region in cross 4.

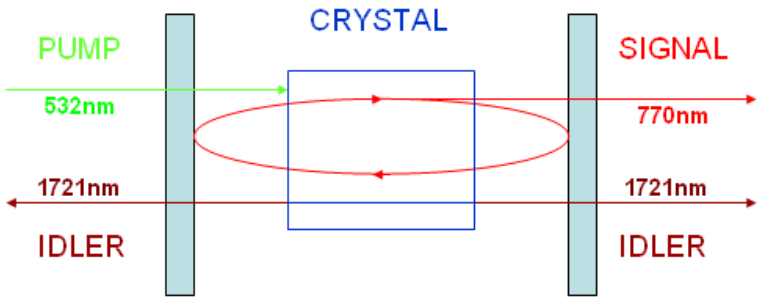

Figure 4.10: Illustration of the OPO operation, which produces the signal and idler pulses. The signal pulse is amplified in the cavity.

Using the laser system in this configuration a broader linewidth is produced and a higher pulse energy in the 243 nm radiation should be obtained. This broadening comes from the OPO unit. An OPO works through the use of a non-linear crystal, in this case a Barium Borate or BBO crystal. The pump wavelength (532 nm from the Nd:YAG laser) enters the crystal where it is converted into two, lower frequency pulses, known as the signal and idler waves. As with the Ti:Sapp laser the BBO crystal position can be controlled by stepper motors resulting in a tunable system.

The BBO crystal is placed in a cavity, such as that shown in figure 4.10, which amplifies the signal radiation so that higher intensity pulses can be produced. Estimates of the pulse energies and linewidths produced using this system can be seen in figure 4.12. The broad bandwidth of the OPO unit dominates the linewidth that is achieved using this system, also from figure 4.12, it is clearly shown that the output power is much higher.

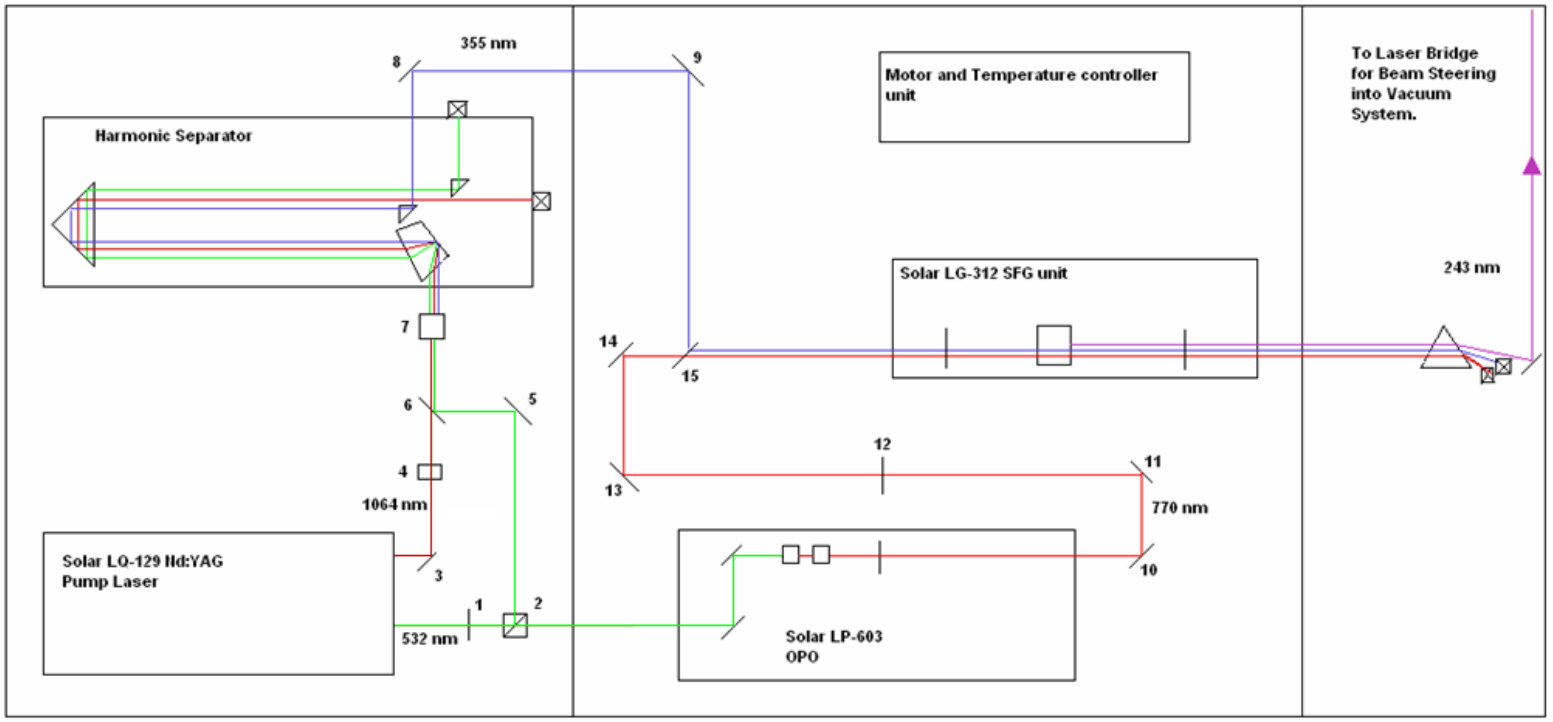

Figure 4.11: Illustration of the new laser configuration currently being constructed to perform the positronium measurements in Swansea.

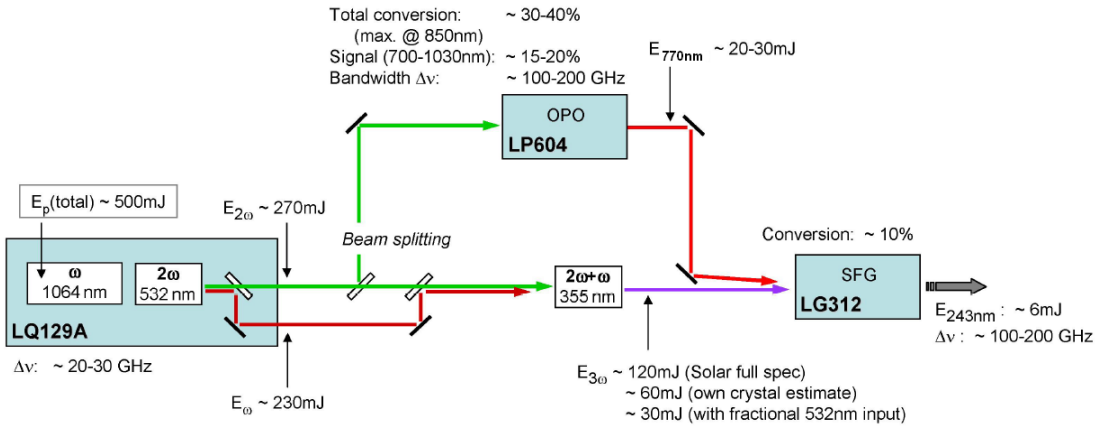

Figure 4.12: Schematic of the proposed broad band 243 nm laser pulse showing pulse energies and estimates of linewidths available.

The implantation energy of the positrons incident on the silica will be increased by biasing the target at 5 kV. It is essential that the design of the mini-trap is altered to accomodate this. There will also need to be changes to the feedthrough of the vacuum system. The proposed new mini-trap design can be seen in figure 4.13. It should also be noted that the Nd permanent magnets have been removed. The CsI detectors will still be mounted onto the back plate of the mini-trap. Additional to this the silica target will be replaced.

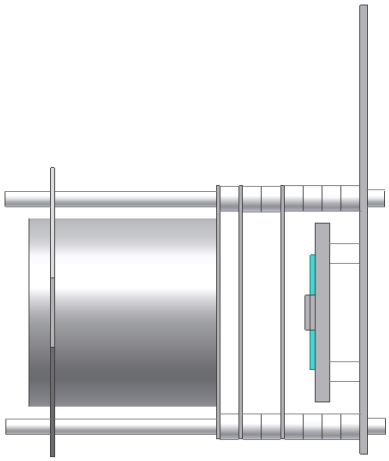

Figure 4.13: Schematic of the the proposed new design for the mini-trap showing the additional insulation around the target plate, to allow for higher voltages to be applied. The tube, grid and electrode remain unchanged from figure 4.8.

Chapter 5

Optimisation of Positron Plasmas in the ALPHA Experiment

The ALPHA positron accumulator has been employed by both the ATHENA and ALPHA collaborations. Over recent years it has needed more than routine/preventative maintainance. Some of the faults developed have proved difficult to trace and have required extended and detailed measurements. During these measurements it became clear that the coldhead used was no longer achieving its base temperature and was failing to grow efficient neon moderators. A new coldhead was purchased which required substantial modifications to the coldhead assembly and the source chamber itself. Additionally, the phosphor screen had become damaged. It is thought that this was due to sparking in the system, and some of the components including the screen itself were replaced.

During the modifications the rotating wall control system was also changed to allow a quadrupole rotating electric field to be applied to the electrodes. A cooling gas line was also incorporated. These repairs and alterations were carried out over the space of a year and due to the time invested in improving the system, and subsequent research conducted, I have been named an author on a number of ALPHA collaboration papers [79, 80, 81, 82]. While the accumulator is still not operating to full efficiency, the positron plasmas produced are improved. The following research has been motivated by an attempt to optimise the accumulator further through the addition of an extra cooling element.

5.1 Introduction

In 1959 the Proton Synchrotron (PS) was built in CERN (Conseil Européan pour la Recherche Nucléaire). At this time it was the highest energy particle accelerator in the world, operating at momenta up to 25 GeV/c. Initially it was responsible for most of CERN's particle physics experimentation but was upgraded, in 1970, with newer, higher energy, accelerators. The PS consists of 277 electromagnets with 100 dipoles which bend the beam around the ring of circumference 628 m. To date it has been used to accelerate protons, alpha particles, oxygen and sulphur nuclei, lead ions, electrons, positrons and antiprotons.

To produce antiprotons, protons accelerated by the PS ring are fired into a metal target. The collision is sufficiently energetic that it causes proton - antiproton pairs to be produced, via reaction (5.1),

$$\mathrm{p} + \mathrm{p} \rightarrow \mathrm{p} + \mathrm{p} + \mathrm{p} + \overline{\mathrm{p}}. \tag{5.1}$$

The antiprotons produced are too energetic to be used in the production of anti-atoms and they need to be slowed down. The first stage of this process is achieved using the Antiproton Decelerator or AD ring, capable of decelerating antiprotons from 3.57 GeV/c to around 100 MeV/c, which corresponds to a kinetic energy of ~ 5.3 MeV (see figure 5.1). The AD became operational in 2000, and it consists of a series of dipole and quadrupole magnets directing the antiprotons around the ring. The particles are decelerated using radio-frequency electromagnetic fields. Consequently, following Liouville's theorem, the transverse momentum becomes more important. Stochastic cooling is employed to counteract this effect. Using this process the antiprotons are decelerated from 3.57 GeV/c to 0.3 GeV/c. Electron cooling is then applied as the energy is brought down further to the range of 100 MeV/c. The deceleration and cooling cycle can be seen in figure 5.1.

The AD ring receives around 5×10^7 antiprotons and has an estimated efficiency[1] of 25 %. This means that around 1.2×10^7 are available in a 200-500 ns wide pulse. The repetition time is 100 s. Once the antiprotons are sufficiently cooled down, a kicker magnet is used to eject the particles into an extraction line

[1]Here efficiency refers to the ratio of $\overline{\mathrm{p}}$ slowed to usable energies when compared to the number of $\overline{\mathrm{p}}$ injected into the AD ring.

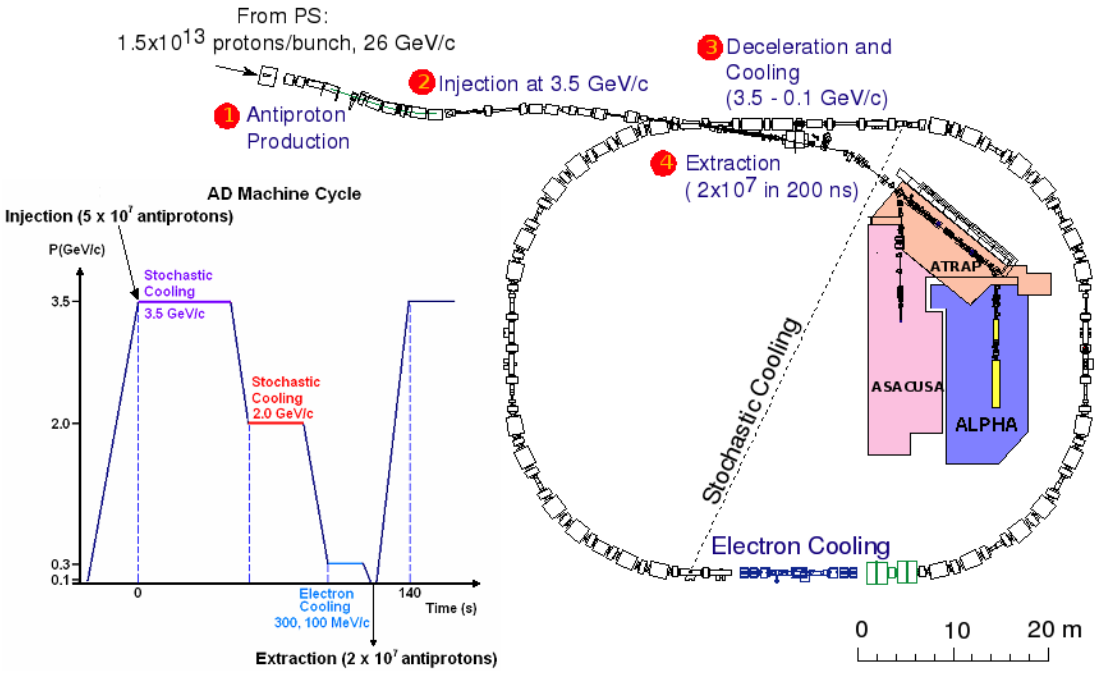

Figure 5.1: Schematic of the AD ring based at CERN, showing the AD cooling cycle.

where they are guided into one of the three main experiments currently running at the AD, namely ALPHA, ATRAP and ASACUSA.

ASACUSA (Atomic Spectroscopy And Collisions Using Slow Antiprotons) began working at the AD in 2000, prior to which it was involved taking measurements using the LEAR ring which was decommissioned in 1996. ASACUSA uses the antiprotons ejected from the AD to produce antiprotonic helium. In their experiment, the antiprotons are fired through a cloud of helium gas. A portion of them annihilate on contact with the matter in the immediate surroundings, however, some combine with the helium to produce the matter-antimatter hybrid, antiprotonic helium. Laser beams are then used to excite the atom facilitating precise measurements of the mass of the antiproton.

ATRAP (the Antihydrogen TRAP) aims to make precise laser or microwave spectroscopy measurements of antihydrogen to test CPT symmetry. Positrons are produced from a ^{22}Na source and accumulated over a 100 s cycle in a positron accumulator (see chapter 3). Ninety five electromagnets guide the accumulated

positrons down a 7 m tube, which has a sharp 105 degree decline into a vertical 1 T solenoid. Electrodes contained inside the 1 T solenoid are used to trap the positrons, where two e^+ pulses from the accumulator are stacked, producing a plasma containing $\sim 1 \times 10^7$ positrons, which subsequently cool via the emission of synchrotron radiation.

Antiprotons from the AD ring are injected into the ATRAP system via a beryllium degrader foil, where they lose energy, becoming trapped in a 10 cm long Penning trap constructed of 45 electrodes. The antiprotons lose kinetic energy via collisions with the electrons, further energy loss occurs via the emission of synchrotron cooling radiation, due to the magnetic field present. Around 30000 antiprotons are captured per AD pulse, which are stacked to produce 0.6 million particles. Antihydrogen will then be produced within an Ioffe trap through either three-body recombination in a nested trap or by laser controlled charge exchange. For more detailed information on ASACUSA and ATRAP see references [83, 84] and [85].

The ALPHA (Antihydrogen Laser PHysics Apparatus) collaboration was formed in 2005 as the successor of ATHENA, which produced cold antihydrogen in 2002 for the first time [6]. ATHENA's results were confirmed later that year by ATRAP [86, 87]. The inner part of the antihydrogen apparatus employed in the ALPHA experiment consists of an electrode array separated into three distinct trapping regions. Radial confinement is provided through the use of a 1 T superconducting solenoid, and around the catching trap an extra field of 2 T can be applied by the inner solenoid (see figure 5.2).

Antiprotons are injected into the ALPHA apparatus every 100 s, where they are further decelerated through the use of a 218 μm thick aluminium degrader foil. Only around 0.1 % of the incident antiprotons emerge from the foil with a kinetic energy suitable for trapping. Subsequently, the antiprotons enter the first trapping region, known as the 'catching' trap. The antiprotons in the trap are cooled, using electron cooling, to energies of around 5 meV, equivalent to a temperature of ~ 60 K. The temperature of the antiprotons can be further decreased through the use of evaporative cooling, achieving temperatures of around 9 K. In the catching trap, the antiprotons from a series of AD shots can be stacked, increasing the total number of antiprotons trapped for antihydrogen production.

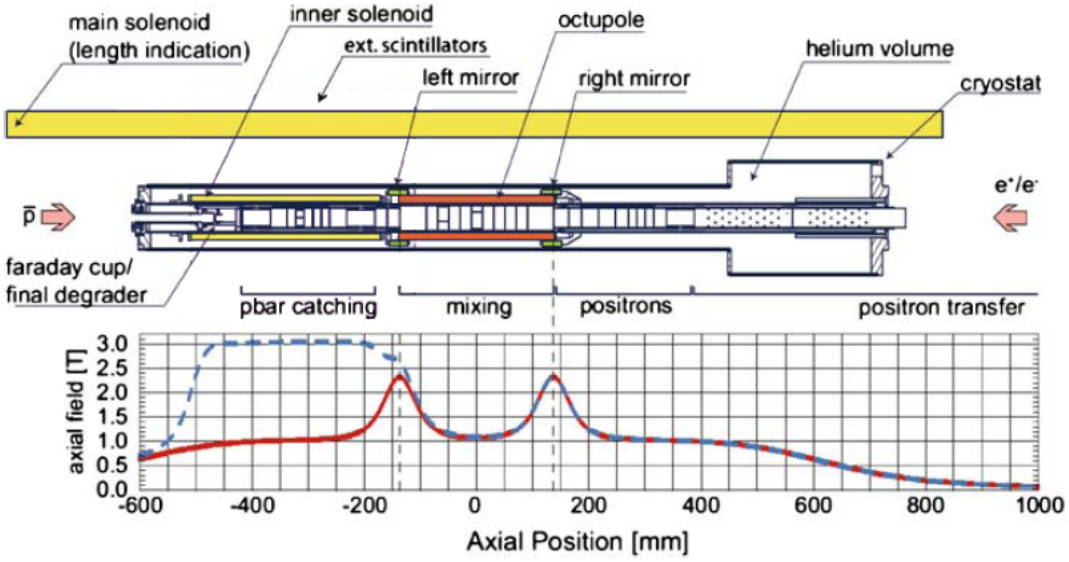

Figure 5.2: Schematic view of the ALPHA antihydrogen trap showing all three trapping regions. The graph shows the longitudinal magnetic field on axis due to the solenoids and mirror coils. The dashed curve is the field with the inner solenoid energized, whilst the solid line is that without.

Typically 2 such AD shots are currently stacked per measurement to give $\approx 2\times10^5$ $\overline{\text{p}}$s. A weak rotating wall electric field (see section 3.4) is applied to the antiprotons and cooling electrons contained in the trap. The electron plasma is slowly compressed by the rotating electric field and in turn sympathetically compresses the antiprotons to increase the antiproton density whilst decreasing the radius. This method of compressing the antiproton plasma is beneficial as the presence of the electrons provides continual sympathetic cooling. The electrons are then removed before the mixing phase. Simultaneously, positrons are trapped and accumulated using the equipment outlined in section 5.2.1.2. The accumulated positrons are held in the accumulator where a rotating wall electrode is used to compress the positrons into a small, dense plasma.

Both positrons and antiprotons are transferred into the 'mixing' trap where a nested potential well [88] is set up (see figure 5.3), allowing both particle species to be held simultaneously. The positron plasma is transferred into the central well whereas the antiprotons are moved into the side wells. The antiproton cloud is allowed to overlap with the positron plasma where they can lose energy via

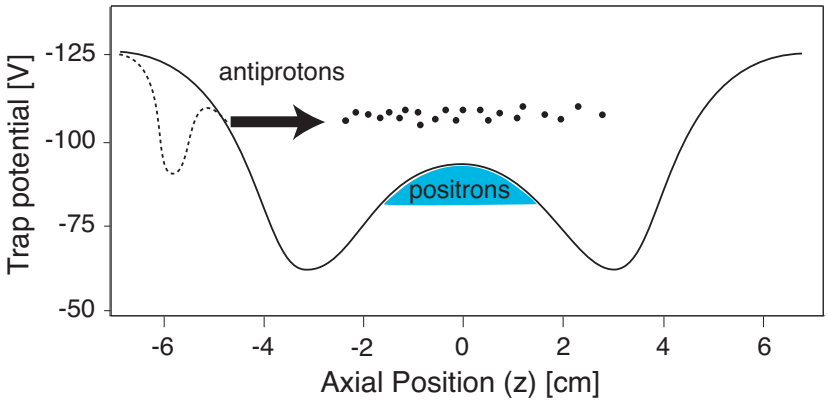

Figure 5.3: Illustration of the nested Penning trap configuration used by ATHENA and ALPHA (pre-2010) for mixing positrons and antiprotons to produce antihydrogen.

interactions with the positrons. When the energy of the antiprotons is sufficiently low, antihydrogen can be formed. In order to perform laser spectroscopy of cold antihydrogen, a future goal of the ALPHA collaboration, the $\overline{\mathrm{H}}$ atoms have to be confined. The antihydrogen formed is not constrained by the magnetic and electric fields of the Penning trap and so a neutral atom trap had to be constructed. An octupole field is superimposed upon the mixing trap (see figure 5.2) which provides radial confinement of the antiatom, whereas two mirror coils, located either side of the mixing trap, constrains the atom axially. Using a trap of this configuration a three dimensional magnetic minimum is produced within which the antihydrogen can become trapped. The well produced is around 0.5 K deep, but only a small fraction of the $\overline{\mathrm{H}}$ can be held. The magnetic field is quenched allowing any trapped antihydrogen to drift to the chamber walls where it annihilates. A specially designed detector consisting of three layers of silicon is used to detect the charged pions, given off in the annihilation. Reconstruction of the particle tracks through the detector are used to locate the annihilation vertex, and pinpoint the position of annihilation.

5.2 Experimental Set-Up

The research presented in this chapter focuses on the optimisation of positron plasmas produced using the ALPHA positron accumulator. Therefore the remainder of this chapter will be concerned exclusively with the equipment used in this investigation and results obtained.

5.2.1 The Positron Beamline

A 40 mCi ^{22}Na positron source is mounted on a closed cycle refrigerator cold head (see sections 4.3.1.1 and 5.2.1.1). In order for neon to condense on the cone and source capsule, a temperature of around 7 K needs to be maintained. The neon condenses onto the cone which is biased at 80 V, and a low energy e^+ beam, of typical intensity $> 5 \times 10^6$ e^+s^{-1}, is produced.

A series of watercooled, 'cheesecake' coils are used to guide the positrons from the source end through an initial vacuum chamber, containing a small kink for energy selection, into the main vacuum line. A $\sim$1 m long pumping restriction, housed in a solenoid capable of producing a magnetic field of 30 mT on axis, connects the source end of the system to the accumulation region. A gate valve (see figure 5.4) is used to separate the two regions at the end of this pumping restriction. A NaI detector is mounted close to the valve to measure the beam strength of the emitted positrons. For leak testing purposes a residual gas analyser is connected to pump box 1 of the vacuum system. The moderated positrons, emanating from the source cone, pass into the accumulator, consisting of eight cylindrical electrodes of varying length and diameter. A 1.5 m long, water cooled, electromagnet (see section 5.2.1.2) is used to provide a field of 0.14 T in the accumulator region. Here the positrons are trapped and manipulated using rotating wall techniques (see section 3.4) before being transfered into the antihydrogen production region.

A phosphor screen detector system, identical to that used in the Swansea positron beamline (see section 4.3.1.3), is employed in the second pump box of the vacuum system. Two grids, used for energy selection, are mounted in front of the phosphor screen (biased at 5 kV), but which were grounded for all the

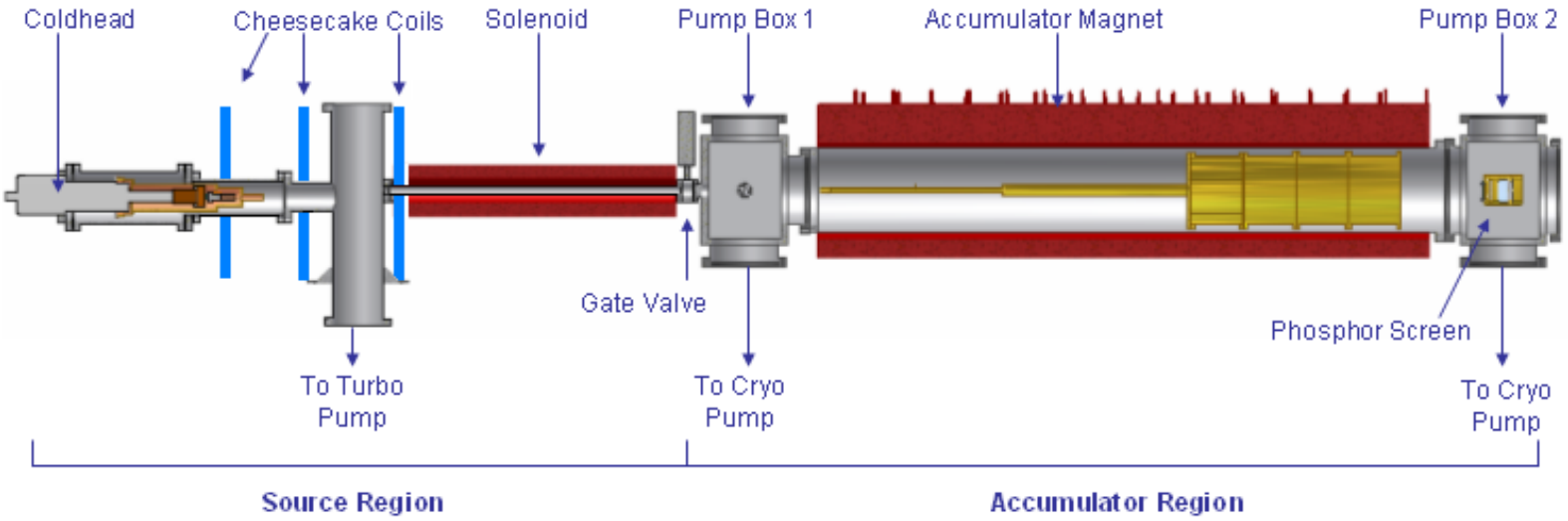

Figure 5.4: Schematic (section view) illustration of the ALPHA positron beamline. The coldhead and accumulator positions are clearly shown along with the magnets guiding the particles through the system. The accumulator magnet which provides the radial confinement required for trapping is also highlighted.

measurements presented here. The phosphor screen assembly is mounted inside a gold plated Faraday cage which is attached to a vertical linear drive at the front of pump box 2. Using the phosphor screen system, images of the positron dumps from the accumulator can be taken. In the situations where transfer to the antihydrogen production and trapping region is required, the phosphor screen can be moved out of the beam path and a transfer electrode, connected to the base of the Faraday cage, is used.

The vacuum in the source and accumulation regions is maintained using a magnetically levitated turbo-molecular pump, backed by a scroll pump, and two cryogenic pumps. For evacuation of the nitrogen buffer gas line (see section 5.2.1.2) a combination of a turbo pump, diaphragm pump and drag pump is used. A schematic diagram of the pumping system of the ALPHA positron beamline can be seen in figure 5.5. The pressure in the system is monitored at various locations, with a range of pressure guages. Using this pumping arrangement a typical base pressure of 3×10^{-10} mbar is obtained.

5.2.1.1 The Coldhead and Coldhead Assembly

The coldhead employed in this system is an SRDK-408E Sumitomo coldhead capable of achieving temperatures of around 3.6 K, similar to that described in section 4.2.1.2. An operating temperature of around 5 K is achieved through the use of a heater located inside the source holder base of the coldhead assembly (see figure 5.6) and is maintained by a Lakeshore 331 temperature controller which can output the temperature reading to a labview program for monitoring. The coldhead used here is of a slightly different design to that used in the Swansea positron beamline. The source holder, biased at 80 V for moderator growth, is electrically isolated from the coldhead by a sapphire disk of diameter 20 mm and thickness 2 mm. A heat shield attached to the first stage of the coldhead at a putative temperature of $\sim$ 40 K, reduces the heatload on the coldhead.

5.2.1.2 The 3-Stage Positron Accumulator

The ALPHA positron accumulator is of a similar design to that developed by Surko and co workers in 1989 [39], and was initially tested at University College

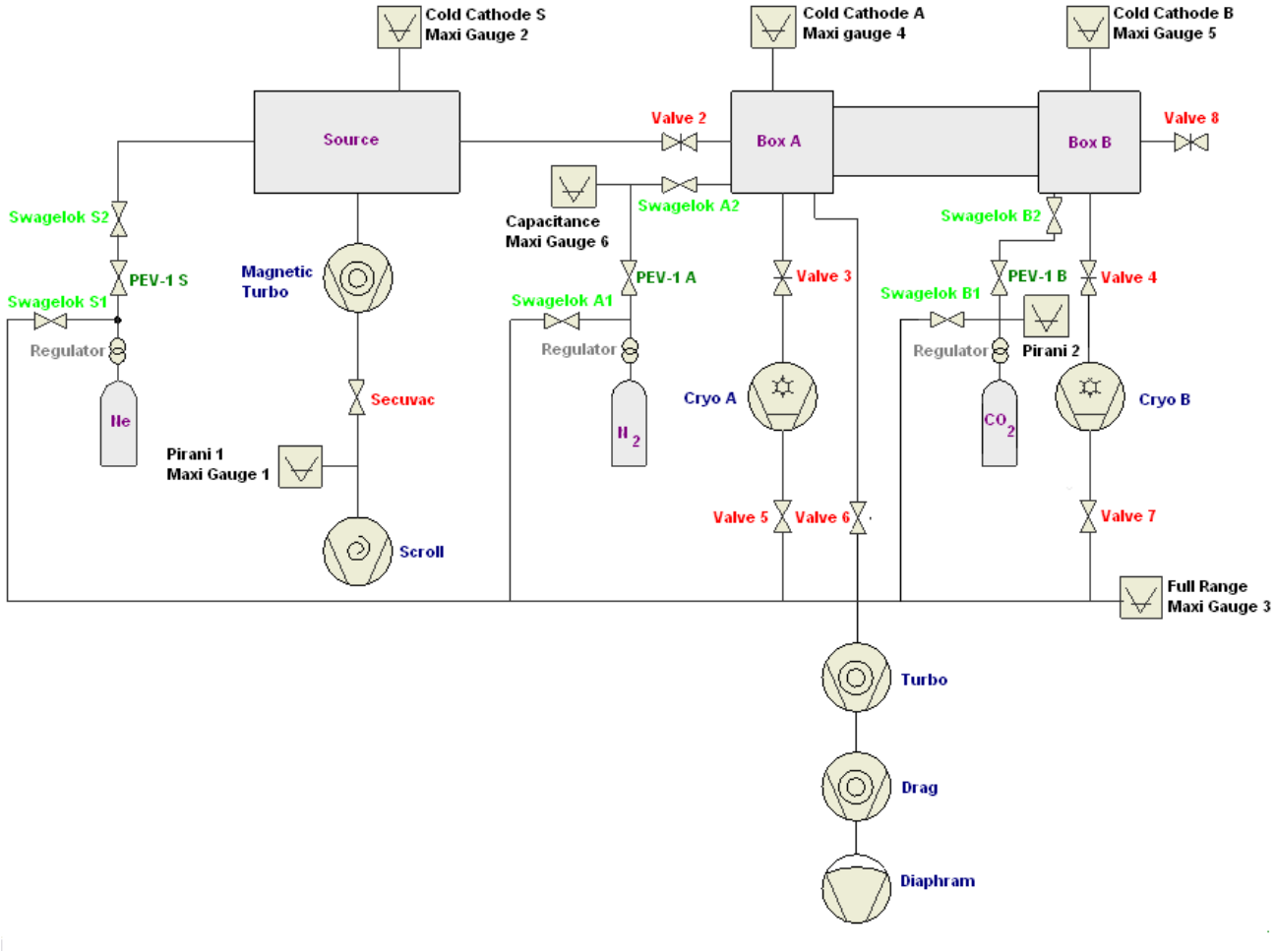

Figure 5.5: Schematic of the ALPHA positron beamline pumping system.

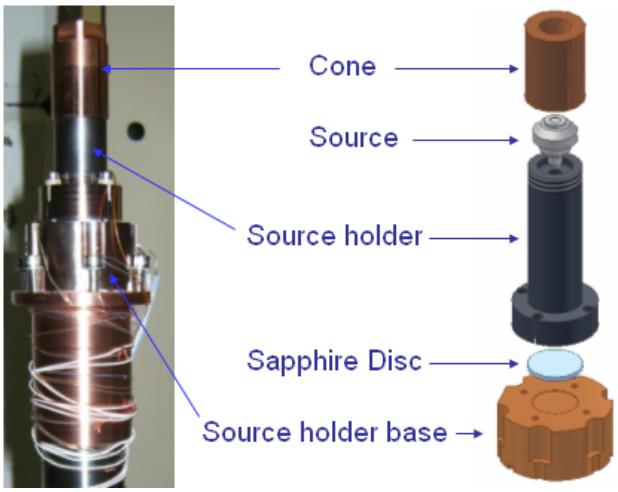

Figure 5.6: Photograph of the ALPHA coldhead assembly alongside a broken down view of the components. The white wires, visible in the photograph, provide a voltage to a heater located inside the source holder base, whereas the orange wire, connected directly to the source holder, provides a bias voltage.

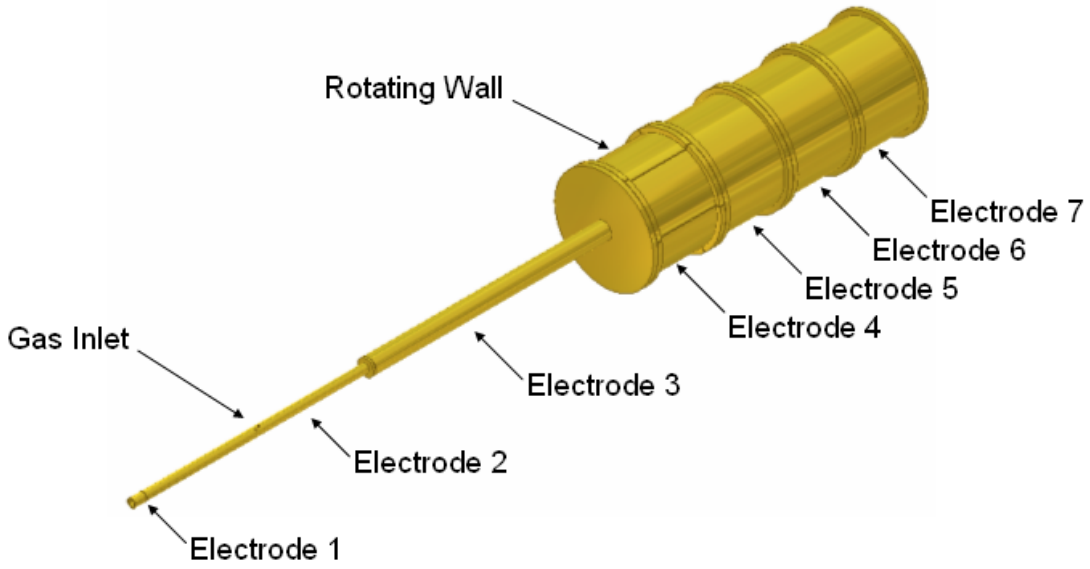

Figure 5.7: Schematic of the ALPHA positron accumulator. The gas is injected through an inlet at the centre of electrode 2. Electrode 4 has been divided into six equal segments which can be used to provide the rotating wall.

London. It consists of three stages made up of seven, gold-plated, electrically isolated electrodes of varying diameter, as shown in figure 5.7. Nitrogen buffer

gas is inserted at the centre of the second electrode. The nitrogen pressure is regulated by a PEV valve, located in the gas line, controlled by a labview program. A capacitance gauge, located outside pump box 1, monitors the gas entering the system. The pressure at each end of the accumulator is measured by two cold cathode gauges situated at the top of each pump box. The electrodes seen in figure 5.7 are separated from each other by means of 2 mm sapphire balls. The dimensions of the accumulator electrodes are given in table 5.1.

Table 5.1: The specifications of the positron accumulator. The potentials applied to the electrodes (E1-E7) for the 'trap' and 'dump' routine are also shown.

	E1	E2	E3	E4	E5	E6	E7
Length [mm]	21.0	509.6	359.8	154.0	154.0	154.0	154.0
Diameter [mm]	12.7	12.7	30.5	200.7	200.7	200.7	200.7
Trap [V]	75.7	70.7	62.0	51.9	51.9	52.0	340.0
Dump [V]	110.0	70.7	62.0	51.9	51.9	52.0	0.00

The process of accumulation is discussed in chapter 3, so only a brief overview will be included here. The accumulator works according to a 'trap' and 'dump' routine, depicted in figure 5.8. During the 'trap' phase the potential on the first electrode is set just below 80 V, the energy of the moderated positrons, to allow the positrons to enter the trap, where they lose energy through collisions with the nitrogen gas. The potential of the gate electrode (electrode 7) is kept at 340 V, providing a barrier to the positrons. The particles are reflected by the barrier towards the trap entrance. With the energy of the positrons being lower than when they entered the trap, the potential on the first electrode is too high for them to overcome and they are captured. Subsequent collisions with the nitrogen molecules cause further energy loss and the positrons to become trapped in the well in the third stage of the accumulator. Here they can be manipulated by the rotating wall before being 'dumped'. In the 'dump' phase the potential on the

gate electrode is dropped to zero, allowing the plasma to leave the trap.

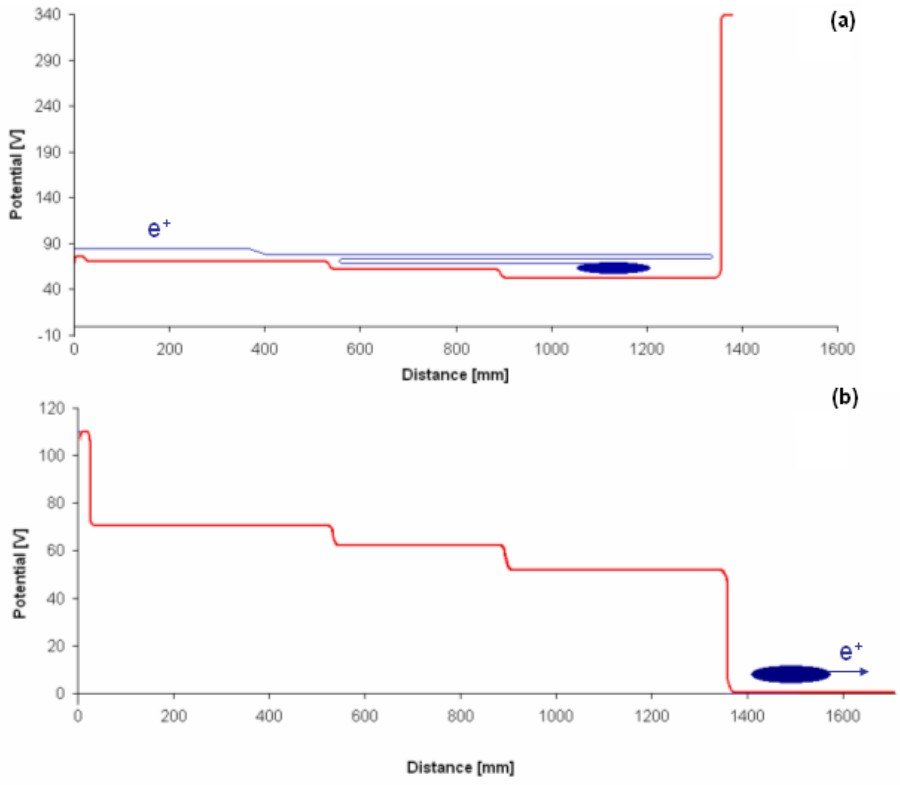

Figure 5.8: Illustration of the electrical potentials applied to the accumulator during the trap (a) and dump (b) routines.

A rotating wall electrode (described in more detail in the following section) is located in the third stage of the accumulator. As previously stated (see section 3.4), when a rotating electric field is applied to a plasma, it is heated up resulting in particle loss [50]. For this reason a second gas line was constructed to allow the optional use of CO_2 as a cooling element to counteract this heating affect. The cooling gas is inserted into the second pump box where it can drift into the third stage of the accumulator. A PEV is used to regulate the CO_2 gas pressure, which is monitored by a Pirani guage positioned outside pump box 2.

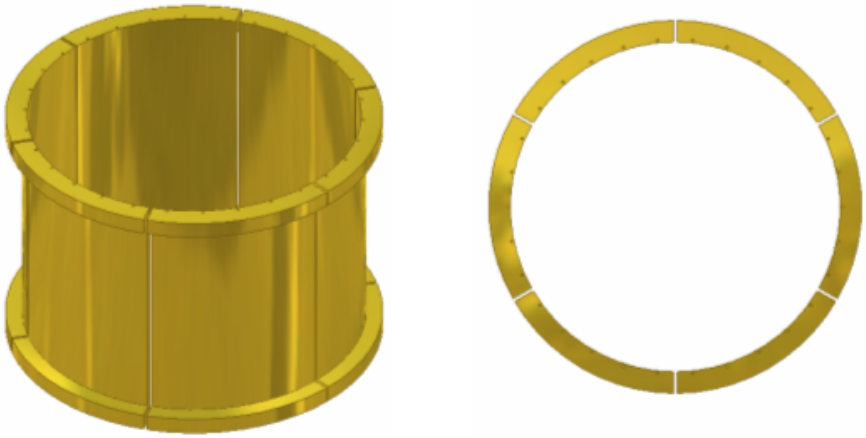

Figure 5.9: Schematic of the rotating wall electrode in the ALPHA system. Each segment is equal in size. Sapphire balls provide electrical isolation between the rotating wall electrode and the remaining accumulator electrodes, see figure 5.7.

5.2.1.3 The Rotating Wall

In the ALPHA beamline, a rotating wall electric field can be produced using a sinusoidal voltage, phase shifted on each part of the segmented electrode, labelled electrode 4 in figure 5.7. It is composed of six segments (see figure 5.9) and can be run in a dipole or quadrupole mode. The rotating wall is controlled using a series of labview programs. The control computer sends the rotating wall settings to a Beckhoff modular control unit which relays the information via an RS232 connection to a rotating wall generator, as shown schematically in figure 5.10. The rotating wall generator receives a trigger signal directly from the computer. Upon receiving this signal it applies a wavefunction to each of its six outputs. These outputs are out of phase by an angle determined by the mode (i.e. dipole or quadrupole) selected. These waveforms pass through an RC circuit (which behaves as a low/high pass filter) where a bias voltage is applied. The total voltage applied to the rotating wall electrodes is of the form $V_{Total} = V_{Bias} + V_0 \sin(\omega t + \phi_i)$, where ϕ_i represents the phase applied to electrode i. For dipole operation a phase difference of $\pi/3$ is applied, whereas a phase difference of $2\pi/3$ is required to achieve a quadrupole field.

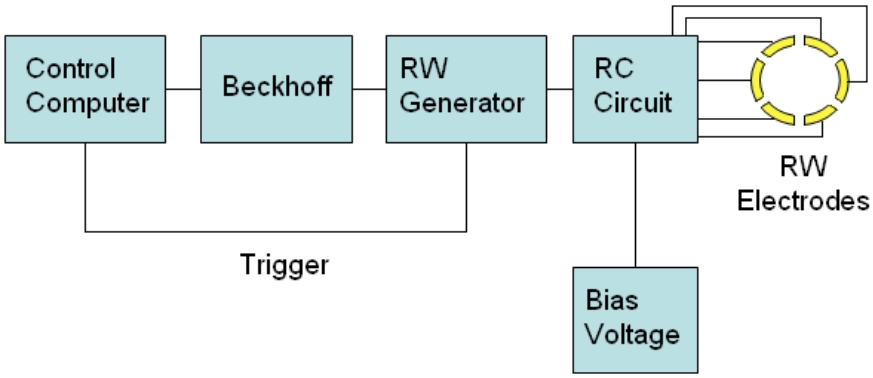

Figure 5.10: Schematic of the rotating wall electronics.

5.3 Results and Discussion

5.3.1 Detection

The phosphor screen, biased at 5 kV during operation, is used to measure the plasma radius and the total number of the accumulated positrons. The total charge, Q, of the plasma is measured on the phosphor screen. The number of particles, N, in the plasma can then be obtained, via;

$$N = \frac{Q}{q} = \frac{VC}{1.6 \times 10^{-19}}. \tag{5.2}$$

where C is the capacitance of the phosphor screen and V is the measured voltage.

Additional to the phosphor screen, two Caesium Iodide (CsI1 and CsI3) detectors are used. CsI1 is mounted approximately 2 m above pump box 2, whilst the position of CsI3 changes depending on the measurement being conducted. For these data it was located approximately 1 m above pump box 2. The CsI detectors monitor the annihilation signals of the positrons dumped onto the phosphor screen. A transient recorder registers the voltage pulses produced by the detectors and the phosphor screen. These signals are sent to a computer where they are inserted into a labview program. Positrons were accumulated for 100, 200 and 300 s accumulation times and the signals from the CsI detectors and phosphor screen were recorded. Using an oscilloscope the charge on the phosphor

screen was also measured, which was substituted into equation 5.2 to determine the number of particles dumped in each case. Dividing the number of positrons in the dump by the measured pulses from the transient recorder for each detector the following calibration constants were obtained for the labview program,

$$N = 270000(\pm 500) \times \text{Phosphor Signal}, \tag{5.3}$$

$$= 140000(\pm 400) \times \text{CsI1 Signal and} \tag{5.4}$$

$$= 71000(\pm 300) \times \text{CsI3 Signal}. \tag{5.5}$$

It should be noted here that an additional CsI detector (CsI2) is located around pump box 2 for alignment purposes but due to its position it saturates when a plasma is dumped on the screen, and so has been excluded from this list.

Plasmas ejected from the accumulator are incident on the screen where the plasma charge causes the screen to phosphoresce, an image of which is directed via a mirror to a cryogenically cooled CCD camera located outside pump box 2. Images of the plasmas can be taken[2], examples of which will be included later, and from these the diameter and the central density of the plasma can be determined. The CCD images were calibrated (1 pixel = 0.486 $\pm$0.005 mm) by comparing the known phosphor screen diameter (50 mm) to the measured diameter of an image of the screen.

The uncertainty in the above calibration values was determined by calculating the standard error in the counts measured. The studies presented here are only concerned with relative plasma sizes and densities under varied trapping and manipulation conditions. As the same detector is used and its position is not changed, the uncertainty in each value will be the same across the range of all measurements, therefore the uncertainties will be disregarded in the following sections.

[2]A background image, produced by applying a bias to E1 which was high enough to block the low energy beam, was subtracted for each measurement. Only high energy particles, that had not been filtered by the magnetic field, reached the screen.

5.3.2 N_2-Only Results

5.3.2.1 Positron Lifetime Measurements

Positrons were accumulated for a set time period after which the resulting cloud or plasma was dumped onto the phosphor screen, using the aforementioned trap and dump routine (see section 5.2.1.2), and the number of incident positrons measured. By plotting the number of positrons trapped over a range of accumulation times, an accumulation curve is produced. A series of such measurements were conducted with this apparatus for various nitrogen gas pressures. The results can be seen in figure 5.11.

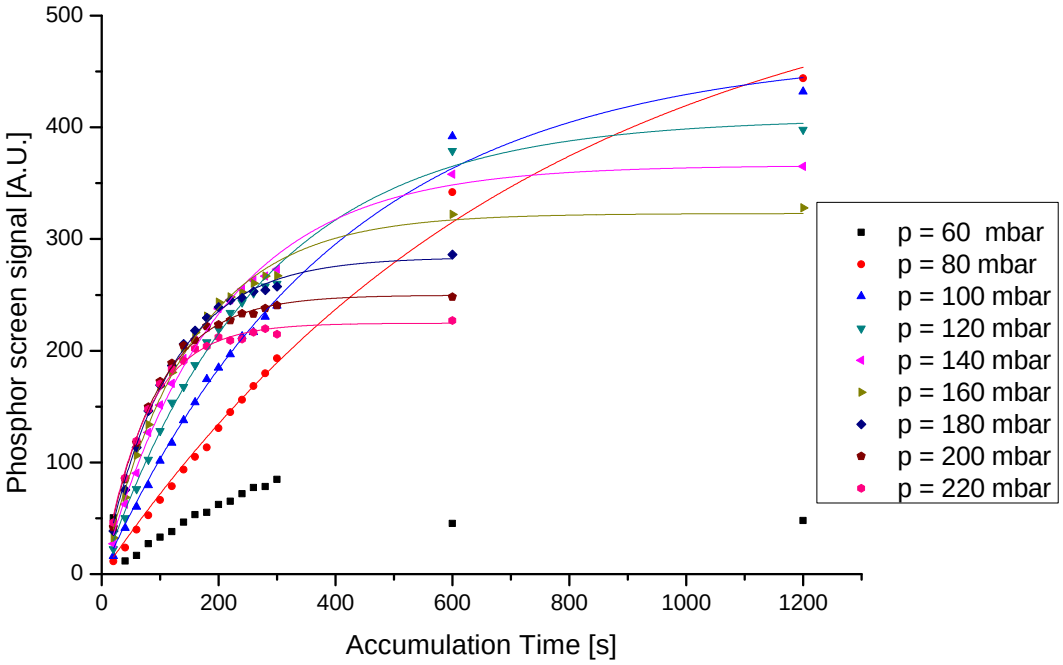

Figure 5.11: Accumulation curves taken with respect to the nitrogen gas pressure, measured in mbar. The accumulation time ranges from 20 - 1200 s in 20 s steps. Here the pressure is measured by a capacitance gauge located just outside pump box 1.

The curves shown in figure 5.11 were fitted with equation 3.15. The fit of these curves allows the lifetime of the particles in the trap, τ, and the saturation point, $N(\infty)$, to be determined with respect to pressure, P, see section 3.2.

These values can be substituted into the following equation in order to obtain the trapping rate, R,

$$R = N(\infty)/\tau. \tag{5.6}$$

At low pressures R is proprtional P, and should tend to a constant value as P becomes larger, therefore the positron number $N(t)$ should increase at a steeper gradient with respect to pressure, which is clearly observed in figure 5.11. At high pressure the saturation point $N(\infty)$ is achieved at shorter accumulation times as expected, and is of a lower value, meaning that less particles are contained in the trap. At lower pressures significantly higher $N(\infty)$ values are obtained for long accumulation times.

In an accumulator it is expected that the lifetime of the particles in the trap is dependent upon pressure with lower pressures yielding higher lifetimes. This is evident for all these data, bar one which will be discussed later. From the fit of these curves the lifetimes have been calculated to range from around 80 s, for a pressure of 220 mbar, to 1000 s for 80 mbar.

The interesting result here is that of 60 mbar, here the accumulator appears to follow the expected behaviour shown with the other pressures, but at long accumulation times the number of positrons in the trap declines. The lifetime of the particles in the trap is inversely proportional to the pressure and as such with less gas in the system there should be fewer losses, resulting in a higher $N(\infty)$. This is not the case for these data. It is not understood why this has arisen and therefore more investigation into this is required

From figure 5.11 it can be seen that the accumulator was optimised, for maximum positron yield, with a buffer gas pressure of 160 mbar at 200 s accumulation time. This gas pressure and time period was therefore used for all subsequent measurements.

5.3.2.2 Dipole RW

Positrons were accumulated as above for 200 s. During the whole accumulation period a RW dipole field was applied. The application of the rotating wall produces smaller, more dense, positron plasmas. The magnitude of the effect that the rotating wall has on the plasma is dependent upon the frequency and

amplitude of the applied electric field. After the 200 s accumulation period the resulting plasma was dumped onto the phosphor screen. A range of rotating wall frequencies were investigated with varying rotating wall amplitudes applied. A text file was produced for each measurement, which was loaded into a labview program in order to determine the positron number, true diameter and central density. The labview program retrieves the value of the charge on the phoshor screen which can then be converted into positron number using the calibration factor stated above. Using the text file a 2D profile of the plasma can be produced in pixels. From this a value for the plasma diameter[3] and the peak position were determined. Here the central density is the number of particles contained in the central 9-pixels of the 3D peak. The results can be seen in figure 5.12.

The application of the rotating wall causes a compression of the plasma as seen in figure 5.12 (c). This compression causes the plasma to heat up, which in turn causes a decrease in the particle lifetime and the loss of particles in the trap. Operating the rotating wall at high frequency and amplitude has a detrimental affect on the plasma with a loss in the number of particles trapped and fewer particles residing in the central density, this is due to the inefficient cooling of the nitrogen. From this it is clear that obtaining dense positron plasmas using the rotating wall under the above conditions is best achieved by using a low rotating wall frequency with 600 kHz giving the best results.

5.3.2.3 Quadrupole RW

The measurements outlined in the previous section were repeated with the use of a quadrupole rotating electric field. Only nitrogen gas at a pressure of 160 mbar was present in the trap. As above a range of rotating wall frequencies were examined with respect to the rotating wall amplitude applied. The rotating wall amplitude was increased in 0.1 V increments. The charge measured on the phosphor screen was recorded and converted to allow the number of particles in the plasma to be plotted. Images of the plasmas were taken for each measurement allowing the central density and diameter, as previously defined, to be determined. The results can be seen in figure 5.13.

[3]This is the value of the full width at half maximum which is obtained from a Gaussian fit of the profile and then converted into mm using the calibration factor previously stated.

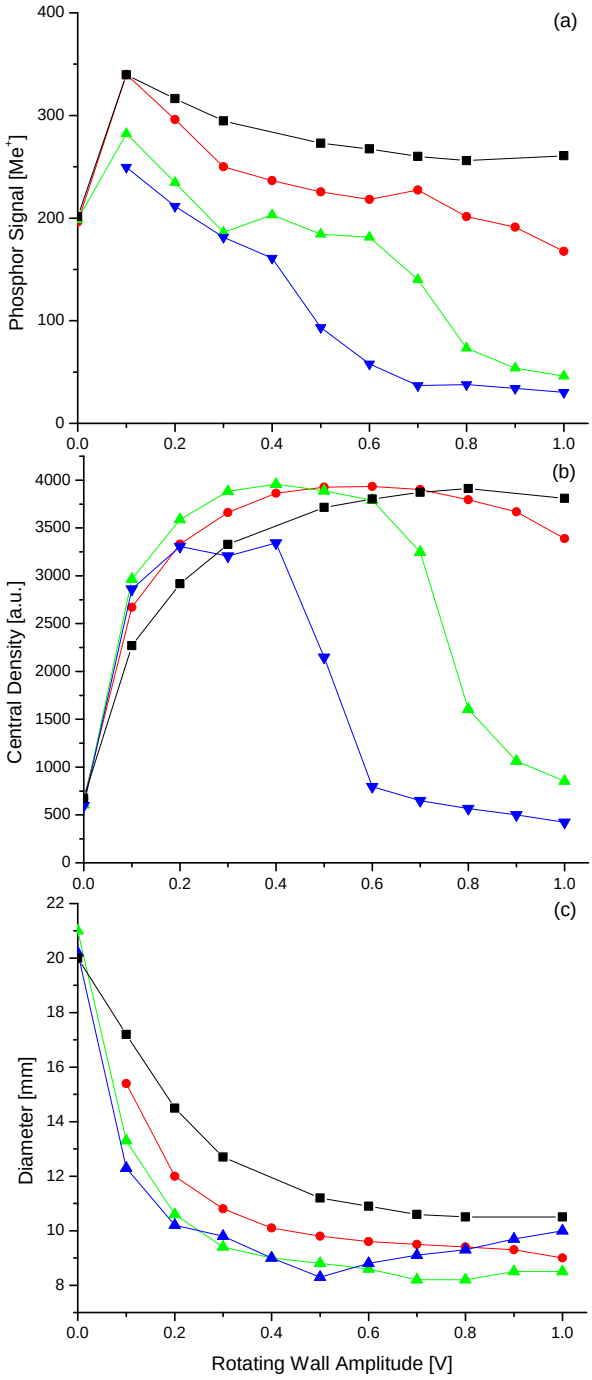

Figure 5.12: Data produced for plasmas accumulated over 200 s with an N_2 set point of 160 mbar at varying rotating wall amplitudes. The dipole rotating wall was employed at various frequencies: squares = 600 kHz, circles = 700 kHz, green triangles = 800 kHz and blue triangles = 900 kHz. Figure (a) shows the charge on the phosphor screen converted using the calibration factor, given in section 5.3.1, into positron number, (b) shows the number of particles contained in the central density of the plasma, and (c) is the diameter of the plasma produced.

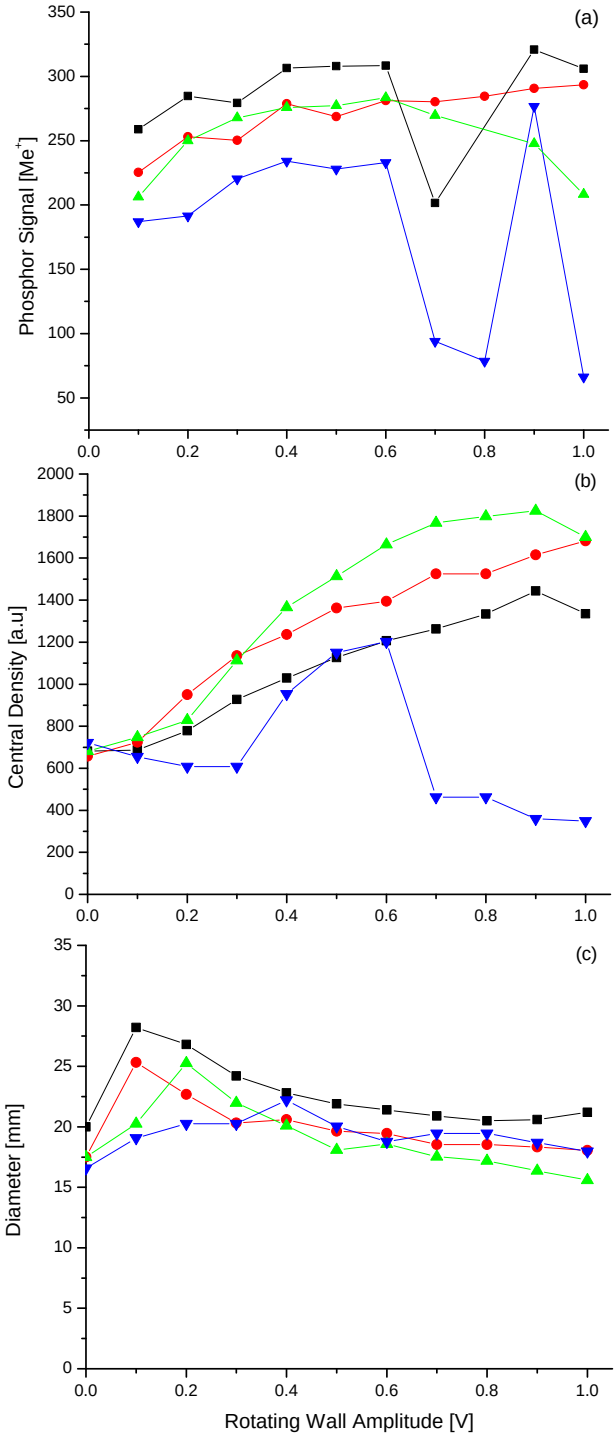

Figure 5.13: Data produced using the quadrupole rotating wall, with an N_2 pressure of 160 mbar, for various frequencies: squares = 600 kHz, circles = 700 kHz, green triangles = 800 kHz and blue triangles = 900 kHz. The rotating wall amplitude ranged from 0-1 V in 0.1 V increments. The nitrogen pressure was set to 160 mbar. Figure (a) shows the charge on the phosphor screen converted using the calibration factor (see section 5.3.1) into positron number, (b) shows the number of particles contained in the central density of the plasma, and (c) is the diameter of the plasma produced.

Comparing these data to the dipole case (see figure 5.12), it is clear that there is no improvement in the yield of low energy positrons contained in the plasma. There is also less than half of the number of positrons in the plasma, detected in the central density, than in the dipole case. The plasma diameter is almost doubled, with the lowest diameter achieved being around 15 mm, 7 mm greater than the plasmas produced with the dipole. While the quadrupole field appears to be more effective at larger amplitudes, a decrease in particle number is still present when the rotating wall is operated at 900 kHz.

When a dipole rotating wall is applied to a plasma the field in the centre of the trap is constant, and this is not true for the quadrupole. In an attempt to overcome the lower effective field at the plasma, the range of the rotating wall amplitude was increased to include up to 10 V, as shown in figure 5.14.

It is clear here that the quadrupole rotating wall has a detrimental effect on the plasma, when used at increased amplitudes. Nitrogen has been shown to be a poor cooling gas [54] and the data here seems to agree, in that the high amplitudes and frequencies shown cause a significant number of particles to be lost, and the plasma diameter to expand. Plasmas produced in this way would not be beneficial for antihydrogen production due to the severe decline in particle number. With only N_2 in the system, the rotating wall needs to be operated with a dipolar field to achieve the best results.

5.3.3 CO_2 Results

Using the rotating wall induces heating into the plasma, as previously discussed in chapter 3. In order to counteract this heating effect, CO_2 gas was inserted into pump box 2 of the ALPHA system where it could drift into the third stage of the accumulator. In order to determine how much CO_2 gas was required, the accumulator was run for 200 s at various CO_2 pressures, the accumulated plasma was dumped onto the phosphor screen where the signal size, central density and plasma diameter were recorded. The results can be seen in figure 5.15.

The rotating wall was employed at a frequency of 875 kHz in each of the measurements shown in figure 5.15, with four different amplitudes being used. The number of particles in the plasma decreases with increasing CO_2 pressure

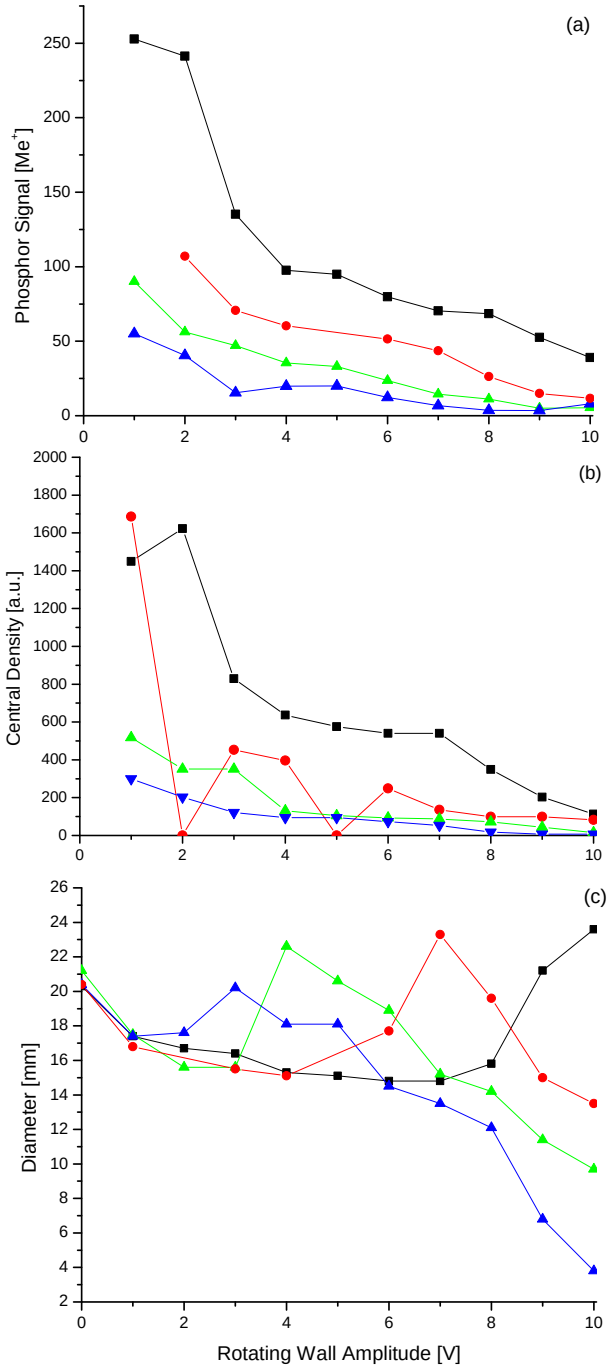

Figure 5.14: Data produced using the quadrupole rotating wall, with an N_2 pressure of 160 mbar, at various frequencies: squares = 600 kHz, circles = 700 kHz, green triangles = 800 kHz and blue triangles = 900 kHz. The rotating wall amplitude ranged from 1-10 V in 1 V increments. Figure (a) shows the charge on the phosphor screen converted using the calibration factor from section 5.3.1 into positron number, (b) shows the number of particles contained in the central density of the plasma, and (c) is the diameter of the plasma produced.

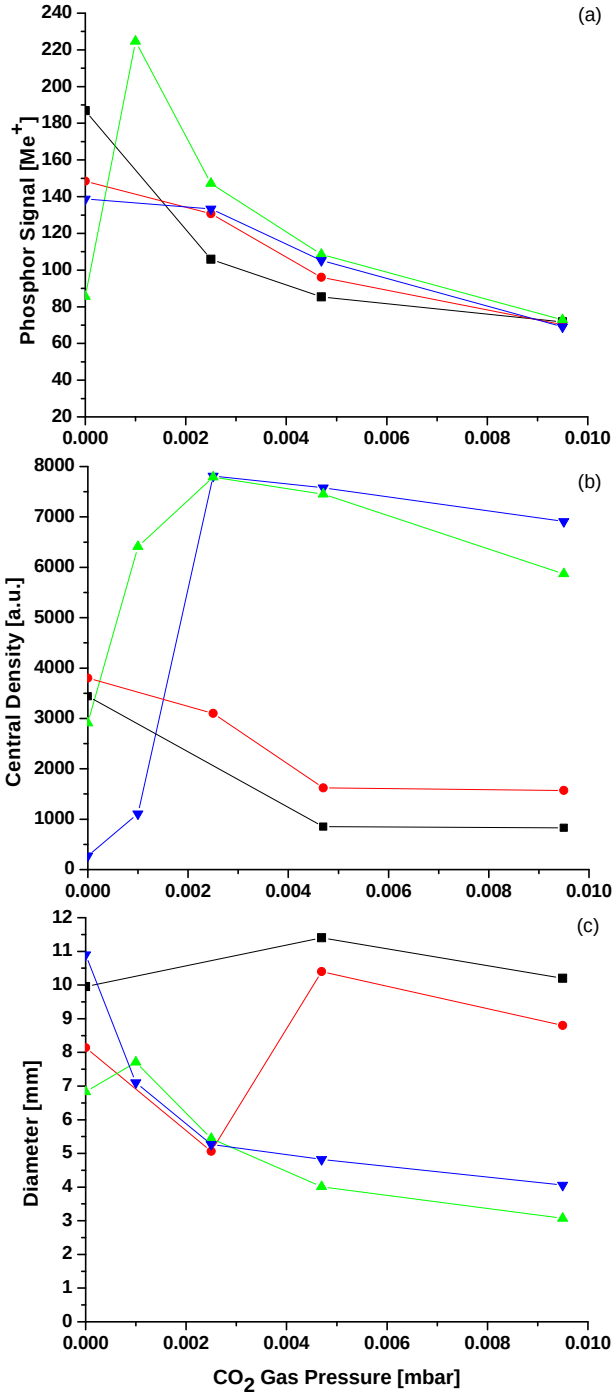

Figure 5.15: Data produced over a 200 s accumulation time with varying CO_2 gas pressure. The dipole rotating wall was employed at various amplitudes: squares = 0.12 V, circles = 0.25 V, green triangles = 4 V and blue triangles = 8 V. Figure (a) shows the charge on the phosphor screen converted using the calibration factor, given in section 5.3.1, into positron number, (b) shows the number of particles contained in the central density of the plasma, and (c) is the diameter of the plasma produced.

with all rotating wall amplitudes. At low amplitudes the number of particles in the central density of the plasma is not improved with increasing cooling gas pressure, however the diameter of the plasma is slightly smaller. In the case of high rotating wall amplitude the results are more significant with more of the particles trapped being contained in the central density. These data clearly show that the optimum plasma conditions, i.e. a small dense plasma with as few particles lost as possible, is achieved with a CO_2 gas pressure of 2.5×10^{-3} mbar, such that this pressure was therefore chosen for all of the following measurements.

To determine the effect the cooling gas had on the lifetime of the particles in the trap an accumulation curve was produced. The accumulation time was increased from 50 s to 500 s in 50 s intervals. Accumulation curves were produced both with and without rotating wall and with and without cooling gas. The results can be seen in figure 5.16. A rotating wall frequency of 850 kHz was used with an amplitude of 5 V. The curves shown in figure 5.16, were fitted

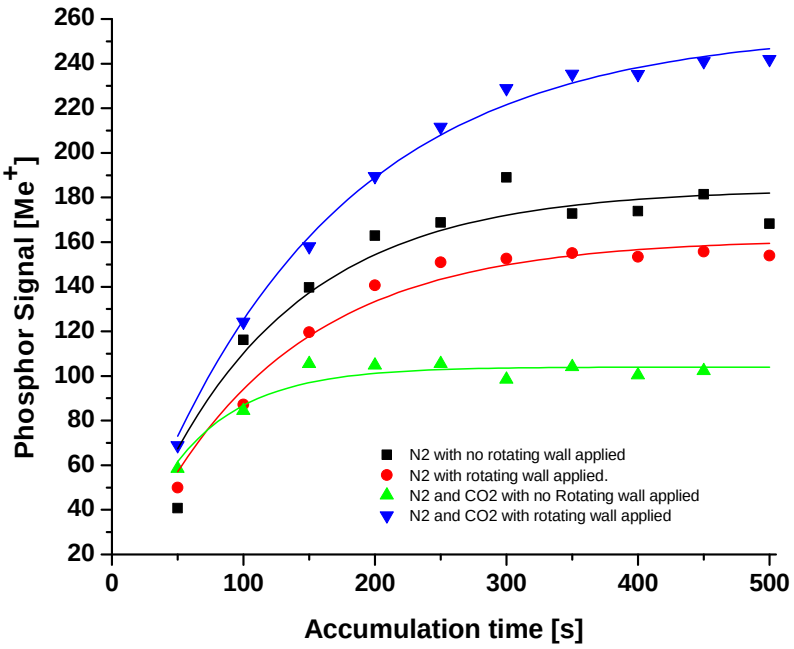

Figure 5.16: Accumulation curves produced with and without rotating wall, frequency = 850 kHz with an amplitude of 5 V, applied both with and without cooling gas in the system.

to equation 3.15 to determine the lifetime, $N(\infty)$ value and accumulation rate

and their values are displayed in table 5.2. From these data it can be seen that the use of the CO_2 gas significantly improves the number of particles trapped when used in conjuction with the rotating wall. With no rotating wall employed, the presence of CO_2 is detrimental to the number of positrons trapped and the lifetime of the particles in the trap.

Table 5.2: The calculated values for $N(\infty)$, lifetime and accumulation rate determined though the fit of the curves shown in figure 5.16. Data are presented for N_2 only measurements and for N_2 with CO_2 in the system both with and without the dipole rotating wall (RW). $N(\infty)$ and rate values displayed here are in millions of positrons.

Data Set	$N(\infty)$	lifetime [s]	Rate [s^{-1}]
N_2 only without RW	184 ± 8	109 ± 17	1.7 ± 0.3
N_2 only with RW	162 ± 4	115 ± 9	1.4 ± 0.1
N_2 and CO_2 without RW	104 ± 2	56 ± 6	1.9 ± 0.2
N_2 and CO_2 with RW	256 ± 4	149 ± 6	1.7 ± 0.1

5.3.3.1 Dipole RW

Again positrons were accumulated for a 200 s time period with a dipole rotating electric field applied throughout. In this measurement CO_2 was inserted into pump box 2, at a pressure of 2.5×10^{-3} mbar, where it drifted back into the second stage of the accumulator. The resulting plasma was dumped onto the screen and images were produced. These images were analysed by a labview program to determine the number of particles in the dump, the diameter of the plasma and how many particles were contained in the central density. The results obtained were plotted with respect to rotating wall amplitude for different rotating wall frequencies, as can be seen in figure 5.17.

For the measurements conducted with only N_2 present, the rotating wall was ineffective at high frequencies and amplitudes, most likely due to the fact that

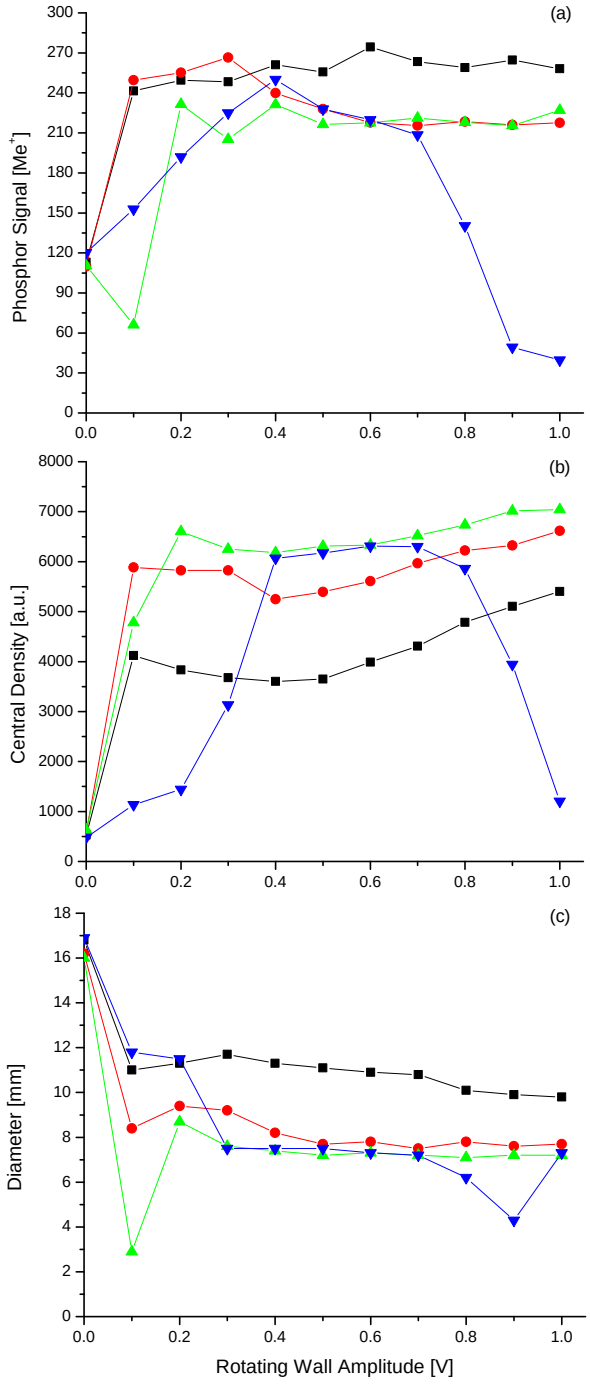

Figure 5.17: Data produced over a 200 s accumulation time with a CO_2 pressure of 2.5×10^{-3} mbar. The dipole rotating wall was employed at various frequencies: squares = 600 kHz, circles = 700 kHz, green triangles = 800 kHz and blue triangles = 900 kHz. The rotating wall amplitude ranged from 0-1 V in 0.1 V increments. Figure (a) shows the charge on the phosphor screen converted using the calibration factor (see section 5.3.1) into positron number, (b) shows the number of particles contained in the central density of the plasma, and (c) is the diameter of the plasma produced.

applying the rotating wall at these magnitudes caused more heating in the plasma, and the N_2 was unable to provide sufficient cooling. In this case the presence of the CO_2 shows an improved performance at higher frequencies. The best overall charge is achieved at a rotating wall frequency of 600 kHz, however the highest central densities and smallest diameters occur at high frequencies. This data indicates that greater compression of the plasma is achieved when CO_2 is present, showing greater cooling at higher rotation, hence achieving smaller diameters.

5.3.3.2 Quadrupole RW

The measurements outlined in the previous sections have been repeated with a quadrupole rotating electric field applied. The accumulation time used was again 200 s with the both N_2 (160 mbar) and CO_2 (2.5×10^{-3} mbar) present in the system. The rotating wall was applied throughout accumulation. the resulting plasmas were dumped from the accumulator onto the phosphor screen where the images produced were analysed to determine the central density and plasma diameter. The charge measured on the screen was used to determine the number of particles incident on the screen. Data were taken for four rotating wall frequencies at amplitudes from 0-1 V in 0.1 V increments.

The data displayed in figure 5.18 shows that plasmas produced using the quadrupole rotating wall are not improved with the prescence of the CO_2, over the range of 0-1 V amplitudes. The plasmas produced are comparable to those with N_2 only in the accumulator. In order to achieve fields of the same magnitude as the dipole rotating wall in the centre of the rotating wall electrode, the range over which the rotating wall amplitude was applied was increased as described in section 5.3.2. The results are displayed in figure 5.19.

The data shown in figures 5.13 and 5.14 demonstrated that the quadrupole rotating wall was ineffective with only N_2 in the accumulator. The presence of CO_2 does not improve this, with significantly lower numbers of positrons contained in the plasma than in the dipole case. Also the increase in amplitude does not appear to overcome the lower effective field at the plasma. From figures 5.18 and 5.19 it would appear that the plasma diameter and the number of positrons present in the central density are dependent upon the frequency used, which war-

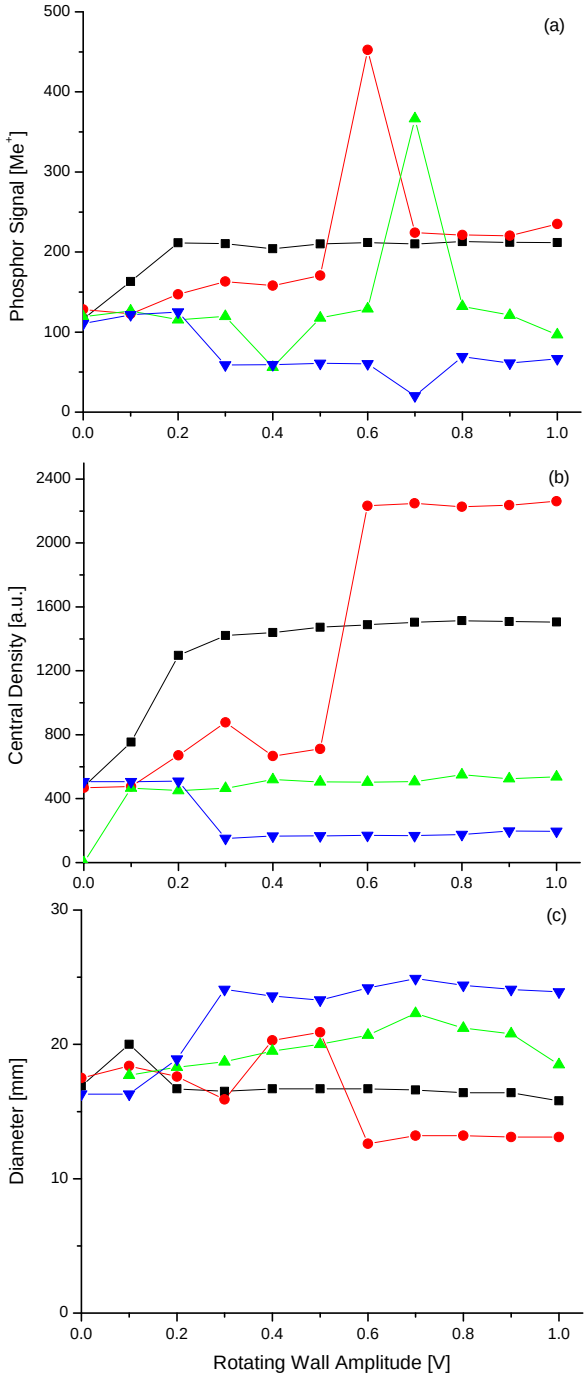

Figure 5.18: Data produced using the quadrupole rotating wall at various frequencies: squares = 600 kHz, circles = 700 kHz, green triangles = 800 kHz and blue triangles = 900 kHz. The rotating wall amplitude ranged from 0-1 V in 0.1 V increments. An N_2 set point of 160 mbar and CO_2 pressure of 2.5×10^{-3} mbar were used. Figure (a) shows the charge on the phosphor screen converted using the calibration factor given in section 5.3.1 into positron number, (b) shows the number of particles contained in the central density of the plasma, and (c) is the diameter of the plasma produced.

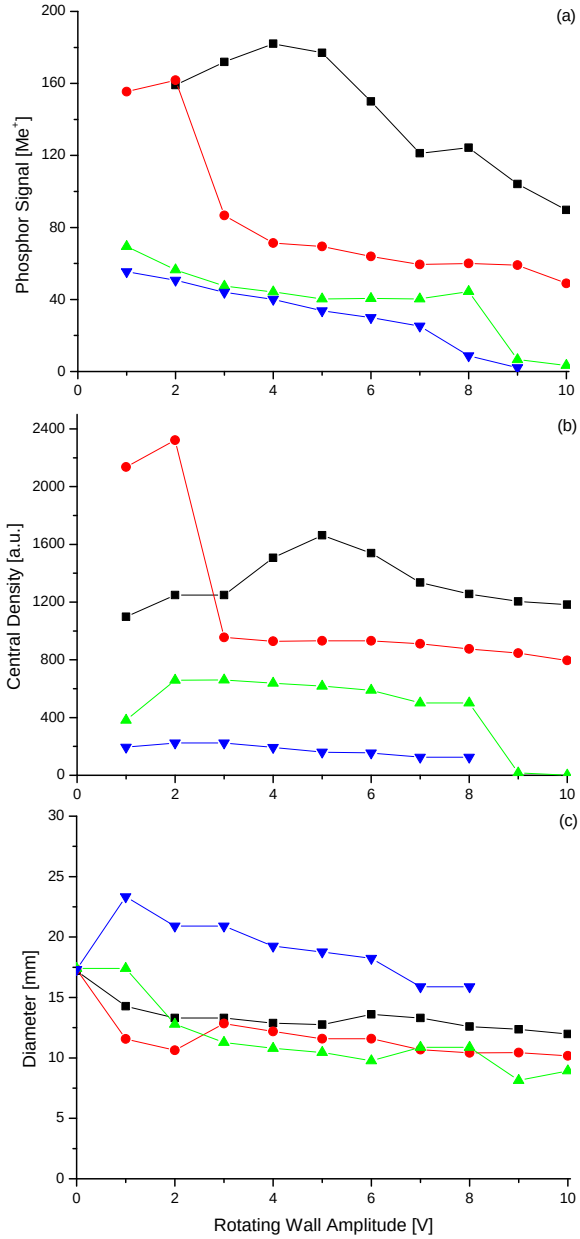

Figure 5.19: Data produced using the quadrupole rotating wall at various frequencies: squares = 600 kHz, circles = 700 kHz, green triangles = 800 kHz and blue triangles = 900 kHz. An N_2 set point of 160 mbar and CO_2 pressure of 2.5×10^{-3} mbar were used. The rotating wall amplitude ranged from 1-10 V in 1 V increments. Figure (a) shows the charge on the phosphor screen converted using the calibration factor above into positron number, (b) shows the number of particles contained in the central density of the plasma, and (c) is the diameter of the plasma produced.

rants further investigation. While the quadrupole does perform better at higher amplitudes than in the N_2 only case, the dipole rotating wall with CO_2 in the system remains significantly more effective.

5.3.4 Plasma Shape

Images were taken for each of the previously outlined measurements, which were used to determine the central densities and the plasma diameter. In each case the images produced were inserted into a labview program to obtain a 2-dimensional cross sectional view of the plasma and a 3-dimensional representation of the plasma produced. The profiles of the resultant plasmas are very interesting and will be discussed here. Only one profile for each of the accumulation conditions has been selected here as a representation of the dataset, the data can be found in the appendix.

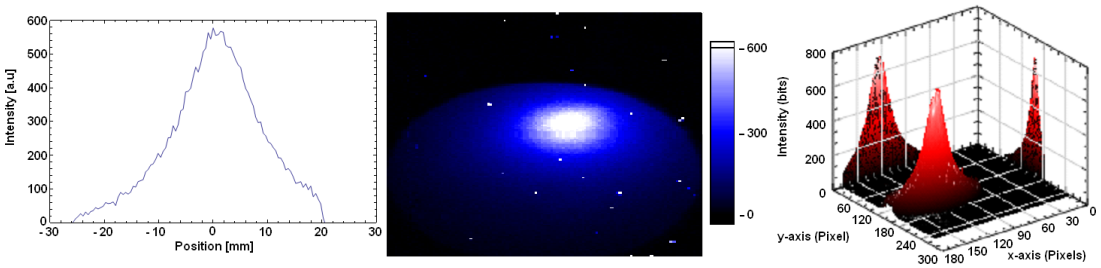

Figure 5.20: An image of the plasma produced when no rotating wall is present, a 2-dimensional profile of the plasma is shown as well as a 3-dimensional representation.

The first image to be considered is that when no rotating wall was applied. In this case nitrogen was present during accumulation, the profile is given in figure 5.20. This figure shows that when no rotating wall is present the plasma is very broad ($\sim$ 20 mm wide FWHM). The intensity of the produced plasma is very low achieving a maximum of around 600.

The plasmas produced when the rotating wall is used, with nitrogen only in the trap, are much improved as illustrated in figure 5.21. In the case of the dipole rotating wall the profile is much narrower with an intensity of around 4000. With the dipole rotating wall the plasma profile appears to be Gaussian, this shape is

consistent for all amplitudes and frequencies. From the data in the appendix it can be seen that the highest intensities are achieved when lower amplitudes and frequencies are used.

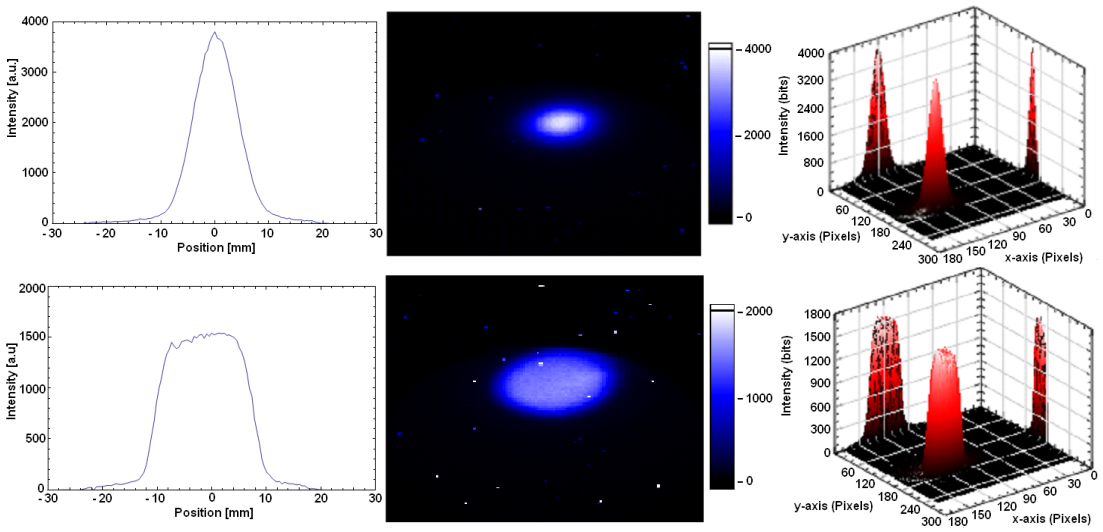

Figure 5.21: Images of the plasmas produced with a dipole rotating wall, top image, and the quadrupole rotating wall, bottom image, with only nitrogen in the system. A 2-dimensional cross section is shown along with a 3-dimensional representation.

The profiles of the plasmas produced with the quadrupole rotating wall, in the presence of nitrogen, are dependent upon the frequency and amplitude used. At low frequencies, the plasma is very square and broad as shown in figure 5.21. As the amplitude is increased the plasma becomes narrower. The intensity of the dump is three times larger than that when no rotating wall is used, however significantly lower than the dipole. This is not the case at higher frequencies. Here the shape changes and begins to return to the no rotating wall applied case (see appendix A).

The most interesting data by far are those when CO_2 is present. Two distinct plasma shapes are observed. The first is that of the dipole where the plasma appears to be hollow as illustrated in figure 5.22. The intensity of the plasma is much greater than all the previously produced data with a maximum intensity of ~ 8000. The hollow plasmas are not observed for all of the dipole CO_2 data,

with the high frequencies producing more Gaussian-like profiles. What can be seen from the data contained in the appendix is that the central position changes. This is confirmed by the images taken. The reason for this shift in position is currently unknown.

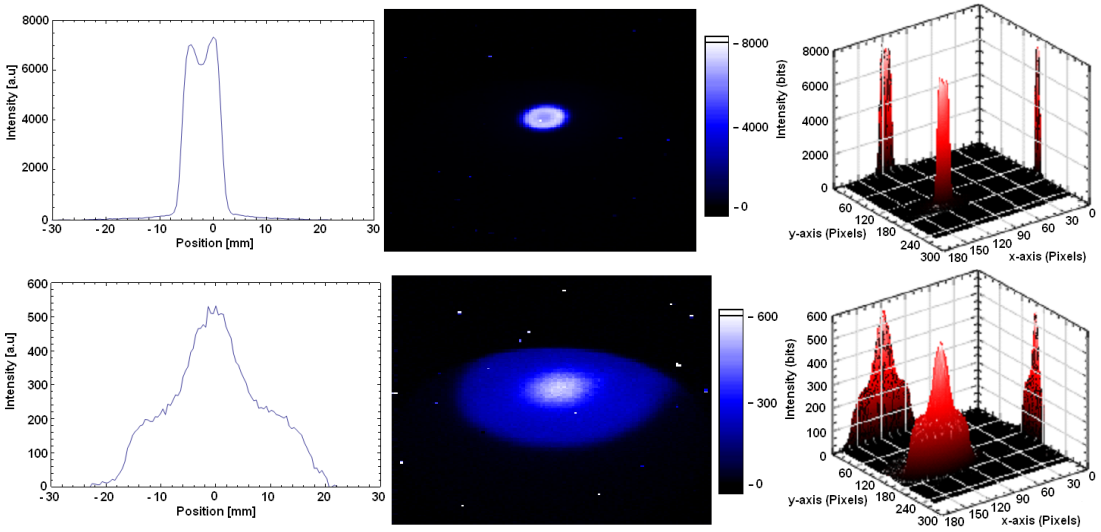

Figure 5.22: An image of the plasmas produced with a dipole rotating wall, top image, and the quadrupole rotating wall, bottom image, with nitrogen and carbon dioxide in the system. A 2-dimensional cross section is shown along with a 3-dimensional representation.

The final shape to be mentioned is that of a plasma with shoulders to the profile. This was initially observed only in the case of the quadrupole data with CO_2 present. Subsequent measurements have shown that this shape can be also be produced with a dipole when CO_2 is present (see figure 5.23) and the quadrupole with only nitrogen present, the latter of which is shown in the appendix.

When a quadrupole rotating wall is applied at low frequency, the plasma shape is initially flat topped and very similar to the N_2-only quadrupole profiles. As the frequency is increased the intensity decreases and the width of the plasma expands, it is at this point that the shoulders start to appear. At the highest frequency, 900 kHz, high amplitudes are required to achieve any intensity but this is clearly significantly less than the dipole case. At this frequency, low amplitudes

result in a loss in the plasma density.

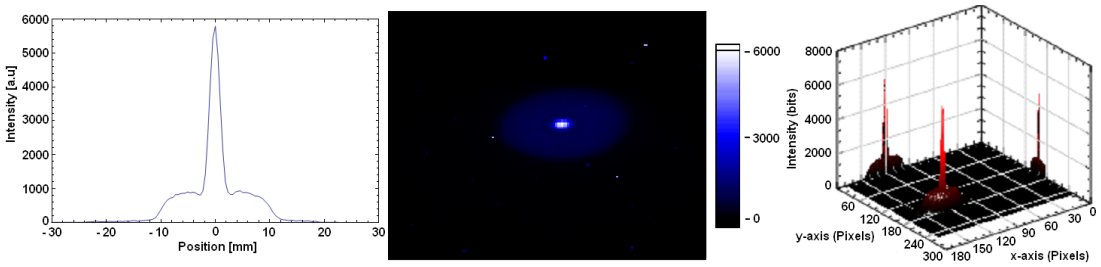

Figure 5.23: An image of the plasmas produced with a dipole rotating wall, with nitrogen and carbon dioxide in the accumulator. A 2-dimensional cross section is shown along with a 3-dimensional representation. Note the massive increase in the peak compared to the shoulders. The peak in this case is very narrow ~ 3 mm.

Figure 5.23 has been included here as an example of the profile produced when the dipole is used with CO_2. The profile here is from a dataset that has not been presented in this thesis. This profile clearly illustrates a dramatic effect in the plasma profile. The shoulders here are very dominant with a very narrow, intense central density being produced.

5.4 Concluding Remarks

Measurements have been taken in an attempt to optimise the positrons plasmas produced in the ALPHA accumulator, these measurements include the introduction of a cooling gas and investigations into the use of both dipole and quadrupole rotating electric fields. With no CO_2 in the system it is clear that the use of the quadrupole is not beneficial with a significant loss in particle number. For the dipole rotating wall the optimum frequency is 600 kHz. With no CO_2 present operating the dipole rotating wall at high frequencies and amplitudes has a detrimental effect on the plasma.

The situation is different when CO_2 is used, with more particles being compressed into smaller plasmas. The highest overall charge measured on the screen is still produced at a frequency of 600 kHz however, the higher frequencies and amplitudes do respond better achieving lower diameter plasmas with higher cen-

tral density, twice that of the nitrogen case. This indicates that the cooling provided by the CO_2 becomes important at the higher frequencies. The use of the quadrupole while improved from the nitrogen only case is still considerably less effective than the dipole. What is interesting here and warrants further investigation is the dramatic dependence on frequency for central density and diameter.

Images were taken for all of the measurements outlined in the previous sections and the profiles for all the data has been included in the appendix. From these profiles five plasma shapes were identified as being of interest. The plasma shapes produced are not fully understood and will require further study, especially those when CO_2 is present.

Chapter 6

Studies of Positron Emission from Solid Argon Moderators

6.1 Introduction

As mentioned in chapter 2, research has been conducted into positron moderation since the 1950's, with groups around the world striving to achieve ever more efficient positron beamlines. Prelimary data [34] shows that when a rare gas solid moderator is plated with a layer of additional gas, the gas layer may subsequently charge causing an increase in positron yield. A beamline system was designed and built to study this effect further. Three plating gases were chosen, namely nitrogen, oxygen and air. The efficiency of both plated and unplated argon moderators has been investigated with respect to growth temperature and argon gas pressure. The following sections describe the equipment used and the results obtained.

6.2 Experimental Arrangement

6.2.1 The Positron Beamline

The moderation studies beamline can be seen schematically in figure 6.1. This beamline has been purpose-built for studies into positron moderation. Positrons

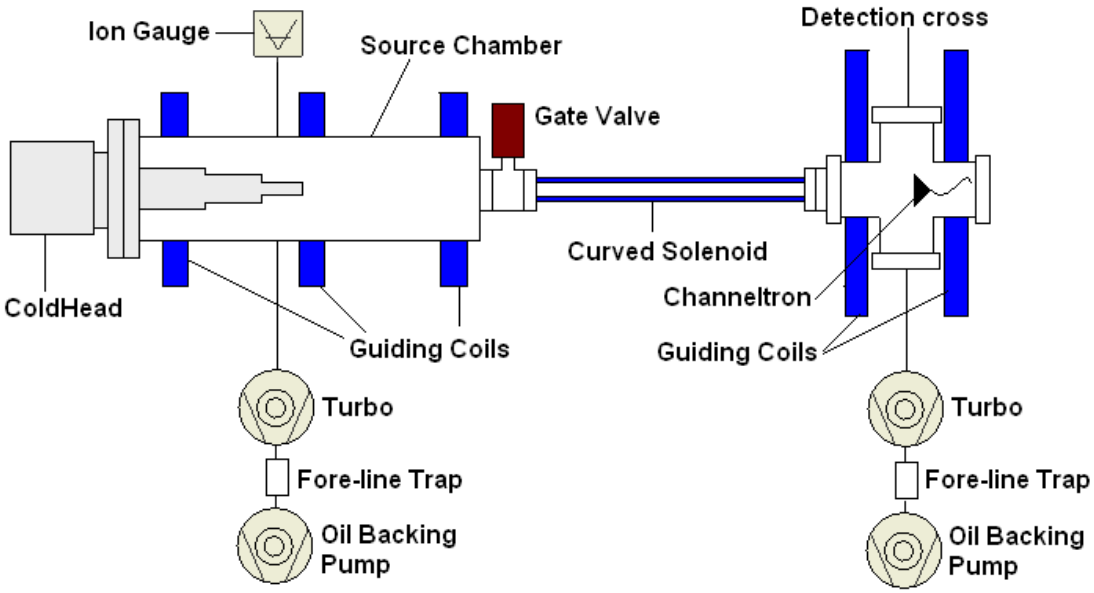

Figure 6.1: Schematic of the moderation studies positron beamline.

emanate from a ^{22}Na radioactive source of strength 18.5 MBq[1]. The emitted positrons enter the moderator where they lose energy via inelastic collisions, including the creation of electron-hole pairs, exciton and Ps formation and the creation of accoustic phonons. The positrons diffuse epithermally to the surface where they can be re-emitted into vacuum (see chapter 2). The moderated positrons are guided through the source chamber by a series of three coils, each providing a magnetic field of 1 mT on axis. They then pass through a curved solenoid, able to produce a magnetic field of around 5 mT which filters the remaining high energy β^+ particles from the moderated flux, to reach a channel electron multiplier (CEM), or channeltron, detector. Two additional coils of 400 turns provide a field of 6 mT, when a current of 6 A is passed through them, in the detection region.

The rare gas used for these moderators was argon. Argon moderators can be grown in the range of 10-30 K, however with the present apparatus the coldhead base temperature, around 15 K (see figure 6.2), proved to be too low and the gas condensed on the heatshield (similar to that described in section 4.3.1.1), as will be discussed later. For this reason a higher temperature ($\sim$ 20 K) was required

[1]As calculated on the 16$^{\text{th}}$ of April 2010.

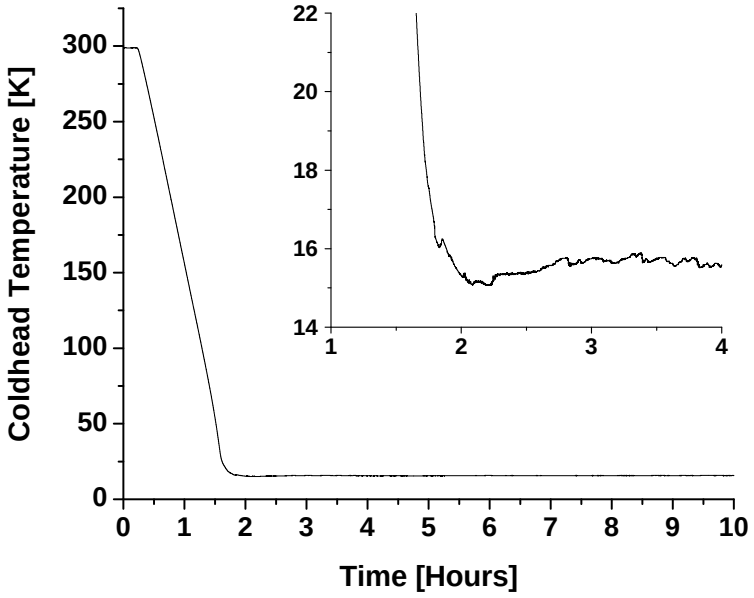

Figure 6.2: Coldhead cooldown curve showing the base temperature (∼15 K), and stability. The inset graph is a zoomed-in view of the lowest temperature achieved. It is clear that the temperature of the coldhead is stable after around 2 hours of operation.

for growth. The temperature could be monitored using a chromel-gold (0.07 % Iron) thermocouple in conjuction with a Lakeshore 330 temperature controller.

In order to investigate the effect that the growing temperature had on the moderator, a heater was mounted inside the source holder base of the cold finger assembly. A diagram of the coldfinger assembly used in this system can be seen in figure 6.3. By allowing a current, typically maintained at 200 mA, to run through the heater a temperature increase of around 5 K was achieved. The coldhead temperature was left to stabilise before growth was attempted. The argon gas condensed on the surface of a copper cone, shown in figure 6.3, which was biased at 20 V. A 2 mm thick, 20 mm diameter, sapphire disc was located between the source holder base and the source holder to electrically isolate the source holder from the coldhead itself, whilst maintaining thermal contact. The

coldhead used in this beamline was an APD DE-204SLB-6.5 model alongside a HC4 compressor.

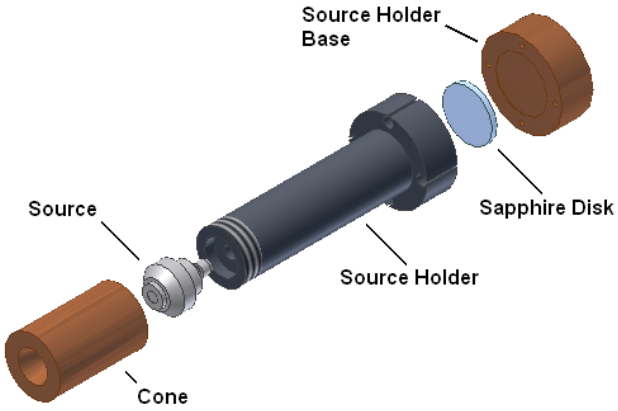

Figure 6.3: Diagram of the coldhead assembly used in the moderation beamline.

A Labview program was written for moderator growth based on the PID regulation (see section 4.3.1) of the gas pressure. The program monitors coldhead temperature, pressure and positron countrate. Once grown, the same program can be used to maintain and monitor the pressure of the plating gas.

The vacuum in the system is maintained using two turbo pumps, with the first located beneath the source chamber, and the second beneath the detection region. These pumps are backed out with two oil pumps as can be seen in figure 6.1. A fore-line trap is located between each turbo and backing pump to prevent oil being drawn into the system. The base pressure achieved using this arrangement is 1×10^{-9} mbar.

6.2.2 The Gas Inlet System

A dual gas inlet system was designed to facilitate growth of the dual gas moderators outlined in this chapter. A diagram of the system can be seen in figure 6.4.

A piece of Swagelok tubing was welded directly onto a DN40 flange connected to the side port of the source chamber to provide the interchange from the UHV chamber to the pressure fitting of the gas line. An isolation valve (labelled V1 in

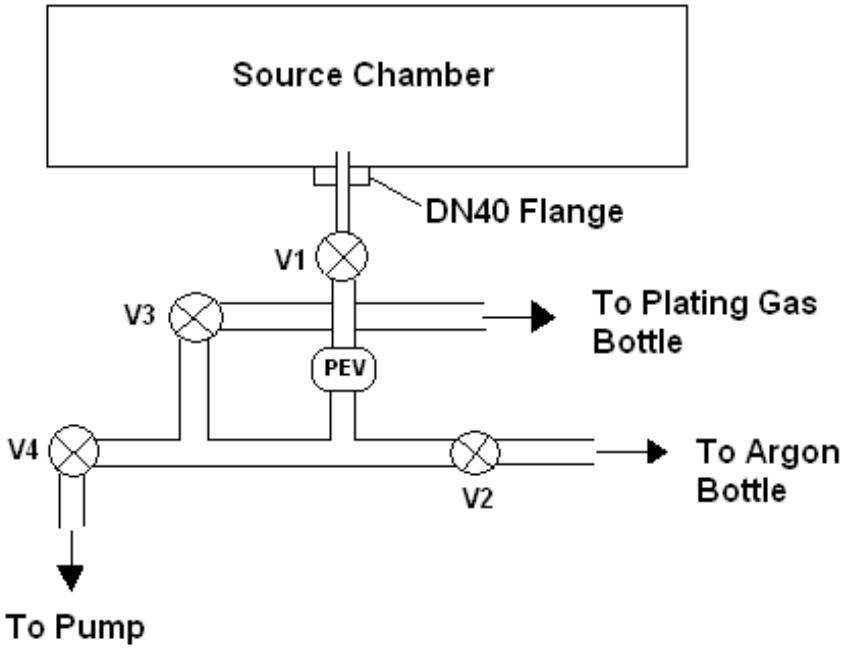

Figure 6.4: Diagram of the gas inlet system used in the positron moderator investigation beamline.

figure 6.4) was installed to enable the UHV system to be isolated from the gas lines. The pressure was regulated using a Piezo Electric Valve (PEV) controlled by the Labview program outlined in section 6.2.1. The PEV regulates both the rare gas and the plating gas. The gas line could be evacuated by opening valve V4 which connects directly to the backing pump of the source turbo pump, as shown in figure 6.1. The argon gas bottle and the plating gas bottle can be isolated using valves V2 and V3 respectively.

6.2.3 Positron Detection

The moderated positrons were detected by a CEM. Positrons incident on the front of the channeltron liberate around four electrons. These electrons are accelerated inside the CEM to a secondary point where each electron further amplifies the signal. Subsequent collisions reinforce this process until $\sim 10^8$ electrons have been produced, resulting in an output pulse which is about ~ 10 ns wide. A grid

used as a retarding energy selector (see section 6.3.1), was mounted on the front of the channeltron (see figure 6.5). The channeltron grid was grounded during growth with voltages of −200 V being applied to the front of the channeltron and +2.3 kV applied to the back of the device.

Figure 6.5: Photograph of the channeltron detector showing the energy selection grid, which was grounded during moderator growth.

As shown in figure 6.6, the CEM signal was passed through a HVA-200M-40-B femto Amplifier (FA), with an amplification of 10, followed by a timing filter amplifier (TFA), providing an additional 10 times amplification. The amplified signal then passed through a constant fraction discriminator (CFD) unit. The CFD output was sent to a computer via a National Instruments PCI 6221 (DAQ) card in conjunction with a BNC 2120 box, where it was monitored by the aforementioned Labview program.

The CEM detection efficiency was calibrated by taking a coincidence measurement with a caesium iodide (CsI) detector. If the efficiency of the CEM is denoted by ϵ_{CEM} and the efficiency of the CsI detector is ϵ_{CsI}, then the number of coincidence signals N_{coin} can be determined via;

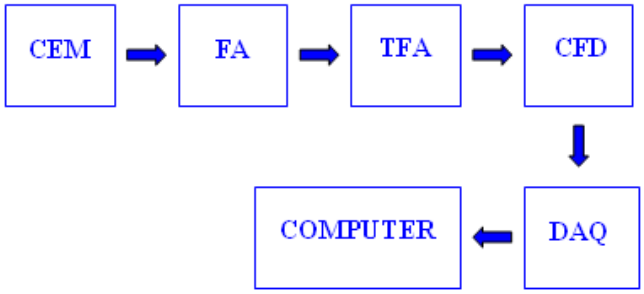

Figure 6.6: Schematic of the moderator beamline signal electronics.

$$N_{coin} = \epsilon_{CEM}\epsilon_{CsI}N, \tag{6.1}$$

where N is the count rate of the beam being monitored. Also it is clear that $\epsilon_{CEM} = N_{CEM}/N$ and $\epsilon_{CsI} = N_{CsI}/N$, where N_{CEM} and N_{CsI} are the measured count rates of the CEM and CsI detectors respectively. Substituting these relationships into equation 6.1 an expression for the absolute count rate can be obtained giving,

$$N = \frac{N_{CEM}N_{CsI}}{N_{Coin}}. \tag{6.2}$$

Counts were monitored for 1000 s. After subtracting a background measurement, the values for N_{CEM}, N_{CsI} and N_{Coin} were substituted into equation 6.2 to obtain N. Using the above relationships the efficiency of the CEM was determined to be 65 ± 6 %, and this correction was applied to the measured countrate in order to give the true positron flux. The efficiency of the CsI detector was calculated to be 1.2 ± 0.4 %.

6.3 Results and Discussion

6.3.1 Argon Moderators

A typical moderator growth curve, as depicted in figure 6.7, shows the number of moderated positrons increase over time until the yield saturates, which in this example is obtained after around 1.2 hours. The time taken to reach saturation

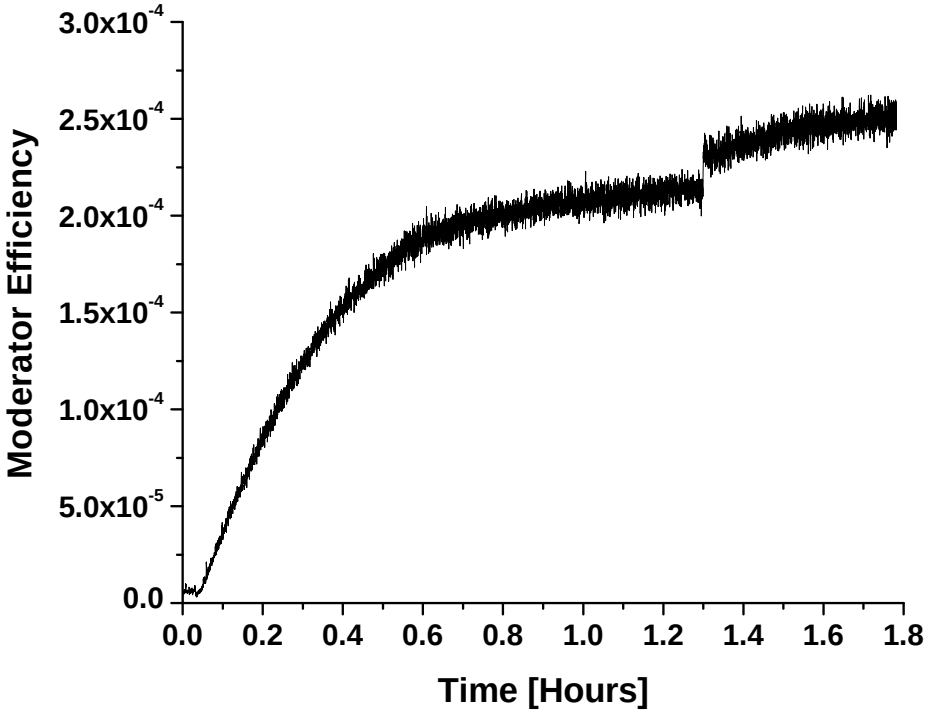

Figure 6.7: A moderator growth curve. Note the yield saturation level and the increase in yield caused by the removal of the gas from the system.

is dependent upon the gas pressure and temperature used for growth, as will be shown later. Once the saturation level has stabilised the gas can be removed from the system. With the removal of the argon gas from the system there is less attenuation in the beam transport to the CEM, and therefore a sharp increase in the number of moderated positrons is observed.

The gas selected, as a base, for these studies was argon as there have been previous measurements conducted elsewhere [34], and due to the capabilities of the system. While neon moderators are the most efficient RGS moderators, boasting an efficiency of $\sim$ 1% [26], they require temperatures lower than 10 K to grow, whilst the coldhead used in this system is only capable of achieving $\sim$ 15 K. Currently the highest efficiency achieved for uncharged argon is 0.07 % [32].

Initially, a purification stage consisting of an adsorbant material, zeolite, which when cooled adsorbed impurities in the argon, was implemented in the gas line system (see section 6.2.2), however the argon gas also began to adsorb and so use

of the purification stage was discontinued. This was not the only complication encountered. The coldhead worked so efficiently that the temperature of the heatshield attached to the coldhead was low enough to allow argon to condense upon on it, such that the moderators took a considerable time to grow. This second complication caused a further problem for the plating phase of the growth. With so much residual argon in the system the chamber pressure remained high enough to prevent the PEV from regulating the plating gas, and so a second gas could not be used. This was remedied by simply removing the heatshield.

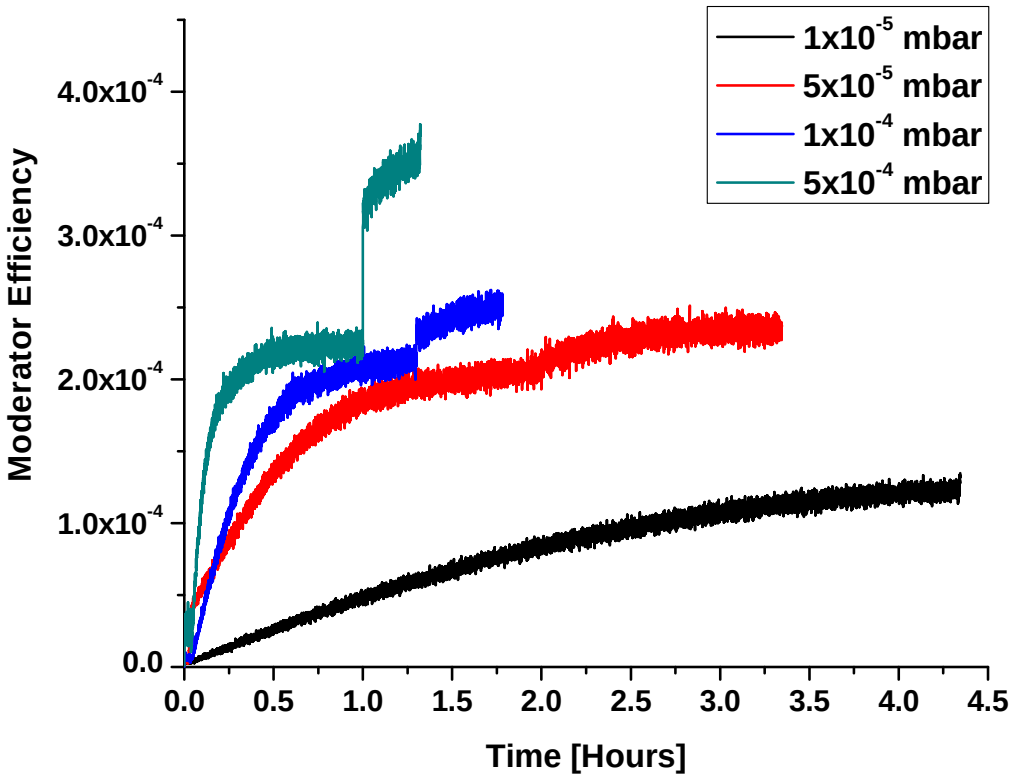

Figure 6.8: Time dependence of the low energy positron intensity for argon moderators grown at different pressures.

A series of moderators were grown at varying gas pressures as can be seen in figure 6.8. Molecular impurities in the bulk of the moderator can cause the positrons to slow down more rapidly, such that they may have insufficient energy to overcome the positive ϕ_+. As these impurities come from residual gas in

the chamber, moderators grown at higher pressure and hence more quickly, will contain fewer impurities in the bulk, leading to higher efficiencies.

Defects in the moderators can be reduced by annealing, which improves the lattice structure of the moderator. While this process has been shown to be sucessful for some positron beamlines [89], annealing showed no increase in yield with the neon moderators grown using the positron accumulator in Swansea [78], and had a detrimental effect on the argon moderators grown as part of these studies. The effect was so adverse that the positron yield from moderators annealed using this system decreased significantly. Annealing was therefore not used in any of the moderators presented.

From figure 6.8, an interesting observation can be made; when the argon gas is removed there is a increase in countrate, which does not level off immediately. Instead the yield continues to rise. While the reason for this is not known it is thought that this effect could be due to the moderator self-annealing[2]. This explanation is tentative as deliberate annealing was deleterious to the moderator efficiency. What can be seen is that this increase appears to be pressure dependent, as it is sharper and larger at higher pressures.

The experiments were repeated at a higher growing temperature, see figure 6.9. Comparing figures 6.8 and 6.9 one can see that the moderators grown at the lower pressure (1×10^{-5} and 5×10^{-5} mbar) are not significantly improved when the heater is employed. The same is true for the highest pressure, 5×10^{-4} mbar. What does appear to be significant is the change in the efficiency in the case of the moderator grown at 1×10^{-4} mbar. What is clear here is that the moderators grown at higher pressures have the highest slow positron yield which is consistent with fewer impurities existing in the bulk. The increase in positron yield, after the gas is removed, is also present here. Again it appears to be pressure dependent, but also temperature dependent at high pressure, indicating self-annealing.

Positrons leaving the moderator do so with a kinetic energy around a few eV such that the 20 V bias applied to the cone of the coldhead gives the positrons an additional 20 eV of kinetic energy. A retarding bias can be applied to the grid in front of the channeltron to prevent detection of the positrons. In this way

[2]Self-annealing is a process where the temperature of the layer is high enough to allow movement of the atoms, improving lattice structure.

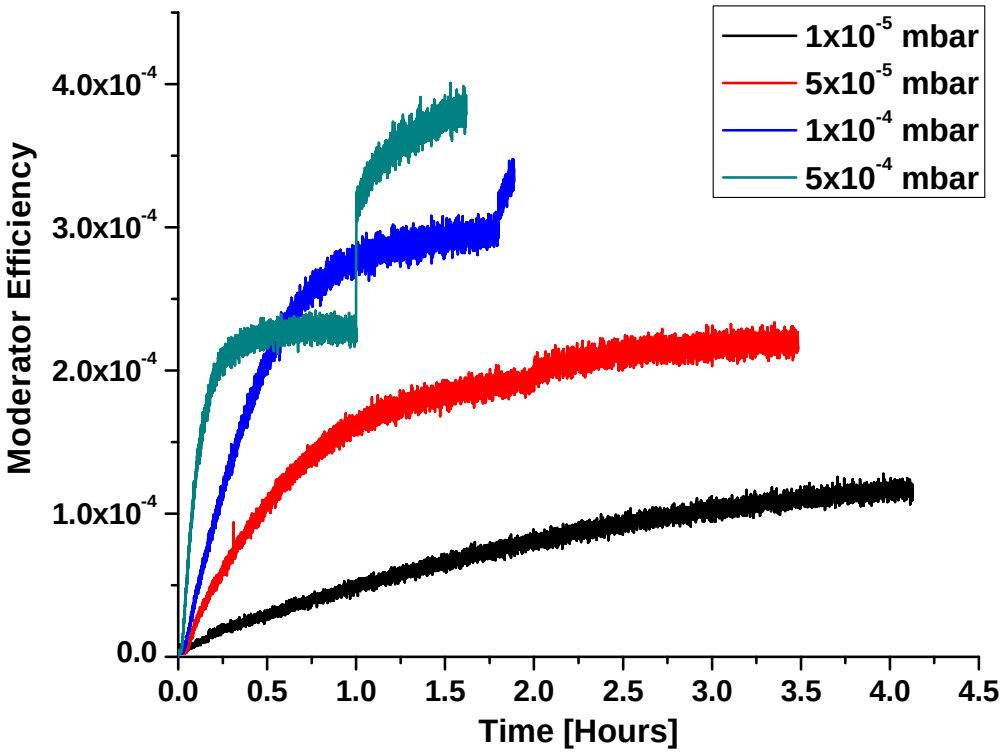

Figure 6.9: Time dependence of low energy positron intensity for argon moderators, grown with the use of the heater at different argon growth pressures.

only positrons with energy higher than the retarding potential are detected. The retarding bias was applied to the grid of the CEM over a range of 20 - 35 V in 60 steps. Each datum was measured for 10 s and averaged. It should be noted that the energy measurement described here is a measurement of the energy parallel to the magnetic field lines. An example of a typical retarding spectrum can be seen in figure 6.10.

By differentiating the resulting signal, the energy spectrum is obtained. As can be seen in figure 6.11, the energy spectrum is assymetric. As there is no accepted funtional form available for the distribution of energies emitted from a rare gas moderator, a Gaussian function was chosen for fitting in order to obtain the full width at half maximum (FWHM), and the peak position. The latter parameter determines the average energy of the emitted beam, whereas

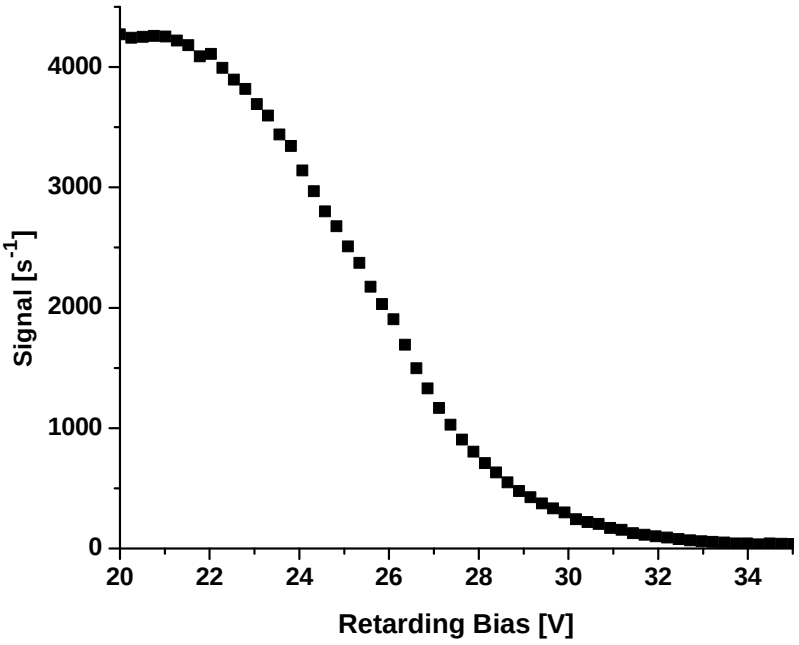

Figure 6.10: A typical retarding spectrum measurement, taken with a retarding bias over the range of 20 - 35 V in 0.25 V steps.

the FWHM value gives an estimate of the energy spread. The Gaussian fit was implemented through the use of the advanced fitting tool, part of the Origin software package.

The energy widths and peaks of the moderators, grown as previously discussed, are summarised in table 6.1 alongside the moderator efficiency. Here the efficiency is the measured signal[3]/source strength. The uncertainties in these values were determined through the error in the fit. The error in efficiency has been calculated from the standard error in the countrate. From table 6.1 it can be seen that when a higher growth pressure is used the overall moderator efficiency increases. The average energy of the emitted positrons, once the moderator bias has been subtracted from the measured peak centre, is around 5 eV. The addition of the heater appears to have a significant affect on the moderator efficiency at a pressure of 1×10^{-4} mbar, though this is not the case for the other pressures used

[3]The measured CEM signal is converted into positron number using the aforementioned calibration constant, and it is this value that is used here.

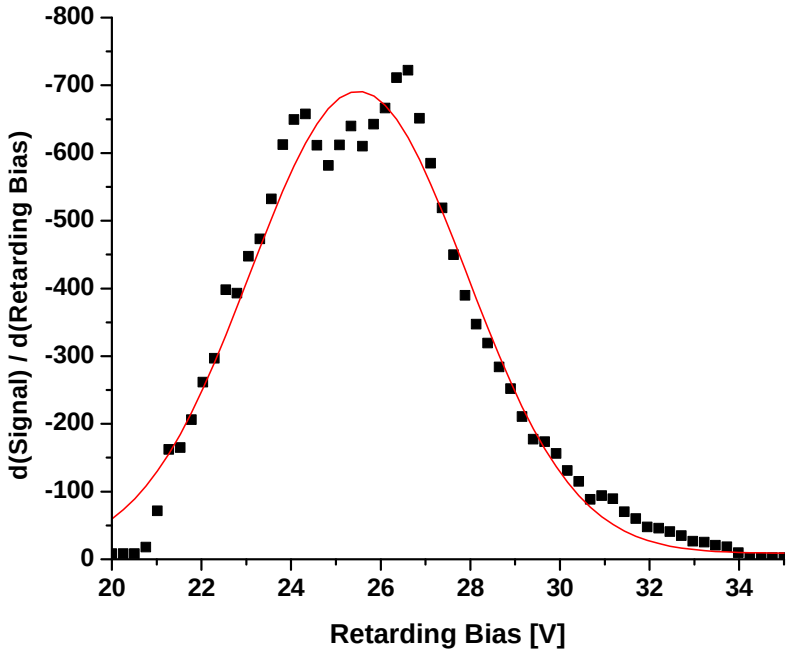

Figure 6.11: Plot of the derivative of figure 6.10 fitted with a Gaussian (the fit can be seen in red).

here. This result is very interesting as the yield of low energy positrons increases considerably when the heater is used, probably due to the higher growth temperature causing a reduction in the defect concentration in the moderator. It is not understood why similar effects are not observed at all pressures.

The argon moderators presented in table 6.1 were all grown over short time periods. Moderators grown at higher pressure in general have a shorter growth time, with the highest pressure achieving maximum yield in approximately an hour and the lowest pressure taking around four hours. In general the saturation point of the moderator, whilst achieved quickly, is maintained for a long period of time (i.e. 20 hours) before the layer of argon gas becomes too thick and the yield of low energy positrons decreases. For comparison purposes a range of moderators were grown over long time periods, which could be set using a time control written into the Labview program.

The moderators shown in table 6.2 were grown at 1×10^{-4} mbar, with this pressure chosen due to experience with the short growth moderators shown in

Table 6.1: The efficiency, FWHM and peak position values of argon moderators when grown at different pressures, both with and without the use of the heater. The uncertainty in the efficiency quoted here is the relative uncertainty. As all the measurements were conducted using an identical method this value is appropriate, However to determine the total uncertainty an additional factor of the 10 % must be included due to the uncertainty in the detector efficiency.

Argon Pressure [mbar]	Heater	FWHM ± 0.2 [eV]	Peak Centre ± 0.04 [eV]	Efficiency $\pm 7 \times 10^{-6}$
1×10^{-5}	No	5.8	25.95	1.2×10^{-4}
1×10^{-5}	Yes	5.2	26.13	1.1×10^{-4}
5×10^{-5}	No	4.8	25.50	2.3×10^{-4}
5×10^{-5}	Yes	5.2	25.50	2.1×10^{-4}
1×10^{-4}	No	5.4	25.63	2.4×10^{-4}
1×10^{-4}	Yes	4.8	25.50	3.5×10^{-4}
5×10^{-4}	No	5.4	25.47	3.7×10^{-4}
5×10^{-4}	Yes	5.4	25.47	3.4×10^{-4}

Table 6.2: The efficiency, FWHM and peak position values of argon moderators when grown at different pressures, both with and without the use of the heater, over a time period of 18 hours. The uncertainty in the efficiency quoted here is the relative uncertainty. As all the measurements were conducted using an identical method this value is appropriate, however to determine the total uncertainty an additional factor of the 10 % must be included due to the uncertainty in the detector efficiency.

Argon Pressure [mbar]	Heater	FWHM ± 0.2 [eV]	Peak Centre ± 0.04 [eV]	Efficiency $\pm 7 \times 10^{-6}$
1×10^{-4}	No	4.9	25.18	2.1×10^{-4}
1×10^{-4}	Yes	4.8	25.11	3.2×10^{-4}

table 6.1. When comparing tables 6.1 and 6.2 it can be seen that there is no significant change in the average energy of the positrons emitted from the long growth moderator, and the width is also not effected. The efficiency for the long growth moderators appears to be slightly lower, which could be related to an increased number of impurities in the moderator bulk. The efficiency difference observed between the heater on and off, for a gas pressure of 1×10^{-4} mbar, in table 6.1 is still present in the long growth moderators.

6.3.2 Ar Moderators Plated with N_2

Argon moderators were grown as previously discussed, with gas allowed into the system until the saturation positron yield was achieved. The system was then pumped out allowing the base pressure of the system to be achieved. Using the gas inlet system described in section 6.2.2 a plating gas could then be admitted. The gas line was flushed with the plating gas prior to the plating phase of the experiment. In this case, nitrogen gas could then be allowed into the system. The purity of the nitrogen used here was 99.998 %. The nitrogen gas pressure was regulated using the PEV valve (see figure 6.4) controlled by a PID algorithm

written into the Labview moderator growth program.

The gas was admitted into the system until the yield of low energy positrons began to decrease, which in general took around five minutes. If the plating pressure was too high the moderator countrate decreased almost as soon as the gas was allowed into the system, as can be seen in figure 6.12. Thus, it was decided to allow the plating gas in at a pressure that did not effect the countrate of the moderator to investigate whether the added gas had an effect on the energy of the emitted positrons; i.e to cause a shift in the average energy of the beam, and whether or not the addition of the second gas effected the energy spread of the emitted positrons. Energy spectrum measurements were taken as described in section 6.3.1 both before and after plating to allow a direct comparison. These data were taken within an hour of each other and so the degradation of the moderator was not a factor. The retarding bias used was over the range of 20 - 35 V in 60 steps. Measurements were taken for a 10 s counting period and then averaged. The results of these measurements are summarised in table 6.3.

The results presented in table 6.3, show no significant change in the energy width. There is, however, a clear shift in the peak position in the negative direction meaning that the average energy of emitted positrons is lower after plating. This effect may be indicative of charging of the surface layer, though the efficiency of the moderator remains unaffected.

6.3.3 Ar Moderators Plated with O_2

Moderators were grown as previously described. In this section the plating gas used was oxygen. The purity of the oxgen used was 99.6 %. Again, argon moderators were grown over a range of pressures both with and without the heater. Once the argon layer was grown the oxygen gas was inserted into the system using the gas inlet system previously described (section 6.2.2). Energy spectrum measurements were conducted after the Argon growth stage and repeated after the plating gas was added.

The oxygen gas pressure appeared to have the same effect as the nitrogen pressure, as shown in figure 6.12, in that if the pressure was too high the moderator countrate dropped significantly. As this was contrary to the aim of this

Table 6.3: The efficiency, FWHM and peak position values of argon moderation when plated with nitrogen gas, both before and after plating. Here, ϵ is the moderator efficiency and δ represents the difference between before and after measurements. The uncertainty in the efficiency quoted here is the relative uncertainty. As all the measurements were conducted using an identical method this value is appropriate, however to determine the total uncertainty an additional factor of the 10 % must be included due to the uncertainty in the detector efficiency.

Argon Pressure [mbar]	Heater	Before Plating			After Plating			δ_{FWHM} [eV] ± 0.45	δ_{Peak} [eV] ± 0.12
		FWHM ± 0.40 [eV]	Peak Centre ± 0.10 [eV]	$\epsilon_{Before} \pm 7 \times 10^{-6}$	FWHM ± 0.20 [eV]	Peak Centre ± 0.06 [eV]	$\epsilon_{After} \pm 7 \times 10^{-6}$		
5×10^{-5}	No	5.01	25.56	2.9×10^{-4}	4.83	25.16	2.9×10^{-4}	0.07	0.40
5×10^{-5}	Yes	5.64	25.96	2.7×10^{-4}	4.83	25.54	3.0×10^{-4}	0.81	0.42
1×10^{-4}	No	4.86	25.96	2.9×10^{-4}	4.81	25.58	2.9×10^{-4}	0.05	0.38
1×10^{-4}	Yes	4.85	25.89	3.6×10^{-4}	4.72	25.29	3.6×10^{-4}	0.13	0.60

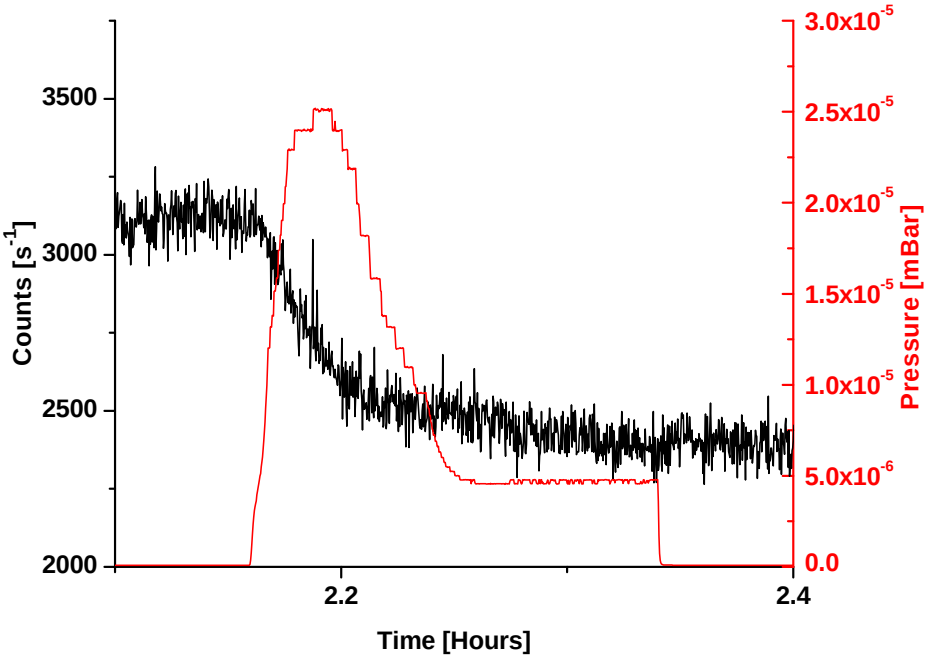

Figure 6.12: Plot showing the effect on the yield of low energy positrons when a plating gas is added at a high pressure. It can be seen here that when the nitrogen gas is inserted (red data), the CEM counts are significantly reduced. The count rate did not recover when the nitrogen was removed.

investigation the pressure used was lowered to 5×10^7 mbar, the point of having no obvious effect on the countrate to again investigate whether the energy profile was affected. Gas was allowed into the system until the countrate began to decrease, which occurred approximately 5 mins into the growth. The oxygen gas was then removed and the system was pumped out to base pressure. Once the beam intensity had stabilised, a retarding bias, over the range of 20-35 V, was applied to the grid at the front of the channeltron. Counts were measured over a 10 s time period and were then averaged. The results of these measurements can be seen in table 6.4.

All the retarding spectrum measurements presented in this section were differentiated with respect to the retarding bias. The differentiated signal was then

Table 6.4: The efficiency, FWHM and peak position values of argon moderation when plated with oxygen gas, both before and after plating. Here, ϵ is the moderator efficiency and δ represents the difference between before and after measurements. The uncertainty in the efficiency quoted here is the relative uncertainty. As all the measurements were conducted using an identical method this value is appropriate, however to determine the total uncertainty an additional factor of the 10 % must be included due to the uncertainty in the detector efficiency.

Argon Pressure [mbar]	Heater	Before Plating			After Plating			δ_{FWHM} [eV] ± 0.36	δ_{Peak} ± 0.10 [eV]
		FWHM ± 0.30 [eV]	Peak Centre ± 0.08 [eV]	$\epsilon_{Before} \pm 7 \times 10^{-6}$	FWHM ± 0.20 [eV]	Peak Centre ± 0.06 [eV]	$\epsilon_{After} \pm 7 \times 10^{-6}$		
1×10^{-5}	No	5.05	25.84	1.1×10^{-4}	4.50	25.54	1.1×10^{-4}	0.55	0.30
1×10^{-5}	Yes	4.82	25.90	1.1×10^{-4}	4.78	25.75	1.1×10^{-4}	0.04	0.15
5×10^{-5}	No	4.82	25.61	1.7×10^{-4}	4.70	25.27	1.7×10^{-4}	0.12	0.34
5×10^{-5}	Yes	4.98	25.39	2.5×10^{-4}	4.73	25.11	2.3×10^{-4}	0.25	0.28
1×10^{-4}	No	4.88	25.49	2.4×10^{-4}	4.59	25.22	2.4×10^{-4}	0.29	0.27
1×10^{-4}	Yes	4.91	25.36	2.6×10^{-4}	4.67	25.11	2.5×10^{-4}	0.24	0.25
5×10^{-4}	No	4.98	25.53	3.7×10^{-4}	4.59	25.12	3.6×10^{-4}	0.39	0.41
5×10^{-4}	Yes	4.72	25.41	3.8×10^{-4}	4.66	25.03	3.7×10^{-4}	0.48	0.48

fitted with a Gaussian function in order to estimate the energy width and the average energy of the positron beam. Table 6.4 shows that in the case of every moderator grown with oxygen the FWHM remains unchanged. A small shift in the average peak energy, towards the lower energy range is evident. This is consistent with a negative surface charge caused by electrons becoming stuck to the adsorbed oxygen molecules. As was found with nitrogen, the moderator efficiency is not significantly affected by the introduction of the second gas.

6.3.4 Ar Moderators Plated with Air

This section describes the results of argon moderators when plated with air. The method for these results was the same as previously described, i.e. argon moderators were grown over a range of pressures both with and without the heater and allowed to stabilise before the air was added to the chamber. In this case the plating gas bottle was removed from the gas inlet system and the pipe was left open to atmosphere. The gas pressure was regulated using the PEV valve and aforementioned labview program. The air pressure, if too high, caused the countrate to decrease in a similar fashion to both nitrogen and oxygen. Therefore, a lower pressure was used which did not affect the yield to investigate whether the energy distribution was altered, and if the shift in peak position observed with both oxygen and nitrogen, was still present when air was used. Energy spectrum measurements were made over the same voltage range as used for nitrogen, oxygen and argon moderators (20-35 V). The retarding bias was increased in 0.25 V steps and the signal measured over 10 s and recorded. The energy spectrum measurements were conducted using a labview program. Again, the energy range was measured after the growth phase and repeated after the plating phase and the results were fitted with a Gaussian function. The results of the energy measurements of argon moderators when plated with air are presented in table 6.5.

From table 6.5 it can be seen that when plated with air, a shift in the peak energy is observed, meaning that a lower average energy of the emitted positrons is achieved, as seen with the other plating gases. The moderator efficiency was not significantly affected by the introduction of the plating gas with most cases having

Table 6.5: The efficiency, FWHM and peak position values of argon moderation when plated with air, both before and after plating. Here, ϵ is the moderator efficiency and δ represents the difference between before and after measurements. The uncertainty in the efficiency quoted here is the relative uncertainty. As all the measurements were conducted using an identical method this value is appropriate, however to determine the total uncertainty an additional factor of the 10 % must be included due to the uncertainty in the detector efficiency.

Argon Pressure [mbar]	Heater	Before Plating			After Plating			δ_{FWHM} ± 0.36 [eV]	δ_{Peak} ± 0.10 [eV]
		FWHM ± 0.30 [eV]	Peak Centre ± 0.08 [eV]	$\epsilon_{Before} \pm 7 \times 10^{-6}$	FWHM ± 0.20 [eV]	Peak Centre ± 0.06 [eV]	$\epsilon_{After} \pm 7 \times 10^{-6}$		
1×10^{-5}	No	5.78	25.95	1.2×10^{-4}	5.12	25.51	1.2×10^{-4}	0.66	0.44
1×10^{-5}	Yes	5.17	26.13	1.1×10^{-4}	4.85	25.72	1.1×10^{-4}	0.32	0.41
5×10^{-5}	No	4.83	25.50	2.3×10^{-4}	4.73	25.05	2.2×10^{-4}	0.10	0.45
5×10^{-5}	Yes	5.16	25.50	2.2×10^{-4}	4.85	25.37	2.2×10^{-4}	0.31	0.13
1×10^{-4}	No	5.35	25.63	2.6×10^{-4}	4.70	25.38	2.6×10^{-4}	0.10	0.45
1×10^{-4}	Yes	4.82	25.50	3.5×10^{-4}	4.72	25.05	3.0×10^{-4}	0.65	0.25
5×10^{-4}	No	5.44	25.47	3.7×10^{-4}	4.88	25.32	3.5×10^{-4}	0.56	0.15
5×10^{-4}	Yes	5.44	25.47	4.2×10^{-4}	4.88	25.32	4.2×10^{-4}	0.56	0.15

no change. While the FWHM values do not appear to be effected the higher pressure measurement begin to show an effect, however this is not compelling.

Table 6.6: The efficiency, FWHM and peak position values of argon moderation when plated with air. The moderators were grown with and without the use of the heater, over a time period of 18 hours.The uncertainty in the efficiency quoted here is the relative uncertainty. As all the measurements were conducted using an identical method this value is appropriate, however to determine the total uncertainty an additional factor of the 10 % must be included due to the uncertainty in the detector efficiency.

Argon Pressure [mbar]	Heater	FWHM ± 0.20 [eV]	Peak Centre ± 0.04 [eV]	Efficiency $\pm 7 \times 10^{-6}$
1×10^{-4}	No	4.5	24.99	2.1×10^{-4}
1×10^{-4}	Yes	4.7	25.05	2.9×10^{-4}

In addition to these moderators the long growth moderators, outlined in table 6.2, were plated with air to see how a moderator grown over a long period of time was affected by a second gas. The result of the charging process can be seen in table 6.6. It is clear that when plated with air there is no significant change in the moderator. While there is a small shift in peak position this only occurs when the heater is not used and the difference is considerably smaller than with the short growth moderators.

6.4 Concluding Remarks

The results of this investigation have been disappointing as no increase in yield was observed, contrary to the preliminary results from elsewhere [34]. What is somewhat more promising is that these data do provide some evidence that surface charging of the moderator is taking place as evidenced by shifts in the peak position being observed for each plating gas. This would suggest that an

electric field has been produced through the surface charging, but that it was not sufficient to increase the low energy positron yield. The behaviour in efficiency observed at 1×10^{-4} mbar, when the heater is used, is very interesting and requires further investigation.

Chapter 7

Concluding Remarks

7.1 The Laser Ionisation of Positronium

For a number of years it has been a goal of researchers in Swansea to perform laser spectroscopy of positronium, as a method for producing Rydberg positronium that could be used for antihydrogen production. A laser system was purchased to do this, however all measurements attempted have been unsuccessful. It has been determined that the causes of this were most likely due to the laser linewidth being too narrow, such that not enough of an overlap with the Doppler profile was achieved, and that the temperature of the positronium was too high.

In order to overcome these problems new designs for both the laser system and the mini-trap have been produced. All the optics for the new laser system have been purchased and some of the components have been installed and aligned. The OPO and tripling units require alignment and the resultant pulses will need to be directed into the laser interaction cross. The power density and linewidth of the 243 nm pulse will need to be measured to ensure that sufficient power and linewidth are achieved. Once the Ps has been excited from the $n = 1$ to $n = 2$ state, efforts to probe the high n-states can begin. An additional laser beam will be required for this.

The new mini-trap needs to be constructed and tested. Simulations should be conducted to establish the best potentials to apply to the minitrap components. The lifetime of the mini-trap will also need to be measured. The new mini-trap

will allow higher implantation energies, around 5 keV, to be used, significantly decreasing the temperature of the Ps. A new silica target will also be installed.

7.2 Optimisation of Positron Plasmas in the ALPHA Experiment

A series of measurements were made in an attempt to optimise the positron plasmas produced in the ALPHA accumulator. These studies examined the introduction of a cooling gas, namely CO_2, into the accumulator, and the use of both dipole and quadrupole rotating electric fields. For a 200 s accumulation time with only nitrogen in the accumulator, the optimum trapping conditions were achieved using a dipole rotating wall with a frequency of 600 kHz. High frequencies appeared to have a detrimental effect on the plasma. Using a quadrupole field instead resulted in a significant loss in particle number.

When a cooling gas (CO_2) was used, the plasmas compressed using a dipole field contained more particles and higher densities were achieved. The data indicated that the cooling provided by the CO_2 becomes important at the higher frequencies, achieving lower diameter plasmas with higher central density, twice that of the nitrogen case.

The application of the quadrupole rotating wall produced broad plasmas with low central densities. Whilst the plasmas produced with CO_2 present were improved from the N_2-only case, the quadrupole was considerably less effective than the dipole rotating wall. The central densities and diameters appear to be dramatically dependent on the frequency, which could be examined further.

Using a CCD camera alongside a phosphor screen, images for all the data presented in chapter 5 were produced. The plasma shapes ranged from Gaussian-like profiles to hollow plasmas. Five distinct plasma shapes were observed and examples of these were given. The plasma shapes produced are not fully understood and will require further study.

There are a number of interesting aspects to this study that could be expanded upon, and many of the results observed were difficult to interpret. The rotating wall was applied throughout accumulation, making the analysis of the experiment

more complicated. The positron accumulator could be used for a given length of time prior to the application of the rotating wall, this would decouple the effects of the rotating wall and the accumulator, possibly providing more insight into the individual factors. The range of frequencies and amplitudes applied to the rotating wall could also be extended.

A study conducted by Greaves and Surko [54] concluded that SF_6 is the most effective cooling gas. These measurements could be repeated using SF_6 and CF_4 in the accumulator to see if better compression could be achieved, and to examine the radial profiles of the resultant plasmas.

The potential well in the trap is not particularly harmonic, different trapping potentials could be applied to the rotating wall to see if by using more symmetric or harmonic wells, higher positron plasma densities can be achieved.

7.3 Moderation Studies

A series of argon moderators were grown at four different pressures, with and without the use of a heater, which raises the temperature during growth by about ~ 5 K. These moderators were plated with an additional gas. The effect of pressure, temperature and plating gas were all investigated. The measurements and results are outlined and presented in chapter 6.

It was shown that moderators grown at higher pressures achieved higher yields of low energy positrons, than those grown at lower pressure. Temperature did not appear to have an effect on any of the results except one, those obtained for a pressure of 1×10^{-4} mbar, which showed a significant increase in efficiency.

The investigation into plated argon moderators was motivated by preliminary data [34] reporting a three-fold increase in yield when an additional plating gas was used. While the yield of low energy positrons was not improved by the introduction of a plating gas in this investigation, some positive results were obtained. The energy widths for most of the moderators grown remained unchanged however, in some cases, specifically with air as the plating gas, the energy widths were narrowed by around 0.5 eV. The average peak positions were also shifted giving a lower average energy for each plating gas. This shift in position is important as it indicates that either a negative surface charge of the moderator has

been produced or that the work function has changed. This would suggest that an electric field must exist across the rare gas solid, but that it is insufficient to improve the low energy positron yield.

It would be interesting to be able investigate argon at a higher gas pressure, which is currently limited by the system. The experimental arrangement allows gas into the system via a DN40 flange on the side of the source chamber. The gas pressure is monitored via an ion guage located at the top of this chamber. The current gas inlet system could be adapted, by attaching a pipe to the inside of the DN40 flange, and positioning it in such a way as to allow gas to be admitted into the chamber directly in front of the cone, attached to the coldhead assembly, without blocking the positron beam. In this way higher gas pressures could be achieved at the coldhead assembly. This adaptation should also allow the heatshield to be reinserted into the system, permitting lower temperatures to be examined.

Increasing the gas pressure in smaller increments would enable more measurements to be conducted. This would allow an investigation into whether the increase in yield observed in the 1×10^{-4} mbar case occurs at other pressures around this value; i.e. is there a pressure window where the higher growth temperature does indeed have an effect. The stability of the moderator over time could also be examined.

Another observation made is that when the gas is removed the yield of low energy positrons does not level off immediately but in fact continues to grow, which occurs at a steeper gradient for higher pressures. While this effect has been noted in this thesis it has not been fully investigated and further study into this could prove to be fruitful.

It has been argued that the increase in yield observed at higher pressure is due to fewer impurities existing in the bulk. A second gas line could be added to the gas inlet system for the specific purpose of allowing low pressures of molecular gas into the chamber during growth. This would provide insight into whether the increase at high pressure is indeed due to residual gas impurities.

Extending the temperature range could prove interesting for a number of reasons. It has been argued that the increase in yield after removal of the gas, could be attributed to self annealing of the moderator. This could potentially

occur quicker if the growth temperature is higher. Also, in the case of the argon moderators grown at 1×10^{-4} a significant increase in yield was observed when a higher temperature was used for growth. With a broader temperature range this effect can studied to see if the higher temperatures induce a similar result at higher pressures.

As neon is the most efficient RGS moderator this study could be extended to encompass plated neon moderators. While this is unachievable with the current system, a different coldhead capable of reaching lower temperatures could be used, or this study could be carried out using the positronium beamline outlined in chapter 4.

Appendix A

Projections of Positron Plasmas Produced in the ALPHA Experiment

As stated in chapter 5, photographs of all the plasmas produced were taken using the phosphor screen system previously discussed. A selection of some of the plasma projections were presented in chapter 5, the full plasma profiles are presented here.

A.1 Nitrogen Data with the Dipole Rotating Wall

Plasma profiles produced with nitrogen only in the accumulator, using a dipole rotating wall at a frequency of 600 kHz.

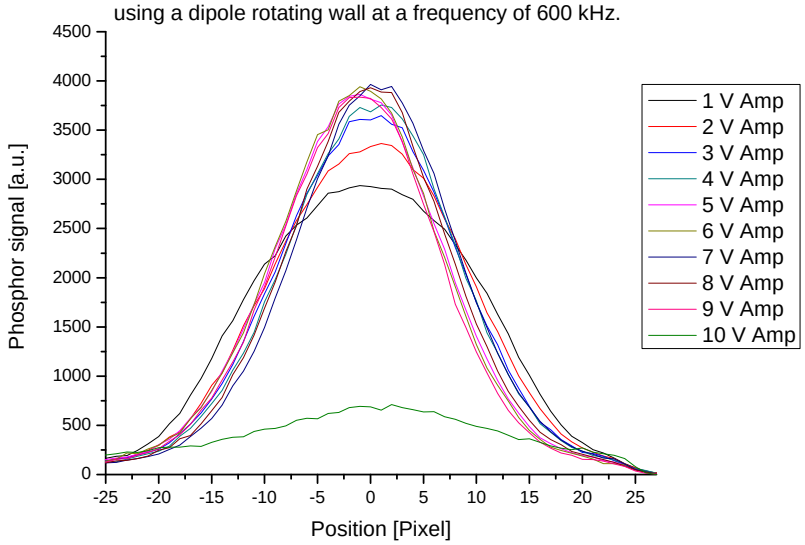

Plasma profiles produced with nitrogen only in the accumulator, using a dipole rotating wall at a frequency of 700 kHz.

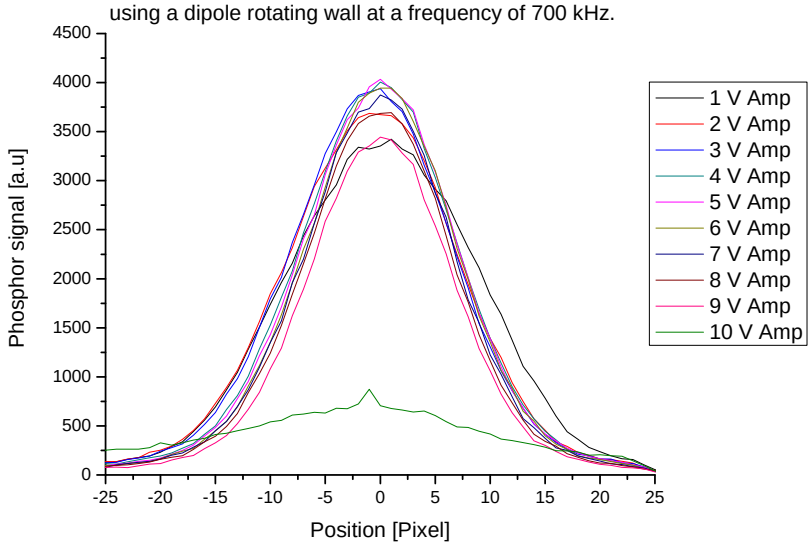

Plasma profiles produced with nitrogen only in the accumulator,
using a dipole rotating wall at a frequency of 800 kHz.

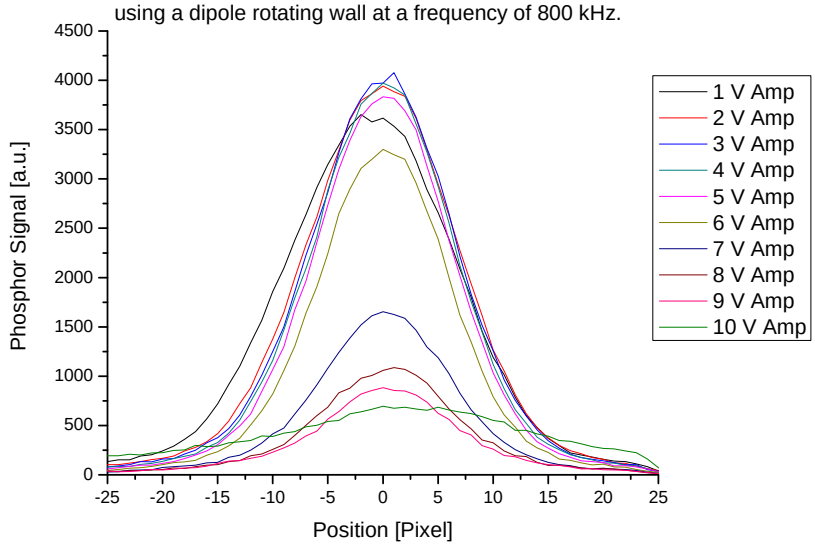

Plasma profiles produced with nitrogen only in the accumulator,
using a dipole rotating wall at a frequency of 900 kHz.

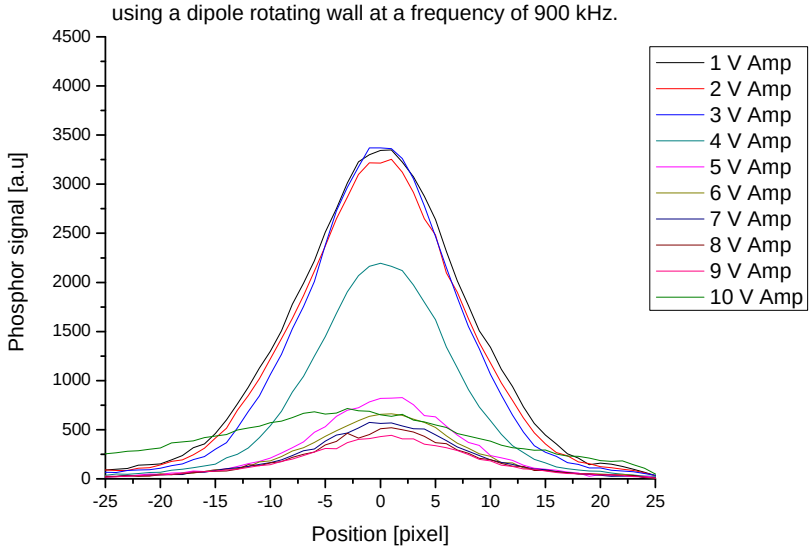

A.2 Nitrogen Data with a Quadrupole Rotating Wall

Plasma profiles produced with nitrogen only in the accumulator,
using a quadrupole rotating wall at a frequency of 600 kHz.

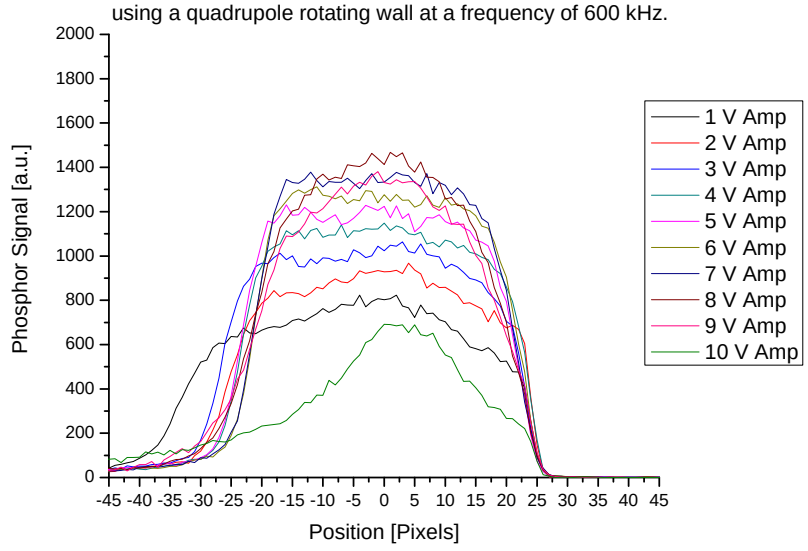

Plasma profiles produced with nitrogen only in the accumulator,
using a quadrupole rotating wall at a frequency of 700 kHz.

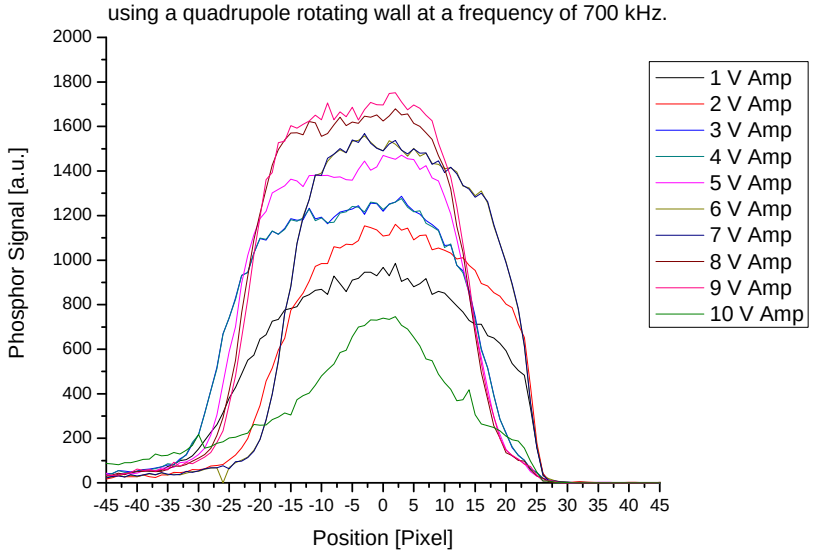

Plasma profiles produced with nitrogen only in the accumulator, using a quadrupole rotating wall at a frequency of 800 kHz.

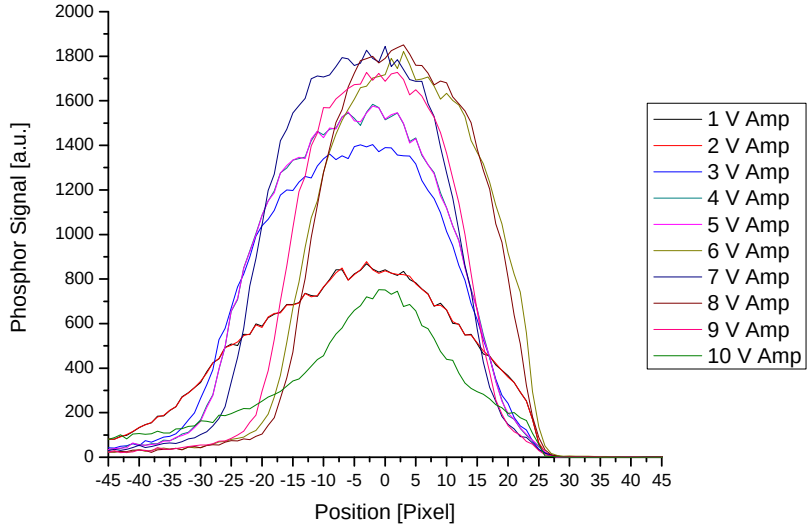

Plasma profiles produced with nitrogen only in the accumulator, using a quadrupole rotating wall at a frequency of 900 kHz.

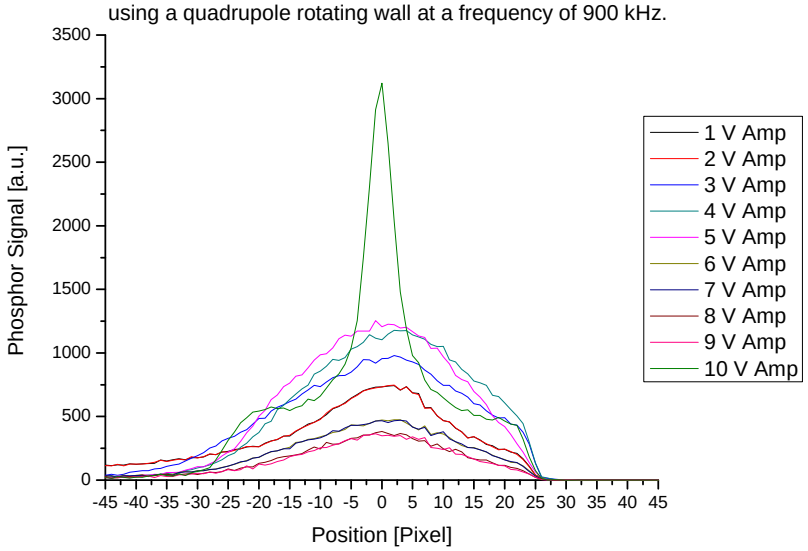

A.3 CO_2 Data with a Dipole Rotating Wall

Plasma profiles produced with nitrogenand carbon dioxide in the accumulator, using a dipole rotating wall at a frequency of 600 kHz.

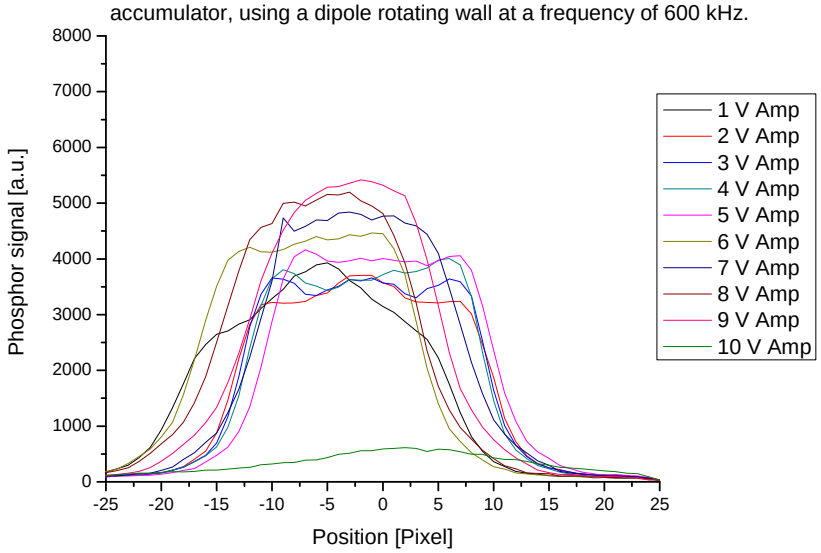

Plasma profiles produced with nitrogen and carbon dioxide in the accumulator, using a dipole rotating wall at a frequency of 700 kHz.

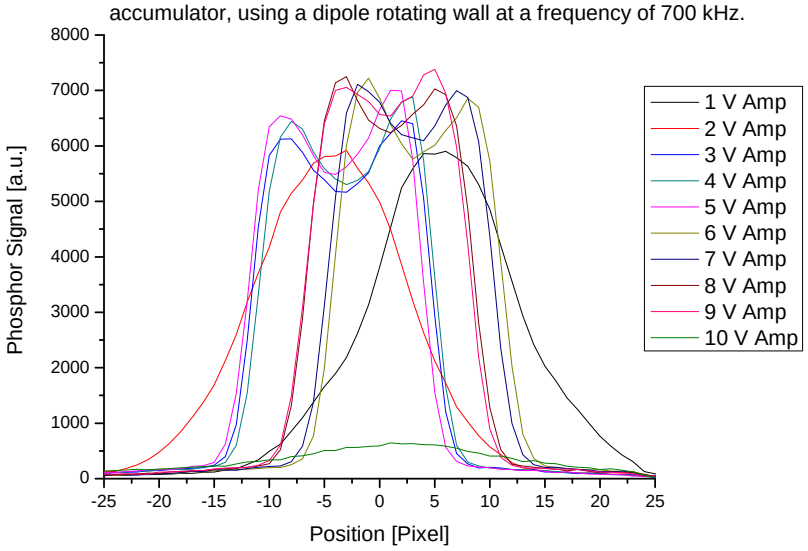

Plasma profiles produced with nitrogen and carbon dioxide in the accumulator, using a dipole rotating wall at a frequency of 800 kHz.

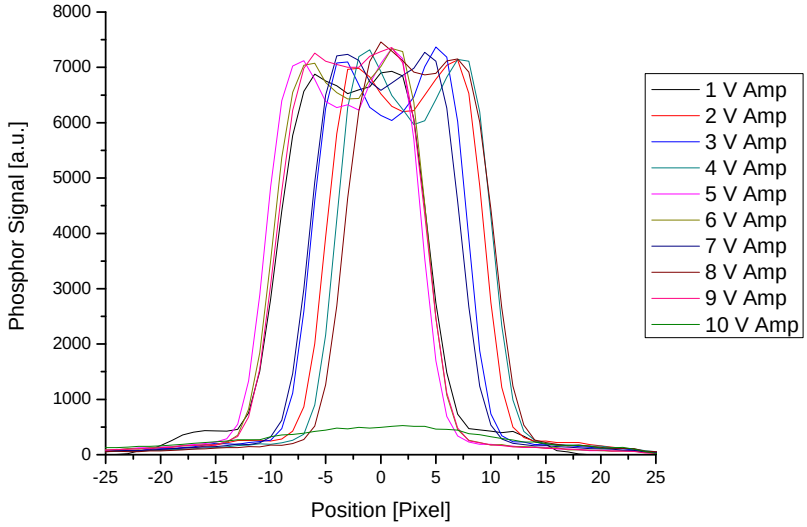

Plasma profiles produced with nitrogen and carbon dioxide in the accumulator, using a dipole rotating wall at a frequency of 900 kHz.

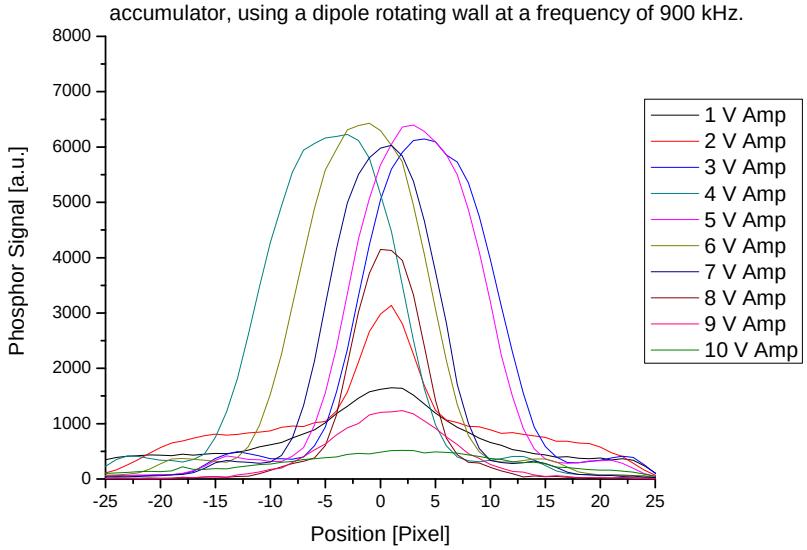

A.4 CO_2 Data with a Quadrupole Rotating Wall

Plasma profiles produced with nitrogen and carbon dioxide in the accumulator, using a quadrupole rotating wall at a frequency of 600 kHz.

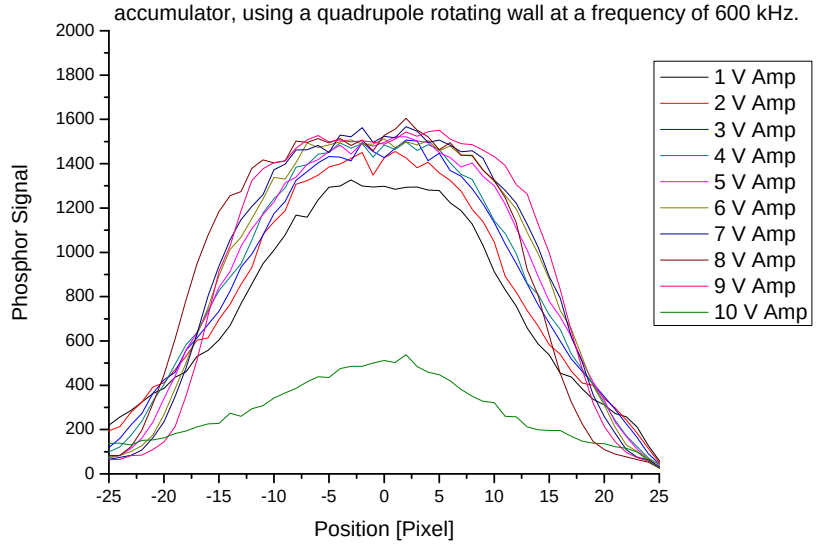

Plasma profiles produced with nitrogen and carbon dioxide in the accumulator, using a quadrupole rotating wall at a frequency of 700 kHz.

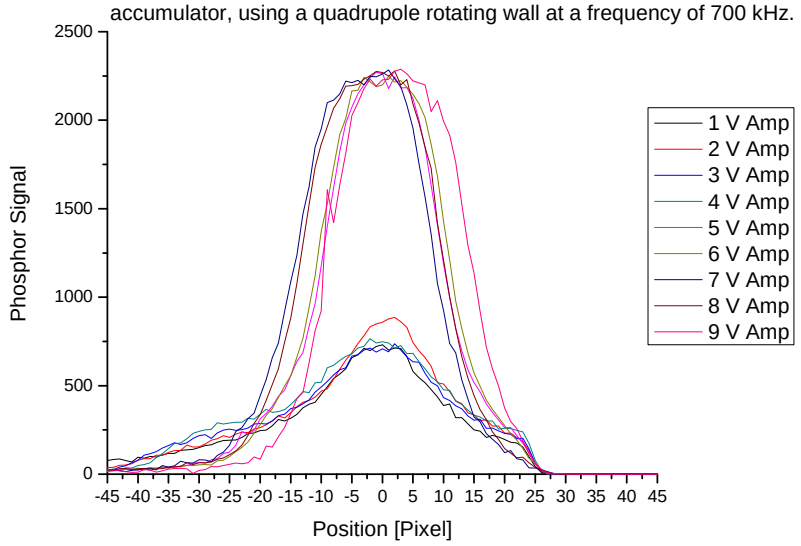

Plasma profiles produced with nitrogen and carbon dioxide in the accumulator, using a quadrupole rotating wall at a frequency of 800 kHz.

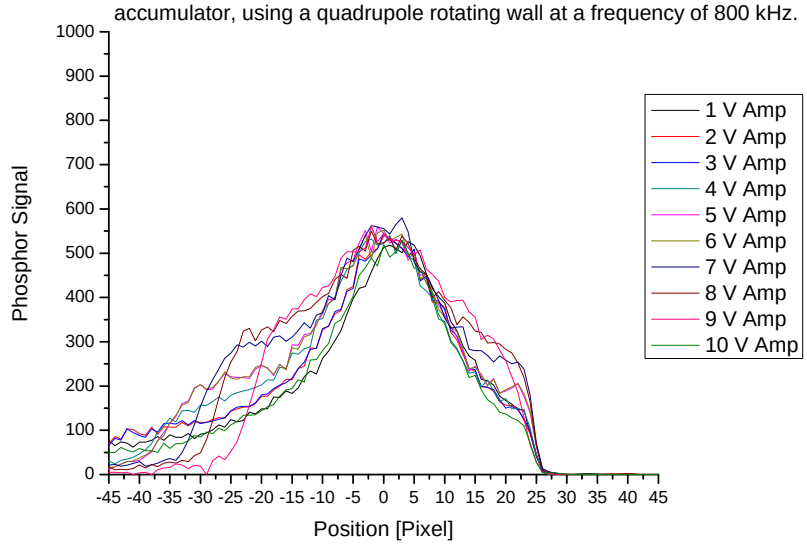

Plasma profiles produced with nitrogen and carbon dioxide in the accumulator, using a quadrupole rotating wall at a frequency of 900 kHz.

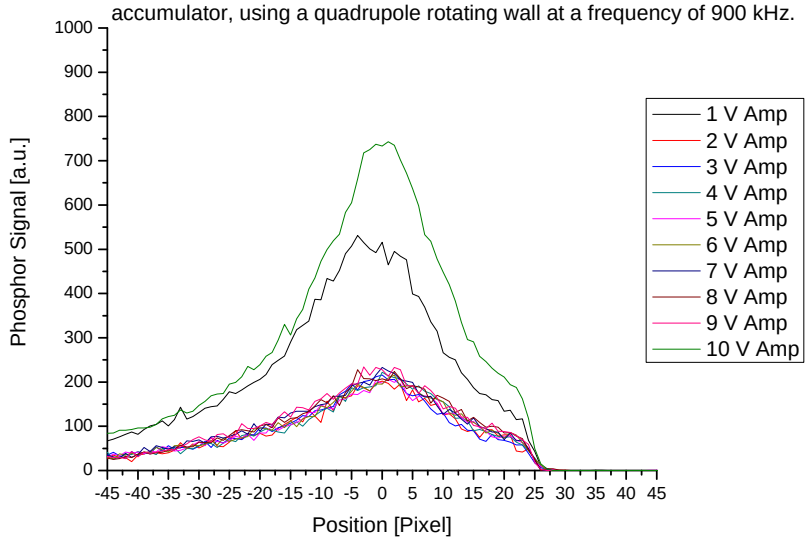

Appendix B

Publications

"Antiparticle sources for antihydrogen production and trapping."

G.B. Andresen, W. Bertsche, P.D. Bowe, C. Bray, E. Butler, C.L. Cesar, S. Chapman, M. Charlton, J. Fajans, M.C. Fujiwara, D.R. Gill, J.S. Hangst, W. N. Hardy, R. S. Hayano, M. E. Hayden, A. J. Humphries, R. Hydomako, L. V. Jørgensen, S. J. Kerrigan, L. Kurchaninov, R. Lambo, N. Madsen, P. Nolan, K. Olchanski, A. Olin, A. P. Povilus, P. Pusa, F. Robicheaux, E. Sarid, S. Seif El Nasr, D. M. Silveira, J. W. Storey, R. I. Thompson, D. P. van der Werf, J.S. Wurtele, and Y. Yamazaki. ,J. of Phys. Conf. Series **262** (2010) 012001

"Antihydrogen formation dynamics in a multipolar neutral anti–atom trap"

G.B. Andresen, W. Bertsche, P.D. Bowe, C. Bray, E. Butler, C.L. Cesar, S. Chapman, M. Charlton, J. Fajans, M.C. Fujiwara, D.R. Gill, J.S. Hangst, W.N. Hardy, R.S. Hayano, M.E. Hayden, A.J. Humphries, R. Hydomako, L.V. Jørgensen, S.J. Kerrigan, L. Kurchaninov, R. Lambo, N. Madsen, P. Nolan, K. Olchanski, A. Olin, A. Povilus, P. Pusa, F. Robicheaux, E. Sarid, S. Seif El Nasr, D.M. Silveira, J.W. Storey, R.I. Thompson, D.P. van der Werf, J.S. Wurtele, Y. Yamazaki ,Physics Letters B **685** (2010) 141

"Magnetised positronium"

D. P. van der Werf , C. J. Baker , D. C. S. Beddows , P. R. Watkeys , C. A.

Isaac , S. J. Kerrigan , M. Charlton and H. H. Telle, J. Phys.: Conf. Ser. **199** 012005 (2010)

"Antiproton, positron, and electron imaging with a microchannel plate/phosphor detector"

G. B. Andresen, W. Bertsche, P. D. Bowe, C. C. Bray, E. Butler, C. L. Cesar, S. Chapman, M. Charlton, S. Seif El Nasr, J. Fajans, M. C. Fujiwara, D. R. Gill, J. S. Hangst, W. N. Hardy, R. S. Hayano, M. E. Hayden, A. J. Humphries, R. Hydomako, L. V. Jørgensen, S. J. Kerrigan, L. Kurchaninov, R. Lambo, N. Madsen, P. Nolan, K. Olchanski, A. Olin, A. P. Povilus, P. Pusa, E. Sarid, D. M. Silveira, J. W. Storey, R. I. Thompson, D. P. van der Werf, Y. Yamazaki, and ALPHA Collaboration, Rev. Sci. Instrum. **80**, 123701 (2009)

"Magnetic multipole induced zero–rotation frequency bounce–resonant loss in a Penning-Malmberg trap used for antihydrogen trapping"

G. B. Andresen, W. Bertsche, C. C. Bray, E. Butler, C. L. Cesar, S. Chapman, M. Charlton, J. Fajans, M. C. Fujiwara, D. R. Gill, W. N. Hardy, R. S. Hayano, M. E. Hayden, A. J. Humphries, R. Hydomako, L. V. Jørgensen, S. J. Kerrigan, J. Keller, L. Kurchaninov, R. Lambo, N. Madsen, P. Nolan, K. Olchanski, A. Olin, A. Povilus, P. Pusa, F. Robicheaux, E. Sarid, S. Seif El Nasr, D. M. Silveira, J. W. Storey, R. I. Thompson, D. P. van der Werf, J. S. Wurtele, and Y. Yamazaki, Phys. Plasmas **16**, 100702 (2009)

"Weakly bound positron–electron pairs in a strong magnetic field"

C. J. Baker , D. P. van der Werf , D. C. S. Beddows, P. R. Watkeys , C. A. Isaac , S. J. Kerrigan , M. Charlton and H. H. Telle, J. Phys. B: At. Mol. Opt. Phys. **41** 245003 (2008)

"Three–body effects in positron annihilation on molecules"

M. Charlton, D. P. van der Werf, R. J. Lewis, P. R. Watkeys and S. J. Kerrigan, J. Phys. B: At. Mol. Opt. Phys. 39 (2006) L329 – L334

Bibliography

[1] C. D. Anderson. The positive electron. *Phys. Rev.*, 43:491, 1933.

[2] O. Chamberlain, E. Segrè, C. Wiegand, and T. Ypsilantis. Observation of antiprotons. *Phys. Rev.*, 100:947, 1955.

[3] B. Cork, G. R. Lambertson, O. Piccioni, and W. A. Wenzel. Antineutrons produced from antiprotons in charge-exchange collisions. *Phys. Rev.*, 104:1193, 1956.

[4] G. Baur, G. Boero, S. Brauksiepe, A. Buzzo, W. Eyrich, R. Geyer, D. Grzonka, J. Hauffe, K. Kilian, M. LoVetere, M. Macri, M. Moosburger, R. Nellen, W. Oelert, S. Passaggio, A Pozzo, K. Röhrich, K. Sachs, G. Schepers, T. Sefzick, R. S. Simon, R. Stratmann, F. Stinzing, and M. Wolke. Production of antihydrogen. *Phys. Lett. B*, 368:251, 1996.

[5] G. Blanford, D. C. Christian, K. Gollwitzer, M. Mandelkern, C. T. Munger, J. Schultz, and G. Zioulas. Observation of atomic antihydrogen. *Phys. Rev. Lett.*, 80:3037, 1998.

[6] M. Amoretti, C. Amsler, G. Bonomi, A. Bouchta, P. Bowe, C. Carraro, C. L. Cesar, M. Charlton, M. J. T. Collier, M. Doser, V. Filippini, K. S. Fine, A. Fontana, M. C. Fujiwara, R. Funakoshi, P. Genova, J. S. Hangst, R. S. Hayano, M. H. Holzscheiter, L. V. Jørgensen, V. Lagomarsino, R. Landua, D. Lindelöf, E. Lodi Rizzini, M. Macrí, N. Madsen, G. Manuzio, M. Marchesotti, P. Montagna, H. Pruys, C. Regenfus, P. Riedler, J. Rochet, A. Rotondi, G. Rouleau, G. Testera, A. Variola, T. L. Watson, and D. P. van der

Werf. Production and detection of cold antihydrogen atoms. *Nature*, 419:456, 2002.

[7] P. A. M. Dirac. The quantum theory of the electron. *Proc. R. Soc. A*, 117:610, 1928.

[8] P. M. S Blackett and G. P. S. Occhialini. Some photographs of the tracks of penetrating radiation. 1933.

[9] S. DeBenedetti, C. E. Cowan, W. R. Konneker, and H. Primakoff. On the angular distribution of two-photon annihilation radiation. *Phys. Rev.*, 77:205, 1950.

[10] A. Dupasquier. *Positron Solid-State Physics*. Proc. Int. School of Physics "Enrico Fermi": Course LXXXIII (North-Holland), 1983.

[11] M. Deutsch. Evidence for the formation of positronium in gases. *Phys. Rev.*, 82:455, 1951.

[12] B. R. Martin and G. Shaw. *Particle Physics*. John Wiley and Sons, $2^n d$ edition, 1997.

[13] M. Charlton and J. W. Humberston. *Positron Physics*. Cambridge University Press, 2000.

[14] G. Gräff, R. Ley, A. Osipowicz, and G. Werth. Intense source of slow positrons from pulsed electron accelerators. *Appl. Phys. A*, 33:59, 1984.

[15] P. J. Schultz and K. G. Lynn. Interaction of positron beams with surfaces, thin films, and interfaces. *Rev. Mod. Phys.*, 60:701, 1988.

[16] L. Madansky and F. Rasetti. An attempt to detect thermal energy positrons. *Phys. Rev.*, 79:397, 1950.

[17] W. Cherry. Phd thesis. 1958.

[18] J. M. J. Madey. Evidence for the emission of slow positrons from polyethylene. *Phys. Rev. Lett.*, 22:784, 1969.

[19] D. E. Groce, D. G. Costello, J. Wm. McGowan, and D. F. Herring. Evidence for the negative work function associated with positrons in gold. *Bull. Am. Phys. Soc.*, 13:1397, 1968.

[20] D. G. Costello, D. E. Groce, D. F. Herring, and J. Wm. McGowan. Evidence for the negative work function associated with positrons in gold. *Phys. Rev. B*, 5:1433, 1972.

[21] B. Y. Tong. Negative work function of thermal positrons in metals. *Phys. Rev. B*, 5:1436, 1972.

[22] K. F. Canter, P. G. Coleman, T. C. Griffith, and G. R. Heyland. Measurement of total cross sections for low energy positron-helium collisions. *J. Phys. B: Atom. Molec. Phys.*, 5:L167, 1972.

[23] K. F. Canter, A. P. Mills Jr., and S. Berko. Observations of positronium Lyman-α radiation. *Phys. Rev. Lett.*, 34:177, 1975.

[24] A. P. Mills Jr. Efficient generation of low-energy positrons. *Appl. Phys. Lett.*, 35:427, 1979.

[25] A. Vehanen, K. G. Lynn, P. J. Schultz, and M. Eldrup. Improved slow-positron yield using a single crystal tungsten moderator. *Appl. Phys. A*, 32:163, 1983.

[26] A. P. Mills Jr. and E. M. Gullikson. Solid neon moderator for producing slow positrons. *App. Phys. Lett.*, 49:1121, 1986.

[27] C. D. Beling and M. Charlton. Low-energy positron beams-origins, developments and applications. *Contemporary Physics*, 28:241, 1987.

[28] C. D. Beling, S. Fung, Li Ming, M. Gong, and B. K. Panda. A theoretical search for possible high efficiency semiconductor based field assisted positron moderators. *Appl. Sur. Sci*, 149:253, 1999.

[29] K. G. Lynn and B. T. A. McKee. Some investigations of moderators for slow positron beams. *Appl. Phys.*, 19:247, 1979.

[30] C. D. Beling, R. I. Simpson, M. Charlton, F. M. Jacobsen, T. C. Griffith, P. Moriarty, and S. Fung. A field-assisted moderator for low-energy positron beams. *Appl. Phys. A*, 42:111, 1987.

[31] Y. Y. Shan, H. L. Au, C. C. Ling, T. C. Lee, B. K. Panda, S. Fung, C. D. Beling, Y. Y. Wang, and H. M. Weng. Semi-insulating GaAs: A possible substrate for a field-assisted positron moderator. *Appl. Phys. A*, 59:259, 1994.

[32] J. P Merrison, M. Charlton, B. I. Deutch, and L. V. Jørgensen. Field assisted positron moderation by surface charging of rare gas solids. *J. Phys. Condens. Matter*, 4:L207, 1992.

[33] L. V. Jørgensen, J. P Merrison, B. I. Deutch, M. Charlton, and G. O. Jones. Positron dynamics in surface-charged solid argon. *Phys. Rev. B*, 52:12402, 1995.

[34] S. Armitage. Private communication. 2007.

[35] G. B. Andresen, M. D. Ashkezari, M. Baquero-Ruiz, W. Bertsche, P. D. Bowe, E. Butler, C. L. Cesar, S. Chapman, M. Charlton, A. Deller, S. Eriksson, J. Fajans, T. Friesen, M. C. Fujiwara, D. R. Gill, A. Gutierrez, J. S. Hangst, W. N. Hardy, M. E. Hayden, A. J. Humphries, R. Hydomako, M. J. Jenkins, S. Jonsell, L. V. Jørgensen, L. Kurchaninov, N. Madsen, S. Menary, P. Nolan, K. Olchanski, A. Olin, A. Povilus, P. Pusa, F. Robicheaux, E. Sarid, S. Seif el Nasr, D. M. Silveira, C. So, J. W. Storey, R. I. Thompson, D. P. van der Werf, J. S. Wurtele, and Y. Yamazaki. Trapped antihydrogen. *Nature*, 468:673, 2010.

[36] G. B. Andresen, M. D. Ashkezari, M. Baquero-Ruiz, W. Bertsche, P. D. Bowe, E. Butler, C. L. Cesar, S. Chapman, M. Charlton, J. Fajans, T. Friesen, M. C. Fujiwara, D. R. Gill, J. S. Hangst, W. N. Hardy, R. S. Hayano, M. E. Hayden, A. Humphries, R. Hydomako, S. Jonsell, L. Kurchaninov, R. Lambo, N. Madsen, S. Menary, P. Nolan, K. Olchanski, A. Olin, A. Povilus, P. Pusa, F. Robicheaux, E. Sarid, D. M. Silveira, C. So, J. W. Storey, R. I. Thompson, D. P. van der Werf, D. Wilding, J. S. Wurtele, and

Y. Yamazaki. Evaporative cooling of antiprotons to cryogenic temperatures. *Phys. Rev. Lett.*, 105:013003, 2010.

[37] S. Armitage, D. E. Leslie, A. J. Garner, and G. Laricchia. Fragmentation of positronium in collision with He atoms. *Phys. Rev. Lett.*, 89:173402, 2002.

[38] W. Sperber, D. Becker, K. G. Lynn, W. Raith, A. Schwab, G. Sinapius, G. Spicher, and M. Weber. Measurement of positronium formation in positron collisions with hydrogen atoms. *Phys. Rev. Lett.*, 68:3690, 1992.

[39] C. M. Surko, M. Leventhal, and A. Passner. Positron plasma in the laboratory. *Phys. Rev. Lett.*, 62:901, 1989.

[40] D. Wineland, P. Ekstrom, and H. Dehmelt. Monoelectron oscillator. *Phys. Rev. Lett.*, 31:1279, 1973.

[41] F. G. Major, V. N. Gheorghe, and G. Werth. *Charged Particle Traps: Physics and Techniques of Charged Particle Field Confinement (Springer Series on Atomic, Optical, and Plasma Physics)*. Springer, 2005.

[42] T. J. Murphy and C. M. Surko. Positron trapping in an electrostatic well by inelastic collisions with nitrogen molecules. *Phys. Rev. A*, 46:5696, 1992.

[43] J. Clarke, D. P. van der Werf, B. Griffiths, D. C. S. Beddows, M. Charlton, H. H. Telle, and P. R. Watkeys. Design and operation of a two-stage positron accumulator. *Rev. Sci. Inst.*, 77:063302, 2006.

[44] J. Clarke. *The Generation and Manipulation of Low Energy Positron Beams*. PhD thesis, University of Wales, Swansea, 2005.

[45] A. W. Trivelpiece and R. W. Gould. Space charge waves in cylindrical plasma columns. *J. App. Phys.*, 30:1784, 1959.

[46] C. S. Weimer, J. J. Bollinger, F. L. Moore, and D. J Wineland. Electrostatic modes as a diagnostic in Penning-trap experiments. *Phys. Rev. A*, 49:3842, 1994.

[47] J. Notte and J. Fajans. The effect of asymmetries on non-neutral plasma confinement time. *Phys. Plasmas*, 1:1123, 1994.

[48] D. J. Heinzen, J. J. Bollinger, F. L. Moore, W. M. Itano, and D. J. Wineland. Rotational equilibria and low-order modes of a non-neutral ion plasma. *Phys. Rev. Lett.*, 66:2080, 1991.

[49] S. L. Rolston and G. Gabrielse. Cooling antiprotons in an ion trap. *Hyp. Int.*, 44:233, 1988.

[50] X.-P. Huang, F. Anderegg, E. M. Hollmann, C. F. Driscoll, and T. M. O'Neil. Steady-state confinement of non-neutral plasmas by rotating electric fields. *Phys. Rev. Lett.*, 78:875, 1997.

[51] F. Anderegg, E. M. Hollmann, and C. F. Driscoll. Rotating field confinement of pure electron plasmas using Trivelpiece-Gould modes. *Phys. Rev. Lett.*, 81:4875, 1998.

[52] E. M. Hollmann, F. Anderegg, and C. F. Driscoll. Confinement and manipulation of non-neutral plasmas using rotating wall electric fields. *Phys. Plasmas*, 7:2776, 2000.

[53] R. G. Greaves and C. M. Surko. Inward transport and compression of a positron plasma by a rotating electric field. *Phys. Rev. Lett.*, 85:1883, 2000.

[54] R. G. Greaves and C. M. Surko. Radial compression and inward transport of positron plasmas using a rotating electric field. *Phys. Plasmas*, 8:1879, 2001.

[55] J. R. Danielson, T. R. Weber, and C. M. Surko. Plasma manipulation techniques for positron storage in a multicell trap. *Phys. Plasmas*, 13:123502, 2006.

[56] J. R. Danielson, T. R. Weber, and C. M. Surko. Extraction of small-diameter beams from single-component plasmas. *Appl. Phys. Lett.*, 90:081503, 2007.

[57] T. R. Weber, J. R. Danielson, and C. M. Surko. Tailored particle beams from single-component plasmas. *Non-Neutral Plasma Physics VII (AIP)*, CP1114:171, 2009.

[58] R. G. Greaves and J. M. Moxom. Compression of trapped positrons in a single particle regime by a rotating electric field. *Phys. Plasmas*, 15:072304, 2008.

[59] C. A. Isaac. *Axialisation of Particles in a Penning-Type Trap by the Application of a Rotating Dipole Electric Field and its Application toPositron Accumulation*. PhD thesis, Swansea University, 2010.

[60] S. Chu and A. P. Mills Jr. Excitation of the positronium $1^3S_1 - 2^3S_1$ two-photon transition. *Phys. Rev. Lett.*, 48:1333, 1982.

[61] S. Chu, A. P. Mills Jr., and J. L. Hall. Measurement of the positronium $1^3S_1 - 2^3S_1$ interval by Doppler-free two-photon spectroscopy. *Phys. Rev. Lett.*, 52:1689, 1984.

[62] M. S. Fee, A. P. Mills Jr., S. Chu, E. D. Shaw, K. Danzmann, R. J. Chichester, and D. M. Zuckerman. Measurement of the positronium $1^3S_1 - 2^3S_1$ interval by continuous-wave two-photon excitation. *Phys. Rev. Lett.*, 70:1397, 1993.

[63] M. S. Fee, S. Chu, A. P. Mills Jr., R. J. Chichester, D. M. Zuckerman, E. D. Shaw, and K. Danzmann. Measurement of the positronium $1^3S_1 - 2^3S_1$ interval by Doppler free two-photon excitation. *Phys. Rev. A*, 48:192, 1993.

[64] K. P. Ziock, C. D. Dermer, R. H. Howell, F. Magnotta, and K. M. Jones. Optical saturation of the $1^3S - 2^3P$ transition in positronium. *J. Phys. B: At. Mol. Opt. Phys.*, 23:329, 1990.

[65] K. P. Ziock, R. H. Howell, F. Magnotta, R. A. Failor, and K. M. Jones. First observation of resonant excitation of high-n states in positronium. *Phys. Rev. Lett.*, 64:2366, 1990.

[66] D. B. Cassidy, P. Crivelli, T. H. Hisakado, L. Liszkay, V. E. Meligne, P. Perez, H. W. K. Tom, and A. P. Mills Jr. Positronium cooling in porous silica measured via Doppler spectroscopy. *Phys. Rev. A*, 81:012715, 2010.

[67] D. B. Cassidy and A. P. Mills Jr. The production of molecular positronium. *Nature*, 449:195, 2007.

[68] H. H. Telle, M. Charlton, and D. P. van der Werf. Research proposal submitted to the EPSRC. 2002.

[69] B. C. Griffiths. *Development of a High-Powered Tuneable Laser System for Spectroscopic Studies of Trace Elements and Positronium.* PhD thesis, University of Wales, Swansea, 2005.

[70] M. Charlton. Antihydrogen production in collisions of antiprotons with excited states of positronium. *Phys. Lett. A*, 143:143, 1990.

[71] B. I. Deutch, M. Charlton, M. H. Holzscheiter, P. Hvelplund, L. V. Jørgensen, H. Knudsen, G. Laricchia, J. P. Merrison, and M. R. Poulsen. Antihydrogen synthesis by the reaction of antiprotons with excited state positronium atoms. *Hyp. Int.*, 76:153, 1993.

[72] F. Castelli, I. Boscolo, S. Cialdi, and M. G. Giammarchi. Efficient positronium laser excitation for antihydrogen production in a magnetic field. *Phys. Rev. A*, 78:052512, 2008.

[73] A. Dupasquier and A. P. Mills. *Physics with Many Positrons.* Proc. Int. School of Physics "Enrico Fermi": Course CLXXIV, 2010.

[74] A. Dupasquier and A. P. Mills Jr. *Physics with Many Positrons.* Proc. Int. School of Physics "Enrico Fermi": Course CLXXIV, 2010.

[75] P. Crivelli, U. Gendotti, A. Rubbia, L. Liszkay, P. Perez, and C. Corbel. Measurement of the orthopositronium confinement energy in mesoporous thin films. *Phys. Rev. A*, 81:052703, 2010.

[76] C. J. Baker, D. P. van der Werf, D. C. S. Beddows, P. R. Watkeys, C. A. Isaac, S. J. Kerrigan, M Charlton, and H. H. Telle. Weakly bound positron

- electron pairs in a strong magnetic field. *J. Phys. B: At. Mol. Opt. Phys*, 41:245003, 2008.

[77] Proxitronic. Phosphor screen data sheet. 2000.

[78] P.R Watkeys. *Towards Laser Excitation of Positronium and Advances in Positron Accumulation Techniques*. PhD thesis, Swansea University, 2008.

[79] M. Charlton, G. B. Andresen, M. D. Ashkezari, M. Baquero-Ruiz, W. Bertsche, P. D. Bowe, C. Bray, E. Butler, C. L. Cesar, S. Chapman, J. Fajans, T. Friesen, M. C. Fujiwara, D. R. Gill, J. S. Hangst, W. N. Hardy, R. S. Hayano, M. E. Hayden, A. J. Humphries, R. Hydomako, L. V. Jørgensen, S. J. Kerrigan, L. Kurchaninov, R. Lambo, N. Madsen, S. Menary, P. Nolan, K. Olchanski, A. P. Povilus, P. Pusa, F. Robicheaux, E. Sarid, S. Seif El Nasr, D. M. Silveira, C. So, J. W. Storey, R. I. Thompson, D. P. van der Werf, D. Wilding, J.S. Wurtele, and Y. Yamazaki. Antiparticle sources for antihydrogen production and trapping. *J. Phys. Conf. Series*, 262:012001, 2011.

[80] G. B. Andresen, W. Bertsche, P. D. Bowe, C. Bray, E. Butler, C. L. Cesar, S. Chapman, M. Charlton, J. Fajans, M. C. Fujiwara, D. R. Gill, J. S. Hangst, W. N. Hardy, R. S. Hayano, M. E. Hayden, A. J. Humphries, R. Hydomako, L. V. Jørgensen, S. J. Kerrigan, L. Kurchaninov, R. Lambo, N. Madsen, P. Nolan, K. Olchanski, A. Olin, A. Povilus, P. Pusa, F. Robicheaux, E. Sarid, S. Seif El Nasr, D. M. Silveira, J. W. Storey, R. I. Thompson, D. P. van der Werf, J.S. Wurtele, and Y. Yamazaki. Antihydrogen formation dynamics in a multipolar neutral anti-atom trap. *Phys. Lett. B*, 685:141, 2010.

[81] G. B. Andresen, W. Bertsche, P. D. Bowe, C. C. Bray, E. Butler, C. L. Cesar, S. Chapman, M. Charlton, J. Fajans, M. C. Fujiwara, D. R. Gill, J. S. Hangst, W. N. Hardy, R. S. Hayano, M. E. Hayden, A. J. Humphries, R. Hydomako, L. V. Jørgensen, S. J. Kerrigan, L. Kurchaninov, R. Lambo, N. Madsen, P. Nolan, K. Olchanski, A. Olin, A. P. Povilus, P. Pusa, E. Sarid, S. Seif El Nasr, D. M. Silveira, J. W. Storey, R. I. Thompson, D. P. van der

Werf, and Y. Yamazaki. Antiproton, positron, and electron imaging with a microchannel plate/phosphor detector. *Rev. Sci. Inst.*, 80:123701, 2009.

[82] G. B. Andresen, W. Bertsche, C. C. Bray, E. Butler, C. L. Cesar, S. Chapman, M. Charlton, J. Fajans, M. C. Fujiwara, D. R. Gill, W. N. Hardy, R. S. Hayano, M. E. Hayden, A. J. Humphries, R. Hydomako, L. V. Jørgensen, S. J. Kerrigan, L. Kurchaninov, R. Lambo, N. Madsen, P. Nolan, K. Olchanski, A. Olin, A. Povilus, P. Pusa, F Robicheaux, E. Sarid, S. Seif El Nasr, D. M. Silveira, J. W. Storey, R. I. Thompson, D. P. van der Werf, J.S. Wurtele, and Y. Yamazaki. Magnetic multipole induced zero-rotation frequency bounce-resonant loss in a Penning-Malmberg trap used for antihydrogen trapping. *Phys. Plasmas*, 16:100702, 2009.

[83] M. Hori, J. Eades, R. S. Hayano, T. Ishikawa, W. Pirkl, E. Widmann, H. Yamaguchi, H. A. Torii, B. Juhász, D. Horváth, and T. Yamazaki. Direct measurement of transition frequencies in isolated $\overline{\mathrm{p}}\mathrm{He}^+$ atoms, and new CPT-violation limits on the antiproton charge and mass. *Phys. Rev. Lett.*, 91:123401, 2003.

[84] H. Knudsen, H.-P. E. Kristiansen, H. D. Thomsen, U. I. Uggerhøj, T. Ichioka, S. P. Møller, C. A. Hunniford, R. W. McCullough, M. Charlton, N. Kuroda, Y. Nagata, H. A. Torii, Y. Yamazaki, H. Imao, H. H. Andersen, and K. Tökesi. Ionization of helium and argon by very slow antiproton impact. *Phys. Rev. Lett.*, 101:043201, 2008.

[85] G. Gabrielse, P. Larochelle, D. Le Sage, B. Levitt, W. S. Kolthammer, R. McConnell, P. Richerme, J. Wrubel, A. Speck, M. C. George, D. Grzonka, W. Oelert, T. Sefzick, Z. Zhang, A. Carew, D. Comeau, E. A. Hessels, C. H. Storry, M. Weel, and J. Walz. Antihydrogen production within a Penning-Ioffe trap. *Phys. Rev. Lett.*, 100:113001, 2008.

[86] G. Gabrielse, N. S. Bowden, P. Oxley, A. Speck, C. H. Storry, J. N. Tan, M. Wessels, D. Grzonka, W. Oelert, G. Schepers, T. Sefzick, J. Walz, H. Pittner, T. W. Hänsch, and E. A. Hessels. Background-free observation of cold

antihydrogen with field-ionization analysis of its states. *Phys. Rev. Lett.*, 89:213401, 2002.

[87] G. Gabrielse, N. S. Bowden, P. Oxley, A. Speck, C. H. Storry, J. N. Tan, M. Wessels, D. Grzonka, W. Oelert, G. Schepers, T. Sefzick, J. Walz, H. H. Pittner, T. W. Hänsch, and E. A. Hessels. Driven production of cold antihydrogen and the first measured distribution of antihydrogen states. *Phys. Rev. Lett.*, 89:233401, 2002.

[88] G. Gabrielse, S. L. Rolston, L. Haarsma, and W. Kells. Antihydrogen production using trapped plasmas. *Phys. Lett. A*, 129:38, 1988.

[89] D. R. J. Mitchard. *Positron and Laser Studies for the Formation of Antihydrogen.* PhD thesis, University of Wales Swansea, 2006.